CATALYTIC OXIDATION OF CARBON MONOXIDE OVER MANGANITE SPINELS

THESIS

submitted to the

GOA UNIVERSITY

for the degree of

DOCTOR OF PHILOSOPHY

in chemistry

by

SHRIDHAR M. GURAV

Department of Chemistry

Goa University

Goa 403206

1997

STATEMENT

I hereby state that this thesis for the Ph.D. degree on 'Catalytic oxidation of carbon monoxide over manganite spinels' is my original work and that it has not previously formed the basis for the award of any degree, diploma , associateship and fellowship or any other similar title to the best of my knowledge and information.

Dr. A. V. Salker
(Research Guide)

Shridhar M. Gurav
(candidate)

CERTIFICATE

As required under the University ordinance, I certify that the thesis entitled 'Catalytic oxidation of carbon monoxide over manganite spinels' submitted by Mr. Shridhar M. Gurav, for the award of Doctor of Philosophy in Chemistry is a record of research done by the candidate during the period of study under my guidance and that it has not previously formed the basis for the award to the candidate of any degree, diploma, associateship, fellowship or other similar titles.

Date : 28.11.1997

Dr. A. V. Salker,
Research Guide,
Department of Chemistry,
Goa University.

ACKNOWLEDGEMENT

With great pleasure I wish to express my deep sense of gratitude to Dr. A. V. Salker for his inspiring and valuable guidance during the course of this work

I am indeed grateful to Prof. V. N. Kamat Dalal, Head, Dept. of Chemistry, for extending necessary facilities.

It is my proud privilege to place on record my sincere thanks to Prof. D. K. Chakrabarty, IIT. Bombay, Dr. Ramchandra Bhatt, HLRC. Bombay and Dr. R. M. Cursetji, ACC. Thane for providing analysis facility.

With due respect I also thank Dr. K. S. Rane, Dr. B. Srinivasan and Dr. Gaurish Naik for their kind help. I thank Dr. R. R. Nair (G.O.D, NIO) for extending the facility of XRD analysis

My sincere thanks to Dr. Felix Dias for his help in analysis.

I thank Mr. Prabhu (G.O.D., NIO) for running XRD's and Jaiprakash (USIC, G.U) for his time to time help.

I thank all my research colleagues past and present who have helped directly or indirectly during the course of this investigation.

Finally I thank my Parents, Brothers and other relatives for their constant encouragement and moral support during the course of this work.

CONTENTS

CONTENTS

CONTENTS

CHAPTER 1

INTRODUCTION

INTRODUCTION

Transition metal oxides (TMO) show interesting catalytic and material properties. Last several decades, the field of transition metal oxides has served as a source of fascinating and challenging research problems to technologists, chemists and material scientists. TMO have become an area of active research for catalytic studies and efforts are being made to replace the conventional noble metal catalyst by oxide catalysts[1-3], which are economical, thermally stable and equally efficient. Extensive study of simple oxide solid solutions led to interesting observations. Above certain critical concentrations of the active metal ions, there is an appearance of new phase of ternary oxides which were identified as perovskites and spinel phases[4]. An investigation of catalytic activity of these pure spinels and perovskite phases showed that they are better catalysts in view of their activity and thermal stability as compared with individual oxides[5-7]

Carbon monoxide (CO) oxidation over TMO is an interesting reaction in terms of practical importance, which is associated with toxicity and the necessity to purify industrial and automobile exhaust gases. There is

a growing demand for the pollution control catalysts either for industries or for the automobiles and to have stable more effective and viable catalysts. The study of CO oxidation has a long history. Although this reaction has the importance of its own, from the point of utility, it has also been used as a model reaction to test the catalysts.

Complex oxides containing two or more cations have attracted attention in recent times because of their growing demand in variety of scientific and technological fields. These oxides find applications in many heterogeneously catalysed oxidation reactions and shown to be active for many oxidation-reduction reactions without poisoning.

Following Volkenstein's[8] electronic theory of catalysis, there is a growing awareness of the role of solid state properties in the catalytic phenomena, since then many correlation's of catalytic activity with defects in solids, electrical and magnetic properties have appeared in the literature.

Ternary oxides chosen for the present investigations are series of spinel systems. Because of their stable structure, spinels have attracted attention in the study of structural and electronic factor in catalysis. These oxides are quiet flexible in the sense that many metal ions with variable valencies could be incorporated into them. Many spinels have found potential applications such as ceramic materials, semi-conductors, magnetic materials, insulators in addition to being good catalysts[9]. It is therefore no wonder that a great concern through research is devoted to these properties to understand and extrapolate, the obtained data to design a new material for specific purposes. The oxide spinels have distinct structural features which play a vital role in determining their electrical, magnetic as well as catalytic

properties. The studies of these systems is quite useful in understanding the fundamental and technological aspects to provide a rational basis for the catalysts selection.

The transition metal manganites discussed in this investigations are prepared by a co-precipitation technique in order to achieve homogeneity and low temperature formation with more surface area, unlike combustion and ceramic methods which require high temperature for their formations, beside the loss in surface area as a result of sintering. In the present study the catalytic oxidation of CO on manganite spinels with reference to activity, selectivity, kinetics and solid state properties has been attempted.

The present investigation includes:

1. Preparation of series of spinels such as [I] $Ni_{1-x}Cu_xMn_2O_4$ [ii] $Zn_{1-x}Cu_xMn_2O_4$ [iii] $Co_{1-x}Cu_xMn_2O_4$ [iv] $Ni_{1-x}Co_xMn_2O_4$ where (x = 0.0, 0.3, 0.5, 0.7, and 1.0).
2. Characterisation of spinels by different methods such as X-Ray Diffraction (XRD), Atomic Absorption Spectroscopy (AAS), and BET Surface Area measurement.
3. Solid state properties of the prepared spinels such as Thermal studies, Magnetic Susceptibility, Electrical Resistivity, and Electron Spin Resonance (ESR) studies.
4. Temperature dependence of CO conversion efficiency over these spinels.
5. Study of kinetics of CO oxidation by oxygen on [i] $Ni_{1-x}Cu_xMn_2O_4$ and [ii] $Zn_{1-x}Cu_xMn_2O_4$.

CHAPTER 2

REVIEW OF LITERATURE

REVIEW OF LITERATURE

2.1. STRUCTURE AND PHYSICO-CHEMICAL PROPERTIES OF SPINELS

Spinels are a class of compounds which are isostructural with the mineral spinel $MgAl_2O_4$ and have a general formula AB_2X_4, where A and B are metal ions and X is a divalent anion, generally an oxide ion. Based on the valencies of A and B ions, the spinels can be divided into three groups namely 6:1, 4:2, and 2:3 spinels, which can be represented with their cationic charges as $(A^{6+} + 2B^{+})$, $(A^{4+} + 2B^{2+})$ and $(A^{2+} + 2B^{3+})$ respectively. The most common spinels are those with A in 2+ and B in 3+ oxidation state on account of their stability. The stability of 2:3 spinels, compared to the other two is due to the less difference between the valencies and the sizes of the A and B ions.

2.1.1. Spinel structure

The unit cell of an ideal spinel structure[10 - 13] is given in fig. 2.1. In this ideal cubic structure the anions form cubic close packing, in which cations occupy partly the tetrahedral and partly the octahedral voids. The unit cell contains 32 anions forming 64 tetrahedral and 32 octahedral interstices, of which 8 tetrahedral and 16 octahedral interstices are occupied by cations. Thus the unit cell contains 8 formula units. The unit cell with perfect cubic-close packing array corresponds to the formula $A_8B_{16}O_{32}$. In the normal spinel structure the eight A ions occupy tetrahedral sites in the face centred cubic oxide lattice and the sixteen B ions occupy octahedral sites as indicated in fig. 2.1a. The tetrahedral and octahedral sites are generally referred to as A and B sites respectively. The spinel structure is fairly empty because only one eight of the tetrahedral and one half of the octahedral sites are occupied. Thus the solubility of the component oxides in the spinel phase is observed, resulting in the appearance of excess cations in the interstitial tetrahedral and octahedral sites.

The crystal structure can be explained easily by subdividing the unit cell into eight octants with edge a/2, where 'a' is the edge length of the unit cell as shown in fig. 2.1c. The oxygen's are arranged in an identical manner in all the octants. Each oxygen is being located on the body diagonal at a distance equal to one-fourth the length of the body diagonal from alternate corners of an octant. Thus each octant contains four oxygen and they form the corners of a tetrahedron. The array of oxygen as a whole

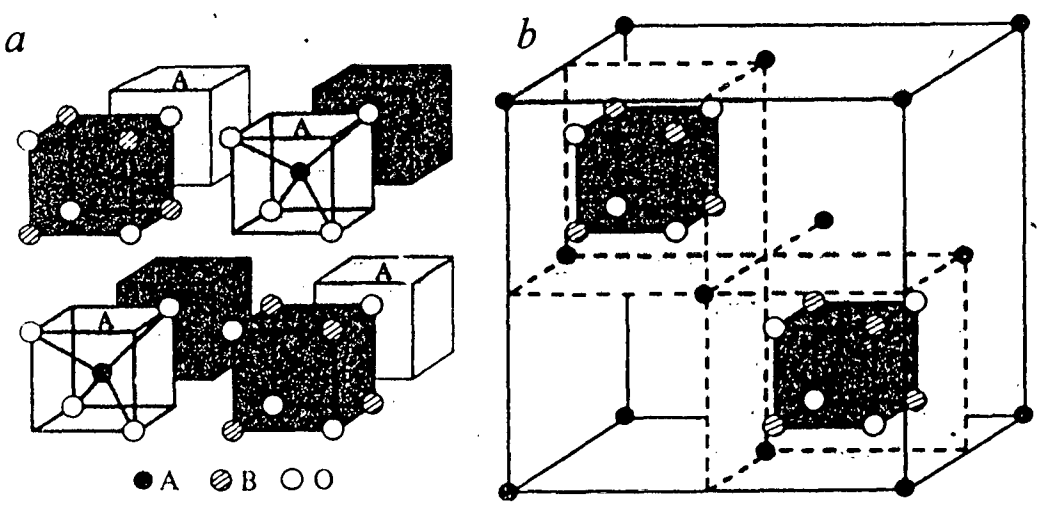

Fig. 2.1. Spinel structure AB_2O_4. (a) Imaginary eight octants of alternate AO_4 tetrahedra and B_4O_4 cubes. (b) Location of two of the B_4O_4 cubes is shown with orientation.

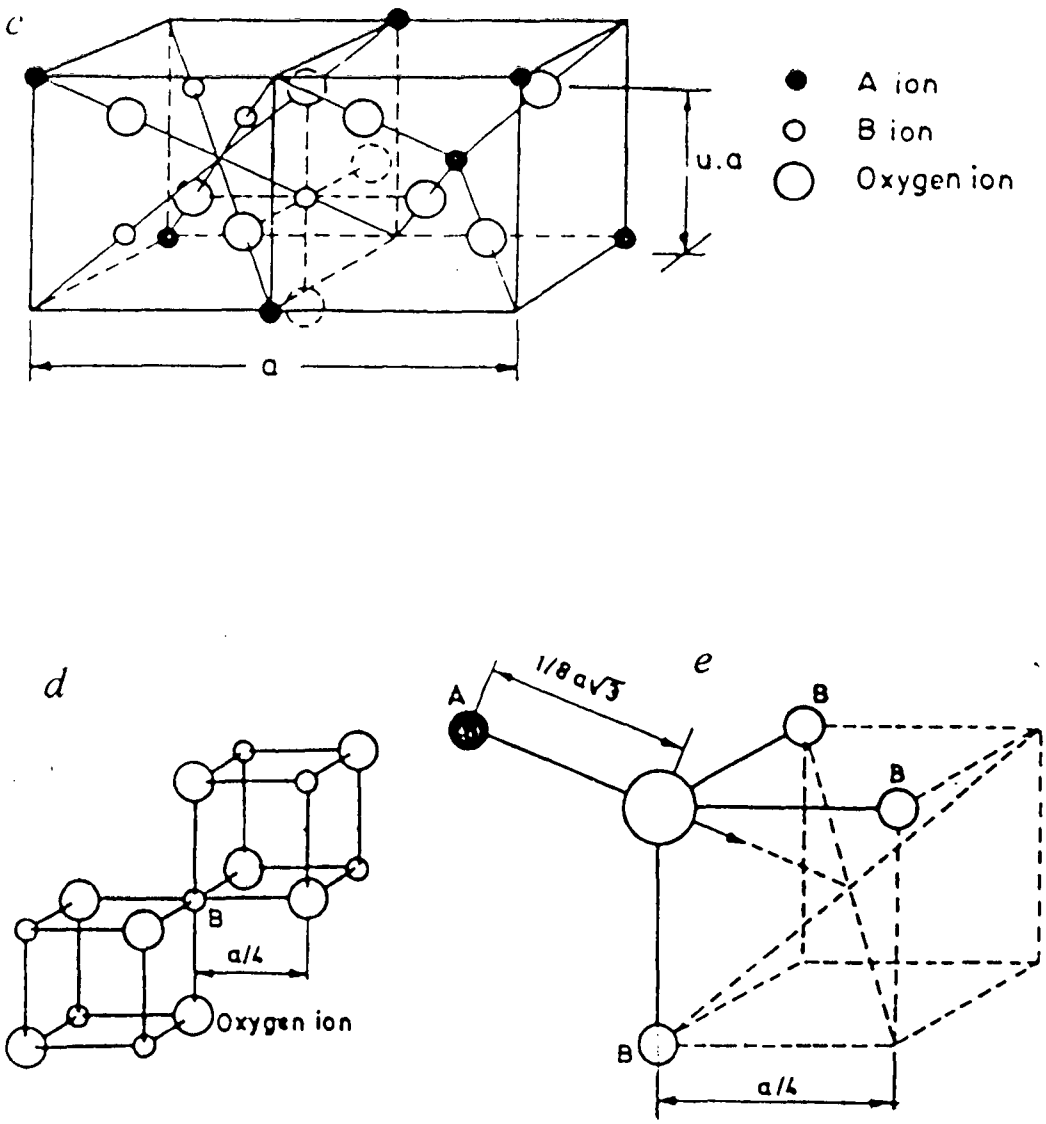

Fig. 2.1. (c) Two octants of the spinel structure. (d) The nearest neighbours of a B-cation. (e) The nearest neighbours of an oxygen ion.

in the crystal constitutes a face centred cubic (f.c.c.) lattice with edge a/2 and there are four such interpenetrating f.c.c. oxygen lattices.

The position of the metal ions are same in alternate octants. The metal ions in octants sharing oxide ion in the face are in different environment, while those sharing the oxide ion in the edge have the same environment. Hence a complete picture of arrangement of metal ions can be obtained if the position of the metal ions in adjacent octants are known fig. 2.1d. In one of the octants an occupied tetrahedral site (A-site) is located at the centre and four more on the alternate corners of the octants. In the adjacent octants the central site is not occupied but the alternate corners are filled. Thus the occupied tetrahedral sites form two interpenetrating f.c.c. lattices, having an edge 'a' which are displaced with respect to each other by a distance $1/4a\sqrt{3}$ in the direction of the body diagonal of a cube. Each tetrahedral ion is surrounded by four other tetrahedral ions which lie at the corner of a regular tetrahedron. There are twelve nearest neighbour octahedral ions for every tetrahedral ion.

There are four octahedral ions (B-site) in each octant and they lie on the body diagonals containing oxide ions but at the opposite ends. The octahedral metal ions are also at one quarter length of the body diagonals from the alternate corners like the oxide ion. Thus the octahedral metal ions form four interpenetrating f.c.c. lattices with edge 'a' which are displaced with respect to each other by a distance of $1/4a\sqrt{2}$ in the direction of the face diagonals of a cube. Each octahedral ion forms a part of two regular tetrahedra, formed from the octahedral ions, leaving the ion under

consideration as common one. There are six tetrahedral ions neighbours around each octahedral ion.

Each oxide ion is surrounded by one tetrahedral ion (A-site) and three octahedral ions (B-site) as shown in fig. 2.4e. Each A ion is shared by four such units and each B ion by six units. The angle A-O-B is about 125° and B-O-B is 90°. The B-B distance is $1/4a\sqrt{2}$ and A-A is $1/4a\sqrt{3}$.

The interstices available in the cubic close packing of oxide ion can accommodate metal ion of radius $r_{tetr} \leq 0.30$ A° in A-sites and $r_{oct} \leq 0.55$ A° in B-sites. Transition metal ions generally have radii above these values and hence to accommodate such ions, both A and B sites expand slightly. However, there is a difference in the expansion of tetrahedral A and octahedral B sites, which is reflected in the values of oxygen parameter 'u'. In an ideal spinel, both A and B sites are enlarged in the same ratio and accordingly the oxygen parameter, which is the distance between A site and oxygen site, is given by $u_{ideal} = 3/8 = 0.375$. The oxygen parameter can be obtained from neutron and x-ray diffraction data[14].

2.1.2. Cation Distribution

An interesting and important property of oxide spinels is the distribution of metal ions between tetrahedral A and octahedral B sites. In a 2:3 spinel, when all the A-sites are occupied by the divalent ions and B-sites by trivalent ions, the distribution is referred to as 'normal' and the spinel is called a normal spinel (as in fig. 2.1a and b). Alternatively, when the divalent ions, either in part or in full, occupy the B -sites, the spinel is termed as 'inverse'.

The cation distribution can be determined by x-ray diffraction, neutron diffraction and magnetic studies. The distribution of metal ions between these two sites is an important factor which determines the structural, solid state as well as the catalytic properties of many oxide spinels.

Factors affecting the cation distribution :

The factors affecting the distribution of cations among A and B sites are:

1. Sizes and valencies of A and B ions
2. Electrostatic energy considerations
3. Polarization and covalency effects and
4. Magnitude of crystal field stabilization energies.

Calculation of Born repulsion forces by Verwey and Heilman[15] for various spinels, considering the bonding to be ionic, showed a normal structure for a 2:3 spinel when 'u' was greater than 0.379 and an inverse structure when it was less than 0.379. But these authors concluded that the observed cation distributions cannot be explained on the basis of electrostatic consideration alone as $CoFe_2O_4$ crystallizes in inverse structure, while electrostatic considerations would favour a normal structure[16].

The transition metal ions have a specific preference for A or B sites. Mc.Clure[17] and Dunitz and Orgel[18] proposed a crystal field model which would explain many of the observed distributions in the spinels, their magnetic properties and the occurrence of Jahn-Teller distortions. In this model five d-orbitals are splitted up by crystal field into a triplet and

doublet. The minimum energy of these two splitted orbitals depend on the site occupancy. Electrons in lower orbitals increase the stabilization energy while those in the upper orbitals decrease the stabilization energy. The degree of stabilization or destabilization is dependent on the magnitude of crystal field (in terms of Dq). The stabilization energy for the respective co-ordinate sites could be obtained from optical spectra. The difference in the stabilization energy of an ion in octahedral and tetrahedral fields gives the site preference energy of the respective ions. Thus, d^3 system has the highest octahedral site preference energy followed by d^4, d^8, d^6, d^9, d^7, d^2, and d^1. The system with d^0, d^5, d^{10}, configuration have no site preference. Blasse[10] employed a purely molecular orbital approach, which considers the overlap of 2p electrons of oxygen with d-electrons of transition metal ion and the overlap of oxygen 2s with metal 4s and 4p electrons. On this basis, system with d^5, d^6, d^7, d^9, and d^{10} configurations favour tetrahedral co-ordination.

Both molecular orbital and crystal field approach predict many of the spinel configurations. However they do not show sufficient difference in tetrahedral stabilization energy between Fe^{3+} and Fe^{2+} or between Co^{2+} and Fe^{3+} to explain the inversion of $CoFe_2O_4$. This problem arises because these approaches consider both tetrahedral and octahedral stabilization energies to be independent of each other. Mössbauer studies of various cobalt spinels carried out by Spencer and Schröeer[19] indicate that the ion occupying the B-site influences the occupancy of A-site

Goodenough and Loeb[20] proposed a qualitative model for spinel crystal chemistry that couples the A and B-site ions. They pointed out that

each oxide ion was bonded to three B-site ions (located in X, Y, and Z directions) as shown in fig. 2.1e. Because of this, if the oxygen orbitals form covalent or partial covalent bonds with the B-site cations, their spatial configurations would make covalent bonds with one A site ion unlikely and vice-versa. There is likely to be error in the calculation of site stabilization energies if A and B ions are treated as independent, since the bonding on one sublattice influences bonding on the other. Goodenough and Loeb[20] also noted that Cr^{3+} ($3d^3$) has an affinity for partial covalent bonding in octahedral symmetry via d^2sp^3 hybrid orbitals, while $Fe^{3+}(3d^5)$ and $Zn^{2+}(3d^{10})$ have an affinity for partial covalent bonding in tetrahedral symmetry via sp^3 hybridization.

2.1.3. Ionic distribution in manganites

The investigation of the cation oxidation state and site distribution in oxide spinels is important from the view point of understanding their behaviour. The ideal spinel is cubic but when certain ions like $Mn^{3+}(d^4)$ or $Cu^{2+}(d^9)$ are present at B-site also $Ti^{3+}(d^1)$ or $Fe^{2+}(d^6)$ ions at the A-site a distortion to a less symmetrical crystal structure occurs due to Jahn-Teller effect[21]. For a co-operative bulk distortion to occur in spinel a minimum fraction of sites (A or B) must be occupied by the Jahn -Teller ions. For example Irani et al[22] have observed that a critical fraction of 0.60 of Mn^{3+} in octahedral sites is required to produce a distortion for several manganites.

The cation distribution in manganite spinels has been studied by a number of workers and there are many conflicting views on them[23-28]. The

cation distribution of the spinel $CuMn_2O_4$, first synthesised by Sinha et al[29] has been studied in detail by many workers [30-35]. Copper Manganite crystallises in a cubic structure although it has two Jahn -Teller ions namely Cu^{2+} and Mn^{3+} ions. The absence of Jahn-Teller distortion could mean that there is no appreciable concentration of Mn^{3+} ions at B-sites. The oxidation state of copper in copper manganite has been a point of contention in many investigations. Thus there are differences of opinion among different investigators regarding the valencies of the cations and their distribution in the A and B-sites in this spinel. The cation distribution in this spinel according to Sinha[36], Kshirsagar[37] and delrome[38] is normal on the other hand Asbrink[34], Ikuo Aoki[28], Zaslavaski et al[39], Sheftal and Pavlotskii[40] found the distribution to be random with varying degree of inversion. The difference in the cation distribution were explained by Millar[41] to be due to the differences in the method of preparation. According to his opinion the degree of inversion increases with sudden quenching and the spinel is normal if the hot sample is annealed gradually. The different ionic structures have been assigned for $CuMn_2O_4$ by different authors, such as

(i) $Cu^{+}Mn^{3+}Mn^{4+}O_4^{2-}$ (ii) $Cu^{2+}Mn_2^{3+}O_4^{2-}$ (iii) $Cu^{2+}Mn^{2+}Mn^{4+}O_4^{2-}$

The first valence structure is arrived at by Sinha et al[36] from the observed cubic symmetry and electrical conductivity, Miyahara[27] from the cubic symmetry, Sinha et al[36] from quantum mechanical considerations, Sabane et al[42] from electrical conductivity and thermoelectric coefficient measurements, Blasse[43] from saturation magnetisation, magnetic

susceptibility measurement and anisotropy, Goodenough[20] from chemical considerations and Jogalekar et al[44] by analogy with similar spinels.

On the other hand, second valence structure is given to this spinel by O' keefe[45] from energy considerations and value of the lattice constant, Kanamori[46] from theoretical considerations, Kshirsagar and Biswas[37] from solid state studies, Millar[41] from x-ray studies, Kshirsagar[47] from electrical conductivity and crystallographic properties and Kulkarni et al[35] from x-ray spectroscopic data. The third valence structure is pointed out by Bongers[48] alone from magnetic susceptibility measurements.

The cubic symmetry of copper manganite changes to tetragonal, when copper ion is replaced by other divalent metal ions at a critical concentration. Naik and Sinha[49] have studied the structural properties of the solid solutions $Cu_xA_{1-x}[Mn_2]O_4$ (where A = Cu^{2+}, Ni^{2+}, Co^{2+}, Zn^{2+} or Mn^{2+}) and they found at a critical concentration of the divalent ions there is a change in the symmetry. This would mean that either copper is present in +1 oxidation state or there is a compensation between the Jahn-Teller distortions produced by Cu^{2+} and Mn^{3+} ions. Hence the most probable ionic distribution of these compound is $Cu_x^{2+}Mn_{1-x}^{2+}[Cu_{1-x}^{2+}Mn_{1-x}^{4+}Mn_{2x}^{3+}]O_4^{2-}$ as suggested by Sheftal et al[50]. The rationalization of the cation distribution in spinels is thus made further difficult, because the concentration and oxidation states of the cation at A and B-sites vary with the preparation methods and the calcination temperature employed. Bhaduri et al[51] studied structural properties of some oxidic spinels $(AMn_2O_4)_{1-x}(MgAl_2O_4)_x$ where A = Mg^{2+}, Mn^{2+}, Zn^{2+}, Cd^{2+} and $0 \leq x \leq 1$. Some of these oxides have been found to be tetragonally distorted from the

cubic symmetry. This type of distortion has been usually ascribed to the covalent bonding properties or to the Jahn-Teller effect caused by the presence of certain metal ions such as Mn^{3+}, Cu^{2+} and Cr^{3+} in the Td and Oh sites. Meenakshisundarm et al[52] studied several manganites and have shown that $NiMn_2O_4$ and $CuMn_2O_4$ exists in cubic structure while $CoMn_2O_4$ and $ZnMn_2O_4$ in tetragonal form.

2.2. ELECTRICAL PROPERTIES OF SPINELS

Spinels possess interesting electrical properties ranging from insulators to metallic conductors. These properties mainly depend on (a) the nature of metal ion and (b) the cation distribution. Conductivity data of many spinels have been related to their magnetic properties, both of which in turn depends on their crystal structure[12, 53]. Goodenough[54] has extended his idea based on chemical bonding to the study of spinels. On the basis of one electron energy diagrams, Goodenough has pointed out that B-site cations are responsible for electrical conduction in spinels, by virtue of their symmetry and other considerations. As B-site ions determine electrical conduction, the B-B interactions become more important in determining the electrical conduction of spinels. Goodenough[55] has defined the critical cation-cation distance (Rc) above which the localised approach is applicable and below this critical value, collective model is applicable.

So long as the cation-cation distance for the B-site ion is greater than the critical cation separation (Rc), the electrons at the B-site ions are localised and conduction occurs by hopping motion of the charge carriers with thermally activated mobility. However, if $R < Rc$ the localised theory

should break down and the overlap of the cation-cation wave functions should be considered giving rise to metallic character. An examination of some vanadium spinels were R tends to Rc, indicated an increase in the conductivity value, supporting Goodenoughs conclusions[56-57]. Oxide spinels in general are semiconductors with conductivity values ranging from 10^{2} to 10^{-11} ohm $^{-1}$ cm $^{-1}$. The electrical conduction in the case of transition metal manganites is through the hopping mechanism proposed by Jonker and Van Santen[58]. In the manganites normally a small fraction of Mn^{4+} is also present which enables the hopping of electrons from Mn^{3+}. The overlap of orbitals with neighbouring atomic orbitals in this case occurs via the excited states. Larson et al[59] have studied the electrical conduction of the system $Ni_{1-x}Mn_{2+x}O_4$ and pointed out that electron transfer between the octahedrally located manganese ion takes place.

Rosenberg et al[60] have studied a series of solid solution systems namely $Cu_xMn_{3-x}O_4$ ($O \leq x \leq 0.2$), $Z_{1+x}Mn_{2-x}O_4$ ($0 \leq x \leq 0.2$) $Mg_xMn_{3-x}O_4$ ($0 \leq x \leq 1$) and $Zn_xMn_{3-x}O_4$ ($0 \leq x \leq 1$). The conductivity data of these systems are consistent with the hopping model involving octahedral site Mn^{3+} and Mn^{4+} ions and they found that these materials are low mobility semiconductors. The hopping involves a shift from a Jahn-Teller ion (Mn^{3+}) to non Jahn-Teller ion which would mean disturbances in the Mn-O bond during the conduction process. The reconstruction of these metal oxygen bonds would lead to a higher activation energy for conduction[61]. This is also seen by the fact that tetragonally distorted spinels have high room temperature resistivity and band gaps, compared to the cubic spinels,

because of the additional activation barriers involved in a change over from a Jahn-Teller ion to non Jahn-Teller ion during the conduction process[62].

Among the manganites, $CuMn_2O_4$ is found to posses a low activation energy for conduction. In case of $CuMn_2O_4$, the electrical conductivity data suggest that the broad 'd' band of Cu^{2+} overlaps with the narrow band of Mn^{4+} ions and the location of the fermi level is such that both Cu and Mn bands are partially filled. The conduction is then explained by hole conduction in Cu^{2+} band and due to hopping exchange between Mn^{3+} and Mn^{4+} ions[49]. Thermoelectric measurements carried out by Mulla and Darshane[63] showed p-type behaviour for $CuMnCrO_4$, $ZnMnFeO_4$ and n-type for $NiMn_2O_4$. Further from their studies on manganites they classified n and p-type conductivity based on the ratio of Mn^{3+}/Mn^{4+}. An n-type conductivity was assigned for manganites with $[Mn^{3+}] < [Mn^{4+}]$ and p-type for $[Mn^{3+}] > [Mn^{4+}]$

Conductivity measurement studies by Meenakshisundaram et al[64] on series of manganites indicated that $ZnMn_2O_4$ is p-type and $CoMn_2O_4$ n-type. Studies by Laberty et al[65] on $NiMn_2O_4$ suggested an ionic arrangement for inverse spinel $Mn^{2+}[Ni_x^{2+}Mn_x^{4+}Mn_{2-2x}^{3+}]O_4^{2-}$, according to them normal manganite spinels are all insulators. The good electrical conductivity of nickel manganite is attributed to octahedrally located Mn^{3+}/Mn^{4+} redox couples induced by Oh Ni^{2+}. However, for x = 1 with ionic arrangement $M^{2+}[Ni^{2+}Mn^{4+}]O_4^{2-}$ does not account for good conductivity of this oxide, from this it is deduced that a part of Ni^{2+} cation must be in tetrahedral site.

2.3. MAGNETIC PROPERTIES OF SPINELS

Spinels exhibit interesting variation in their magnetic properties due to ordering and orientation of spins in the lattices. This kind of ordering of spin results in ferromagnetic, antiferromagnetic and ferrimagnetic spinels.

Ferromagnetism arises out of the parallel alignment of magnetic moments of the ions and leads to higher magnetic moments than ferri and anti-ferromagnetic materials. Antiferromagnetism is due to the opposite alignment of magnetic moments and has zero resultant magnetic moment. Ferrimagnetic materials have resultant uncompensated magnetic moment due to the difference in the magnetic moments oriented in either ways.

The magnetic interactions in spinels are due to the metal ions in octahedral and tetrahedral sites interacting among themselves and with each other directly or through the intervening oxide ions. The interactions through the oxide ions are termed as superexchange and those without the oxide ion are termed as direct exchange. There are three possible modes of interactions between the metal ions in tetrahedral and octahedral sites in spinel type of oxides namely, (i) A-A interactions (ii) B-B interactions (iii) A-B interactions. The A-A and B-B interactions can be a direct exchange or a super exchange through the oxide ion.

The interaction energy between two metal ions depend on (i) The distance between these ions and oxide ion through which the interaction occurs and (ii) The angle M^{I} -----O-----M^{II} (M = Metal ion). The exchange energy decreases very rapidly with increase in the distance and will be greatest if the angle is 180°. Among the different modes of interactions, the

A-B interaction is fairly high because of smaller distances and large angle between them.

The A-B interactions are predominant in the case of spinels and in particular ferrites and hence the A and B site ions will have opposite spins resulting in two oppositely magnetised sublattices A and B. The magnetic moment will be equal to the difference between those of A and B-site ions i.e. $M_S = M_B - M_A$, where M_S is the resultant magnetic moment and M_A and M_B are magnetic moments of sublattices A and B respectively. M_B in general will be greater than M_A.

The magnetic properties of spinel type manganite oxides are dependent on the cation distribution and in many cases, the magnetic susceptibility measurement throw light on the cation distribution of spinels. The absence of distortion, inspite of the presence of two Jahn-Teller ions, namely Cu^{2+} and Mn^{3+} ions has provoked many to investigate the magnetic properties of copper manganite. Copper manganite can be expected to be an antiferromagnetic material if the cation distribution were to be $Cu^{2+}[Mn^{3+}]_2O_4^{2-}$. The valence state of copper and manganese are a point of contention in many investigations. The magnetic susceptibility measurements indicate that it exhibits a ferrimagnetic behaviour due to the B-B interactions between the Mn^{3+}-Mn^{4+} ion pairs[66]. This is further confirmed from the studies on $Cu_xCd_{1-x}Mn_2O_4$, where the magnetic susceptibility decreases with increase in Cd concentration[23]. Studies on chromium substituted $CuMn_2O_4$ spinel indicate that exchange interactions of $CuMn_2O_4$ become weak on addition of chromium into the lattice. The Mn^{4+}-Mn^{4+} interactions will lead to ferromagnetic behaviour. However

when Cr^{3+} is introduced into the lattice, although these two ions are isoelectronic, the higher radius of Cr^{3+} will lead to ferromagnetic behaviour due to the direct B-B interactions[67].

Bhandage and Keer[68] have studied the magnetic behaviour of Mn_3O_4-$NiMn_2O_4$ systems. Mn_3O_4 is paramagnetic and good example of Neels model, while an introduction of Ni into the lattice leads to a complex behaviour. The short range antiferromagnetic A-B interactions between A-sited Mn^{2+} and B-sited Mn^{3+} ions in Mn_3O_4 changes over to complex A-B and B-B interactions in the solid solutions.

Thus in the case of transition metal manganites the B-B interactions and A-B interactions predominate depending on the size and electronic configurations of the A-site and B-site ions. The compounds will exhibit either antiferromagnetic, ferrimagnetic or paramagnetic behaviour depending on the relative strength of these interactions.

2.4. STUDIES ON CARBON MONOXIDE OXIDATION BY OXYGEN

Every heterogeneous catalytic process involves the following steps

1. Diffusion of the reactants from the bulk to the surface of the catalyst
2. Adsorption of the reactants on the catalysts surface
3. Chemical reaction of the adsorbed species on the catalyst surface
4. Desorption of the products from the surface and
5. Diffusion of the products into the bulk.

Depending on the slowest step, the catalytic process can be classified as either diffusion controlled or kinetically controlled. An understanding of

the kinetically controlled catalytic process requires the study of nature of adsorption as well as the reaction mechanism.

catalytic oxidation occurring on the surface of metal oxides has been classified by Voorhoeve et al[69] as intrafacial and suprafacial. Suprafacial is the one involving a relatively less active catalyst surface. The role of the transition metal ion is to provide proper atomic orbitals for the adsorption of the reactant molecules. Even there the surface properties affect the nature and mode of adsorption of the adsorbate and hence indirectly affect the catalytic process. In the intrafacial process the catalyst undergoes a redox type reaction with the reactant (i.e. its surface is alternatively oxidised and reduced during the reaction).

The oxidation of CO can proceed in general in two ways depending on the nature of the surface oxygen that is involved in the reaction.

(a) Reaction with oxygen in the adsorbed state.

This can occur either through a Langmuir-Hinshelwoood or Eley-Rideal type interaction depending on whether CO reacts from an adsorbed state or from gas phase with adsorbed oxygen. The interaction between chemisorbed reactants is referred as Langmuir-Hinshelwood mechanism and other as Eley-Rideal mechanism. The reaction between adsorbed CO and gas phase O_2 is known to be uncommon.

(b) Reaction involving lattice oxygen :

In this mechanism, the adsorbed CO reacts readily with lattice oxygen to form CO_2 and lattice oxygen is then replenished by gas phase oxygen.

2.4.1. Metal and metal oxide surfaces

A review article by savchenko[70] presents the current status of oxidation of CO on metals. Rajadurai and Carberry[71] have demonstrated the structure sensitivity of Pt-catalysts for CO oxidation. Jin et al[72] highlighted the role of lattice oxygen in the case of Pt/CeO_2 catalysts for the oxidation of CO. Kim et al[73] studied the oxidation of CO on CdO/La_2O_3 system and reported that CO essentially chemisorbs on the lattice oxygen of Cd-doped La_2O_3 while O_2 on the lattice oxygen vacancies induced by Cd doping. Carbon monoxide oxidation on Pd/SnO_2 surface was carried out by Bond et al[74] and it was reported that the activity of this catalyst is more than that of SnO_2 or of $PdSiO_2$. Gagarin et al[75] made an attempt to project the role of electronic factor of the catalysts on the catalytic oxidation of CO. Indovina et al[76] studied the CO oxidation on CoO/MgO and observed that the d-electron configuration of Co^{2+} is of primary importance and the nature of matrix and the extent of dispersion are less relevant.

Kobayashi et al[77] by using transient response method suggested a mechanism involving interaction of gaseous CO with the surface anions or neutral oxygen for the formation of CO_2 on ZnO surface. Laine et al[78] studied chromium promoted Raney copper catalyst and observed that presence of chromium inhibited the formation of CuO but not Cu_2O and the activity towards CO oxidation reduced with increase in chromium content.

Jen and Anderson[79] concluded that CO reacts readily with oxygen at the surface to form CO_2 which can immediately bind to O^{2-} to form surface carbonate. Reaction with isolated O^- has a higher barrier on account of O^----CO bond formation with promotion of electron to surface conduction

band, in this case CO_2 gets dissociated from the surface, stabilizing the promoted electron.

Huang and Yu[80] observed a large variation in the surface properties of a commercial copper oxide/γ-alumina catalyst induced by calcination in the temperature range of 723 - 1323 K both in oxidising or reducing atmosphere. Decrease in CO oxidation beyond 1173 K was attributed to the calcination temperature in the region of 1273 K which could be detrimental to the catalyst. Choi and Vannice[81] reported that $PdCl_2$ was much more active than $CuCl_2$ and the addition of water vapour to the feed generally enhances the activity of $PdCl_2$ catalyst but not the $CuCl_2$ catalyst. They proposed a reaction model that involves a water as a reactant with the PdClCO (chlorocarbonyl species as identified by in situ IR spectra) when water vapour is present and in its absence, molecular oxygen appears to interact with PdClCO to produce CO_2. It is further noticed[82] that specific activities for CO oxidation by molecular oxygen over unreduced $PdCl_2$-$CuCl_2$ catalyst are higher than on the reduced bimetallic catalyst. The principle role of copper is the re-oxidation of Pd (0) when water vapour is present (leading to higher activity of 1-3 order) as in the Wacker process, where as it was appeared to be involved as reactive intermediate also containing Pd, CO and O_2 in the absence of water vapour. Kapteijn et al[83] were successful in finding out alternative to noble metal catalyst for purification of auto-exhaust, supported Cu/Cr oxide catalyst were found to be most active for CO oxidation and NO-reduction by CO, further the order of catalytic activity for CO oxidation on carbon supported catalysts was observed in the temperature range of 450 - 600 K as Co > Cu > Ni > Mn > Fe > Cr. Hertz et al[84] in

their study of CO oxidation at low temperature over composite noble metal/reducible-oxide catalyst summarised that high activity for CO oxidation can be obtained over a composite material composed of highly interspersed mixture of one type of site, α, that adsorbs CO and O_2 and another type of site, β, that adsorbs oxygen without significant CO inhibition. As long as oxygen can adsorb on a pair of β-sites, this mode of oxygen adsorption will predominate at low temperatures, where the CO desorption probability is low over other possible modes of oxygen adsorption. Szanyi and Goodman[85] summarises that the presence of certain level of surface oxygen is advantageous during CO oxidation on a Cu (100) catalyst, however, under stoichiometric conditions an oxide layer formed significantly reduces the catalytic activity compared to metallic copper.

Jernigan and Somorjai[86] concluded that mechanism for CO oxidation over the three copper catalysts (copper-0, copper-I oxide, and copper-II oxide) was affected by sub-surface oxygen and oxide formation. The stability of a given oxidation state of copper under reaction conditions was found to be a function of oxidising power of the CO/O_2 partial pressure ratio. Metallic copper, Cu_2O and CuO were stable at 97/3, 90/10 and 66/33 ratios respectively. The rate of reaction at 573 K decreased with increasing copper oxidation state ($Cu > Cu_2O > CuO$) and the activation energy increased with increasing copper oxidation state ($Cu - 9 < Cu_2O - 14 < CuO - 17$ kcal/mol). According to Boccuzzi and Chionno[87], Au/ZnO catalyst prepared by Co-precipitation, expose gold sites, which are able to absorb both oxygen atom and carbon monoxide at the same time and thus easily oxidising CO to CO_2.

Mergler[88] was successful in synthesising a catalyst Pt/CoO_x / SiO_2 which could bring about CO conversion at room temperature. In his opinion during CO oxidation by oxygen, O - vacancies on the CoO_x play an important role as dissociation centres for oxygen. According to mechanism proposed by Hoflund[89] for low temperature CO oxidation on Pt/SnO_x surface during reaction, CO adsorbs on the platinum and associates with a neighbouring hydroxyl group (on a Pt or Sn atom) and a neighbouring O^- ion on Sn to form a surface carbonate, further CO can also adsorb on a Pt by a neighbouring OH^- and form a formate species.

2.4.2. Complex Oxides

Parravano[90] first reported oxidation of CO on strontium substituted manganites. However the work with these catalysts really took off after Meadowcraft[91] reported that $La_{0.8}Sr_{0.2}CoO_3$ can match platinum as oxygen electrode. This prompted Libby[1] to try these oxides as potential auto-exhaust catalysts. Since then elaborate tests were carried out by Voorhoeve and others with transition metal perovskite oxides on automobile emission.

A recent article by Tascon et al[92] summarises the CO oxidation on $LaMO_3$ surface. Rao and Chakrabarty[93] studied the oxidation on $Ln_{1-x}M_xCoO_3$ catalysts and showed that the catalytic activity increases with oxygen deficiency in cobaltites. Vishwanathan and George[94] reported the catalytic oxidation on $LnCoO_3$ and the catalytic activity has been correlated with the magnetic moment and oxygen non-stoichiometry. Gallagher[95]

reported the high activity of copper substituted lanthanum manganites and strong SO_2 poisoning for CO oxidation. Omprakash et al[96] have investigated on $LaCoO_3$ surface and related the activity of the catalysts to the spin and valence of cobalt. Gunasekaran et al[97] investigated on several cuprates and nickelates and reported that the oxidation takesplace through the interaction between the adsorbed species. Korf et al[98] studied the oxidation of CO on several pyrochlores and correlated the activity to the solid state aspects, essentially the electronic properties of the solid. CO oxidation over cobaltites of Lanthanides were carried out by Chakrabarty and Rao[99] to study the effect of A-site substitution in $Nd_{1-x}Ba_xCoO_3$ and $LnCoO_3$ (Ln = La, Sm, Nd, Dy) they observed that compound with cubic structure show maximum activity which decreases with deviation from cubic structure. Salker et al[100] studied the kinetics of redox reactions between NO and CO over perovskite catalysts $LaMnO_3$ and $LaCoO_3$. They were of the opinion that the rate controlling step in the catalytic reduction of NO by CO is presumably the active site reduction process. Chan et al[101] studied the influence of either A and B-site substitution in perovskite type mixed oxides on the catalytic oxidation of carbon monoxide. From the different systems that were investigated, cobaltates were found be more active than the manganates. They concluded that partial substitution of lanthanum manganates or cobaltates with strontium or copper leads to an increased activity for CO oxidation, which was attributed to an increase in

oxygen mobility within the lattice of perovskite, thus explaining the lattice oxygen participation in the reaction even under stoichiometric conditions.

2.4.3. Molecular orbital approach for carbonyl formation

In simple or mixed transition metal oxides, the nature of the carbon monoxide-catalyst bond is considered to be essentially important in understanding the metal carbonyl formation in the mechanistic studies of CO oxidation.

Studies have shown that CO molecule is bonded in carbonyl either linearly with one transition metal atom or forming a bridge between two, or less frequently between three metal atoms as shown by the following scheme.

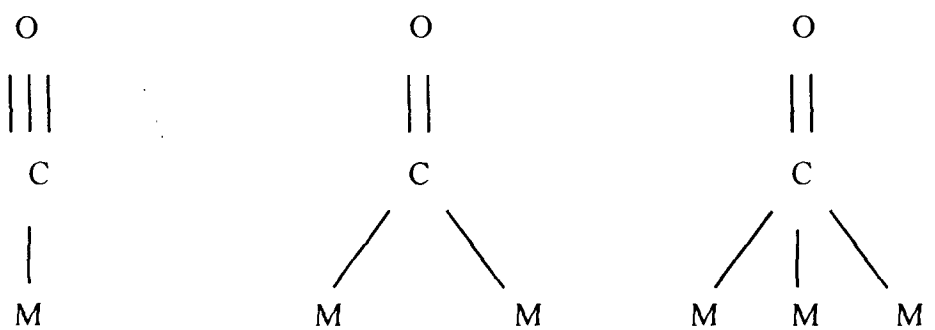

Blyholder[102] demonstrated that the frequency based criterion is incapable of furnishing a sound basis for calling the structure either linear or bridge. Blyholder gave a qualitative description of the chemical bonding in the adsorbed CO from the stand point of the theory of molecular orbitals.

His calculations together with the later findings of the other authors[103-105] explain some particular features of the IR spectra of adsorbed CO. The diagrammatic representation of molecular orbitals of CO and of the adsorptive complex of CO with a transition metal is being reproduced[106] in fig. 2.2. along with the scheme of the overlapping molecular orbitals.

When the CO molecule forms a complex with a metallic ion, the antibonding 5σ orbital produced by the $2P_z$ orbitals of carbon overlaps with the unoccupied d_{z^2} orbital of metal, thus producing the donor-acceptor bond between CO and metal and giving rise to a $5\Sigma^+$ orbital. The back donation of the electron from the occupied d-orbital of metal (d_{yz},d_{xz}) to the unoccupied 2Π orbital of CO produces what is called a dative bond.

In this scheme of molecular orbitals, the formation of donor acceptor bond M←C results in an increase in the frequency of the CO vibration forming a strong bond with the surface. On the other hand, the creation of the dative bond M→C lowers the frequency of CO-vibration and forms a weak bond with the surface. Thus according to Little[107] the shift of electron density to the 2Π antibonding orbitals weakens the C---O bond in carbon monoxide molecule decreasing its stretching frequency from 2143 cm^{-1} in free CO molecule to 2100 - 2000 cm^{-1} for neutral unsubstituted linearly bonded one. The decrease in bond order and bond strength of CO also results in the decreased stretching frequency of CO molecule, which is in the range 1750 - 1850 cm^{-1} for doubly co-ordinated CO molecules

The strength of the donor acceptor bonding M---CO in the first transition series increases steadily from Ca to Ni and decreases with copper. The strength of the back donation bond increases from Ca to Ti, further

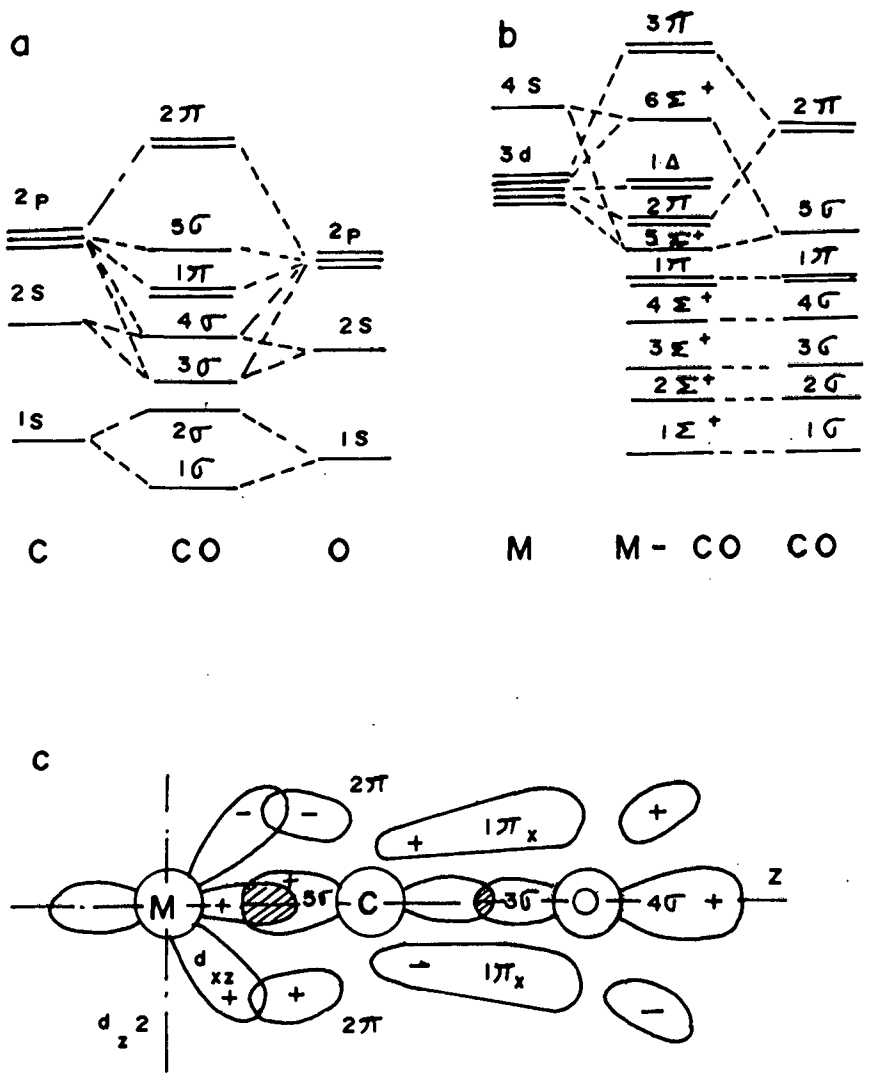

Fig. 2.2. (a) Molecular orbitals of carbon monoxide (b) Molecular orbitals of carbonyl complex (c) Scheme of overlapping of molecular orbitals in the carbonyl complex.

goes down to Ni, and up a little with Cu. The low frequency bands may be explained by multi site adsorption of CO[104]

Semi-empirical calculations of Ni---CO complexes performed by Politzer and Kaster[105] using the extended Hückel method indicate that both the σ-complexing and the charge transfer are responsible for the high frequency bands. The calculations of the electron density in the Ni---C bond indicates the transfer of a large amount of charge from CO to Ni (+ 0.02 for Ni^{+}---CO, + 0.33 for Ni^{2+}---CO, and + 0.59 for Ni^{3+}---CO) which leads to strengthening of bond. In the complex with neutral nickel Ni^{0} ---CO the charge is transferred in opposite direction and the bond is weakened.

According to the calculations using the extended Hückel technique[103], in the adsorptive complexes of CO the electron is transferred from CO to metal on the oxides of trivalent metals (V_2O_3, Cr_2O_3, Fe_2O_3, Co_2O_3) and from metal to CO on the oxides of divalent metals (MnO, FeO, CoO, NiO).

Numerous experiments with the adsorption of CO on the transition metal oxides[108-115] confirm in general the scheme discussed above. A kinetic study by Kobayashi et al[77] of CO oxidation to CO_2 over a partially reduced ZnO showed that there are two reaction paths (I and II). For path-I, the proposed model is the surface reaction of gaseous CO with O^{-}, followed by rapid adsorption of CO_2 formed , path-II is controlled by both the surface reaction of gaseous CO with neutral atomic oxygen species and the desorption of CO_2 formed which is summarised as follows

Path-I

$$CO + O^-_{(ads)} \longrightarrow CO_{2(ads)} + e^- \xrightarrow{fast} CO_{2(g)} + e^-$$

Path-II

$$CO + O_{(ads)} \longrightarrow CO_{2(ads)} \xrightarrow{slow} CO_{2(g)}$$

Jen and Anderson[79] supported the above reaction mechanism. According to them if there were initially an oxygen vacancy site for the partially reduced defect surface, then O_2 could bind to the vacancy and dissociate, placing O^- at the site and O some where on the surface. O^- formed from the adsorption of O_2 forms the superoxide anion O_2^- which dissociates reacts with gas phase CO to form CO_2 plus an electron promoted to the surface conduction band. Electrons are oxidised by O_2 to reform O^- which reacts with CO. CO_2 can rebond to the surface, either on O^{2-} to form the surface co-ordinated monodented CO_3^{2-} or bidentate CO_3^{2-}. CO_2 can also bind strongly to three co-ordinate surface Zn^+ to form co-ordinated CO_2^-. Surface O atoms formed by dissociation of O^{2-} react much more readily with CO, forming CO_2, which is likely to form CO_3^{2-} immediately since there is no surface state electron stabilization accompanying dissociation from the surface. The same energetics were obtained when $2O^-$ are involved in place of O, a possible alternative to the O mechanism . On the defect surface CO_2 can react with O^{2-} to form CO_3^{2-} which is likely to have a bidentate co-ordination, if two Zn^{2+} are available or a monodentate co-ordination if only one is available.

Bheema Raju et al[116] studied CO oxidation on doped NiO catalyst where in electron is transferred from CO to catalyst during its adsorption

which is a slow process and oxygen adsorption is a fast process. They suggested the following mechanism for CO oxidation.

$$CO + h^+ \longrightarrow CO^+_{(ads)} \quad \text{(slow)}$$

$$1/2\ O_2 \longrightarrow O^-_{(ads)} + h^+ \quad \text{(fast)}$$

$$CO^+_{(ads)} + O^-_{(ads)} \longrightarrow CO_2 \quad \text{(fast)}$$

Laser induced desorption of CO_2 by Moller et al[117] from clean and submonolayer-copper covered ZnO surface, it was observed that CO molecules adsorb preferably on Zn^{2+} ions which interacts with lattice oxygen in the ZnO surface layer yielding chemisorbed CO_2^-, which then forms a surface $ZnCO_2^-$ complex. This complex is electrostatically stabilised in the vicinity of a charged oxide vacancy. Further studies[118] of temperature programmed desorption (TPD) on CO from clean and atomic layer Cu covered ZnO surface they came to conclusion that submonolayer amounts of copper on the surface enhance the ability of ZnO to adsorb CO drastically. Recent work by Moller et al[119] from desorption experiments remarked that CO_2 molecular desorption occurs from ZnO areas of the surface and CO molecular desorption from the Cu (or Cu_xO) areas of the surface. Moller et al[119] supported the views of Fu and Somorjai[120] that CO adsorbs more readily on to the copper surface on account of its strong CO sticking probability to the copper surface, which migrate along the surface to open ZnO areas creating CO_2^- complexes on the ZnO surface.

2.4.4. Mechanism of the oxidation of carbon monoxide

The ease of oxidation of CO by different types of materials like noble metal, oxides etc. led to an extensive study of the mechanism of CO oxidation. The rate of the reaction has been observed to vary with catalyst material, temperature, partial pressure of the reactant etc., the reaction has been found to be suprafacial on noble metals and some oxides, where as on some other oxides, it was observed to be intrafacial.

Intrafacial process :

Roginskii[121], one of the earliest worker to study CO oxidation, proposed a mechanism in which he suggested the oxide catalyst as providing oxygen for the reaction followed by a subsequent regeneration of the surface using gas phase oxygen. Around the same period, garner[122] from the experimental thermochemical data, suggested the formation of surface carbonate ions through the lattice oxygen participation. He observed that there was little oxygen adsorption on a bare Mn_2O_3 or Mn_2O_3-Cr_2O_3 surface, but was considerable (half of the adsorbed CO) on a CO preadsorbed surface. Further it was noticed that, the heat of adsorption of CO_2 on Mn_2O_3 is almost equal to the heat of decomposition of a manganese carbonate and this suggests that the common adsorbed species must be a carbonate ion. The process was outlined as follows :

$$M^{2+}\ O^{2-}\ M^{2+} \xrightarrow{CO} M^{2+}\ CO_3^{2-}\ M^{2+} \xrightarrow{1/2O2} M^{2+}\ CO_3^{2-}\ M^{2+}$$

$$O^{2-}\ M^{2+}\ O^{2-} \qquad O^{2-}\ M^{2+}\ 2e^- \qquad O^{2-}\ M^{2+}\ O^{2-}$$

CO interacts with the surface oxide ions forming a carbonate and an anion vacancy which is subsequently filled up by the gas phase oxygen. This explains the increased adsorption of oxygen on a CO pre-adsorbed surface. A simple experimental evidence was given by the x-ray diffraction analysis of CuO on alumina catalysts. Pierron et al[123] noticed reduced Cu_2O and Cu phases when catalyst was activated with CO and hence suggested an alternate redox process on the CuO above 433 K.

Conclusive evidence of carbonate formation has been provided by Winter[124] from the isotopic exchange studies using ^{18}O on Cu_2O and V_2O_5. He observed that both CO and CO_2 readily exchanged oxygen with the whole of the out-gassed oxide surface. Hirota et al[125] found that the concentration of ^{18}O in CO_2 depends on the amount of ^{18}O on the V_2O_5 surface in the temperature region 620 - 685 K from these considerations, the mechanism of CO oxidation with lattice oxygen participation was given by Hughes and Hill[126] as follows

$$M = O + CO \longrightarrow (M = O)CO$$

$$(M = O)CO \longrightarrow M: + CO_2$$

$$M: + 1/2O_2 \longrightarrow M = O$$

From energy considerations, this type of reaction will necessarily be a high temperature process (573 - 873 K). Marshneva et al[127] studied the CO oxidation on V_2O_5 in temperature region 573 - 773 K and pressure range of 1 - 400 torr. He observed that the lattice oxygen participation gains importance above 723 K, so that above 863 K the reaction proceeds through

only lattice oxygen participation. Below 723 K the reaction between the adsorbed species gains importance thus gradually reducing the lattice oxygen participation. Similar observations have been made for TiO_2 and NiO catalysts also .

Suprafacial process :

The intrafacial process expects the oxidation to be a high temperature process, but the reaction has been observed even at low temperatures (253 K) as on hopcalite catalyst containing a mixture of oxides of manganese and copper. This prompted Stone[128] to suggest that a mechanism other than the surface carbonate species must be involved. The lattice oxygen participation is not an essential requirement is further proved[124] by the negative ^{18}O isotopic exchange studies on NiO.

The CO_2 adsorption takesplace only on an oxygen preadsorbed surface and the amount of adsorption was largest for a mixture of $O_2 : 2CO_2$. Stone and his coworkers[128] measured the heat of adsorption of CO, O_2 and CO_2 on the bare as well as on preadsorbed surfaces of Cu_2O, NiO and CoO. They observed that the heat of adsorption of CO and O_2 on the oxygen and carbon monoxide pre-adsorbed surfaces respectively matches well with that of a theoretical surface CO_3 complex species. Further, computations from the heat measurements data by different methods resulted[128] in almost similar heat of formation of surface CO_3 complex, from gaseous CO and oxygen

$$CO_{(g)} + O_{2(g)} \longrightarrow CO_{3(ads)}$$

Unlike CO adsorption the surface shows saturation after CO_2 adsorption and so it can be inferred that CO interacts with the surface adsorbed oxygen to form CO_3 complex as shown below

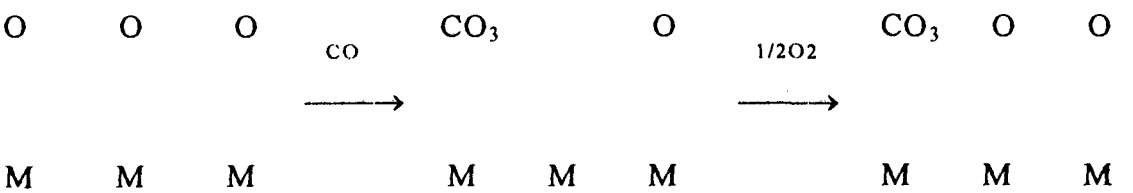

Comprehensive study of Cu_2O were undertaken by Garner et al[129, 130] the observations led to the conclusion that a CO_3 complex has been forming at the oxygenated surface according to these scheme

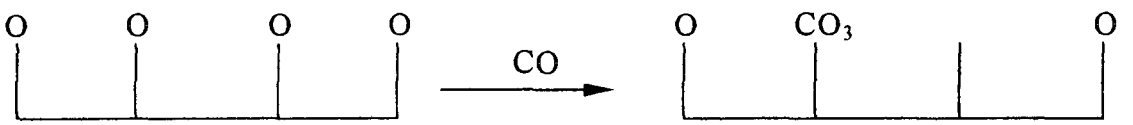

Similar observations were also made on nickel[131] and cobalt oxide[132]. The IR spectra of adsorbed CO on nickel carried out by Blyholder[133] provided confirmatory evidence for the complex formation.

2.4.5 Formation of carbon dioxide

Heat measurements by Rudham and Stone[132] on the incremental CO adsorption on CoO revealed finally the formation of CO_2 from the CO_3 complex. On admission of CO on an oxygen pre-adsorbed CoO, the heat of adsorption showed a gradual fall initially without any CO_2 formation. After

the introduction of few more pulses, the heat of adsorption dropped by 20 kcal/mole with a concomitant formation of CO_2, whose concentration was greater than that of added CO, this indicates the interaction of admitted CO with the CO_3 complex .

This shows that on admission CO first gets adsorbed $CO_{(ads)}$, which then at small concentration reacts with the adsorbed oxygen to form CO_3 complex, while on further addition reacts with the adsorbed complex to yield CO_2. Overall process thus can be written as

(a) $O_{2(g)} = 2O_{(ads)}$ + 55 Kcal

(b) $CO_{(g)} = CO_{(ads)}$ + 20 Kcal

(c) $CO_{(ads)} + 2O_{(ads)} = CO_{3(ads)}$ + 40 Kcal

(d) $CO_{(ads)} + CO_{3(ads)} = 2CO_{2(g)}$ + 19 Kcal

This mechanism was justified by the similarity between the fall of heat of adsorption of CO (20 kcal/mole) and the difference in the heat of adsorption (21 kcal/mole) when reaction (d) takes over from (c). This kind of reaction between the adsorbed species commonly referred to as Langmuir-Hinshelwood mechanism has been observed on CoO and Cu_2O.

An alternative Eley -Rideal mechanism also seems to be possible. The heat of formation of the CO_3 complex from the gaseous oxygen and adsorbed CO is larger (131 kcal/mole) for NiO; as compared to CoO and Cu_2O (111 and 104 kcal /mole respectively). This necessiates the reaction (d) to be an endothermic on NiO unlike the exothermic one on Cu_2O and

CoO and hence is less favourable. So the observed small activity was presumed to be due to the reaction between the CO_3 complex and gaseous CO. Mechanism of CO oxidation on copper chromite has been studied by Hertal and Ferrauto[134] and identified two distinct active sites. A carbonyl has been found to be active at temperature in the vicinity of 333 - 353 K while a less active carbonate species react with O_2 to produce CO_2 at approximately 453 - 473 K. However according to Morgan and Ferrauto[135] active site concentration is determined from the actual catalytic reaction allowing one to differentiate active site from the adsorption sites.

2.5. STUDIES ON SPINELS

Ternary oxides and in particular, the oxides with spinel structure have been reported to be active for oxidation reactions including oxidative dehydrogenation of hydrocarbons. The oxidation could be of two types, namely partial oxidation or mild oxidation in which various partially oxygenated compounds or unsaturated hydrocarbons are obtained and deep oxidation in which products are water and carbon dioxide.

2.5.1 Catalytic activity of oxide spinels

The oxidation characteristics of spinels depend on the bond strength of the surface oxygen. The partial oxidation is favoured by weakly bound labile oxygen through intrafacial catalysis while complete oxidation is promoted by oxides with strongly bound oxygen on the surface through

suprafacial catalysis. The state and strength of the surface oxygen could be determined by oxygen isotope exchange studies. An investigation of the oxygen exchange on 2:3 spinels indicates that the mobility of oxygen and various kinds of exchange do not vary much with change in divalent metal ions. This may be due to the fact that divalent metal ions have the same charge and close values of radii and hence divalent metal ions contribute more or less equal to the stabilization of the cubic packing of oxide ions. However, the energy of the sublattice of the oxide ions in a spinel varies with the trivalent ions due to higher charge difference among them.

The catalytic activity of a spinel, according to Boreskov et al[136] depends mostly on the nature of trivalent ions. They have studied the rate of oxygen exchange reaction on ZnB_2O_4 (B = Cr^{3+} to Co^{3+}) and found it to increase with increase in atomic number and d-electron of trivalent cation. The variation in crystal field stabilization energy (CFSE) and first ionisation potential of B-cations in AB_2O_4 is similar to the variation of Ea for oxygen exchange. The Ea for propylene oxidation on Ni, Co and Mn chromites has been found to be nearly the same, indicating that trivalent chromium ions are responsible for oxidation[137]. However studies on the oxidation of CO on transition metal ferrites[138] and chromites[139] have shown that divalent ions are responsible for the catalytic activity. Boreskov et al[140] found that the reactivity of the surface oxygen in the spinel varies

little when the divalent A-cation is varied and is principally governed by the nature of the trivalent B-cation.

An important aspect of oxide spinels as catalysts for oxidation reaction is their structural stability even under reducing atmosphere which makes them more suitable than binary oxides. Hightower[141] has studied the oxidative dehydrogenation of butene on ferrites using electrical conductivity measurements. The study reveals that a redox mechanism is found to operate with Fe^{3+}/Fe^{2+} as active sites. The electrical conductivity measurements indicate that the catalyst is reduced by hydrocarbons in the absence of oxygen and the re-oxidation by gas phase oxygen is rapid. They have proposed a reaction mechanism involving adsorption of hydrocarbon on the cation and anion vacancies and the C---H cleavage at the rate determining step.

Oxide spinel provide scope for determining the role of site symmetry on the activity. The distribution of cations between the two sites is a unique feature of the spinels and thus provide scope to study the influence of the degree of co-ordination and energetic state of the metal ion on the catalytic activity. Thus the catalytic decomposition of H_2O_2 on $Co_xFe_{3-x}O_4$ indicates that inverse spinels are less active than normal spinels[142]. It has been found that Fe^{3+}/Fe^{2+} couples formed by electron exchange process, are the active centres for decomposition which explains the observed activity pattern. However, in oxidation of CO over transition metal ferrites, the inverse spinels are found to be more active than normal spinels, thus the site symmetry plays a decisive role in the catalytic activity of spinel oxides. The oxide spinels posses interesting solid state properties arising out of

different exchange forces involved between A and B-site ions. These solid state properties bears a direct relation to catalytic activity indicating that such exchange forces are also responsible for the variation in catalytic activity. This aspect is evidenced by the study of the variation of catalytic activity of Ni-Zn ferrites (with composition 0 - 1) and it was found that the variation in catalytic activity and the variation of specific saturation magnetisation with nickel content run parallel and both have maxima at $Ni_{0.5}Zn_{0.5}Fe_2O_4$ composition[138]. Tyurkin et al[143] synthesised complex oxides with structure of 2:3 spinel type based on Co, Ni, Mn, Cr, Al by a self propagating high temperature synthesis (SHS) method. According to them the samples synthesised in the SHS regime are more active than the samples produced by reaction sintering. They are of opinion that lower combustion temperature in the SHS regime results in more defective structure of the synthesised spinels which as a consequence posses higher catalytic activity .

2.5.2 Carbon monoxide oxidation on spinels

In the following studies an attempt has been made to review the utilization of spinels as catalysts.

One of the most effective non precious metal catalysts for CO oxidation was found[144, 145] to be the copper chromium combination. Hertal and ferrauto[134] observed that above 353 K carbonyl intermediate is formed and surface carbonate species are formed above 473 K on $CuCr_2O_4$ and concluded that lattice oxygen participates in the oxidation reaction. Electrical conductivity studies carried on same catalyst by Hertal and

Kingsbury[146] indicated slight reduction of the surface during reaction. Pitchai and Srinivasan[147] found that copper and nickel chromites are highly active among MCr_2O_4 (M = Mg, Cu, Co, or , Ni) which was attributed to the Jahn-Teller distortion associated with these ions. Yu Yao[148] observed that Co_3O_4 readily oxidises CO with the participation of the lattice oxygen, where as introduction of chromium (on B-site) reduces the participation of lattice oxygen and the reaction proceeds via adsorbed oxygen. Severino and Laine[149] studied CO oxidation over copper-chromium-based catalysts, their results led to the postulation of a mechanism of electron transfer between copper and chromium in which copper was reported to be the main active species. Further it was noticed that pre-reduction in CO makes $CuCr_2O_4$ more active than CuO and vice versa when pre-treating in oxidising condition is carried out.

Krishnamurthy et al[150] studied CO oxidation on spinel type ferrites, they found that oxidation of CO on spinel type ferrites obey a first order rate law with reaction rate independent of the partial pressure of either O_2 or CO_2 and showed that the adsorption of CO is the rate controlling step of the overall process. According to Vishwanathan et al[151] activation of CO is a rate limiting step in MFe_2O_4 (M = Mn, Fe, Co, Ni, Cu, or Zn) in which, surface carbonate species are formed as intermediates which then decomposes. They found inverse spinels to be more active than normal spinels. On the other hand according to Schwab et al[152] redox mechanism operates with Fe^{3+}/Fe^{2+} couple as active centres for the reaction in $Mg_xZn_{1-x}Fe_2O_4$, where in normal ferrites are more active than inverse ferrites. It is reported by Yoneda et al[153] that oxidation follows a redox

mechanism and the oxidation power of the catalyst increases (with CO content) in the order Fe_3O_4 < $CoFe_2O_4$ < Co_3O_4. Studies on $CuMn_2O_4$, $MnFe_2O_4$ and $CuCr_2O_4$ by Akhundova and Belenikii[154] showed kinetics of CO oxidation to be first order dependence with respect to CO and $CuMn_2O_4$ exhibits high activity .

Paetour et al[155] obtained the specific activity of Cu^{2+} ions among $CuMn_2O_4$ (M = Mn, Al, Cr) from the activity pattern and chemisorption data. Sultanov et al[156] have discussed the effect of poisoning by SO_2 on $NiCr_2O_4$, $NiAl_2O_4$ $CuCr_2O_4$ and summarised that poisoned and unpoisoned $CuCr_2O_4$ are more active than $NiAl_2O_4$ and $NiCr_2O_4$. Perti and Kabel[157] have put forward a view in their studies of Co_3O_4 /γ-Al_2O_3 that rate depends on partial pressure of CO and temperature and not on oxygen. Thermal treatment carried out by Idem[158] on the same catalyst, showed a reduced catalytic activity due to solid state interactions leading to the formation of $CoAl_2O_4$ which is less active. Piperov and Mekhandzhiev[159] in their study of various supports for $CuCo_2O_4$ led to the conclusion that ideal support for CO oxidation is γ-Al_2O_3 which has structure similar to the spinel. Effect of various impurities (Fe, SO_4^{2-}, Cl^-) on $CuCo_2O_4$ was studied by Piperov[160] and stated that decrease in catalytic activity depends on the kind of impurity where as supported catalysts are not affected by impurities.

Angelov et al[161] reported that in $Cu_xCo_{3-x}O_4$, activity for CO oxidation increases with 'x' and observed no separation of CuO phase on the surface even for the highest copper containing spinels. Resistance towards SO_2 poisoning was also studied on this catalyst by Angelov et al[162], higher copper containing spinels were found to be more resistant to

poisoning due to inverse distribution of Cu^{2+}. On the basis of Vickermann's theory of dilution of active transition metal ion Meenakshisundaram et al[64] explained the catalytic activity in $Zn_xCo_{1-x}Mn_2O_4$, and Co^{2+} in octahedral site has been identified to be active site.

Mekhandzhiev et al[163] studied $Cu_{1-x}Cr_xCo_2O_4$ system for CO oxidation and noticed that catalytic activity for CO decreases with increasing 'x'. According to Laine et al[164] copper rather chromium is an active species for CO oxidation and enhancement in activity produced by pre-reduction with CO of $CuCr_2O_4$ was attributed to an enrichment in Cu concentration at the spinel surface. Studies of CO oxidation on $CuCr_2O_4$ tempted Murthy and Ghose[165] to draw a conclusion that the catalytic activity is due to Cr ions above 500 K and activity per Cr ion increases with Cr dilution due to weaker interaction of the surface Cr ions with its near neighbours, while the activity below 500 K is due to Cu^{2+} ions and their reduction to Cu^{1+} ions leads to decrease in catalytic activity.

Recently further studies made by Murthy and Ghose[166] reported that in oxidation reactions on copper spinel oxide catalyst, the catalytic activity is higher when copper is present on the tetrahedral site of the spinel lattice. They also observed that the activity of $CuRh_2O_4$ is comparable to that of $CuCr_2O_4$ but the activity of $CuFe_2O_4$ is considerably lower.

CO adsorption and oxidation over Cu_2MnO_x catalyst from room temperature to 373 K were studied by Ping et al[167] and found that CO is easier to be oxidised at low temperature. Terelecki-Baricevic et al[168] carried out CO and propylene oxidation on $Cu_{0.8}Co_{2.2}O_4$, $CuCr_2O_4$ and $ZnCr_2O_4$ in a differential recycle reactor where in specific rate of CO

oxidation was found to be highest on copper cobaltite. Activation energy for CO oxidation on two copper containing spinels are similar, where as the activation energy on $ZnCr_2O_4$ is considerably lower. Zarkov and Mehandjiev[169] established that $CoAl_2O_4$ is stable towards SO_2 and its catalytic activity in the oxidation of CO is commensurable with the activity of a platinum catalyst.

Spinel solid solutions of $Co_xMg_{1-x}Al_2O_4$ with x = 0 to 1 have been reported as a catalyst for CO oxidation by Pepe and Occhiuzz[170] and observed that the activity of copper ions was fairly constant over the whole range of cobalt contents as measured by XPS. Takada et al[171] noticed that among the substituted spinel oxides containing cobalt, $ZnCo_2O_4$ posses the higher activity and selectivity for CO oxidation $CoAl_2O_4$ and Fe_2CoO_4 showed lower activity for CO/H_2 oxidation compared with Co_3O_4. They concluded that the main factor determining the activity and selectivity for CO oxidation in the presence of H_2 was the trivalent cobalt ion in octahedral co-ordination on the surface of the catalyst. The catalytic activity of $M(I)M_2(II)O_4$ spinel type complex oxides [M(I) = Cu, Ni, Mn, Zn, Mg, Co, and M(II) = Co, Cr, Al] in the oxidation of CO and ethyl benzene has been investigated by Pirogova et al[172] in which Co containing catalysts were more active than the Cr and Al containing catalysts. They further remarked that higher activities were observed for the catalysts containing two transition elements. Further investigation of Pirogova et al[173] on metal ferrites indicates that the nature of cation affects the catalytic activity and higher activities were observed for the catalyst containing ions with variable valencies in MFe_2O_4 (M = Cu, CO, Ni, Mg, Zn,) and

$M(I)_{0.5}M(II)_{0.5}Fe_2O_4$ [M(I) = Cu, M(II) = Co, Zn, Mg]. Studies by Omata et al[174] on $Zn_xCo_{3-x}O_4$ (x = 0 - 1), $Al_xCo_{3-x}O_4$ (x = 0 - 2.5) and $Fe_xCo_{3-x}O_4$ (x = 0 - 2.5) led to the conclusion that the main factor determining the activity and selectivity for CO oxidation in the presence of H_2 is Co^{3+} Oh on the surface of the catalyst, however other secondary factors also contribute to the activity

2.5.3. Studies on other oxide spinels

Schwab et al[175] reported that inverse spinels are more active than normal spinels, from their studies on $Mg_xZn_{1-x}Fe_2O_4$ they concluded that the catalytic activity increases with increase in degree of inversion. Yur'eva et al[176] in their investigation of the catalytic properties of chromites of copper observed that when a part of copper is replaced by Co or Mg and a part of chromium is substituted by iron the change in Co-ordination of the copper ions in the spinel network leads to change in activation energy of the reaction. Danilova et al[177] synthesised manganites MMn_2O_4 (M = Mg, Cd, Zn, Fe, Co, Ni, Mn) and correlated the activity to the surface oxygen content estimated by pH-iodide method. Presence of Co^{2+} in octahedral site of $Co_xFe_{3-x}O_4$ was found[178] to be superior to Fe^{2+} for H_2O_2 decomposition. The γ-irradiation has significant effect due to variation in active site concentration and cation distribution. Mimani et al[179] have attributed the catalytic activity of MFe_2O_4 and MCo_2O_4 (M = Mn, Fe, Co, Ni, Zn or Mg,)

to their fine particle nature, high surface area and electronic structure. Among these, cobaltites showed higher activity than ferrites. Recent studies made by Lahiri and Sengupta[180] on co-precipitated ferrospinels $M_xFe_{3-x}O_4$ (M = Co, Mn, Cu) showed that H_2O_2 decomposition in alkaline media follows a first order kinetics with respect to H_2O_2 for variable compositions, the high catalytic activity of these catalysts (on the basis of Ea) for H_2O_2 decomposition appeared to be due to surface activity of catalysts which promotes catalytic activity in alkaline media.

Study of methane oxidation on $Mn_{1-x}^{2+}Co_x^{2+}Co_{2-x}^{3+}Mn_x^{3+}O_4^{2-}$ showed[181] $CuCo_2O_4$ to be less active on account of strong inhibition by CO_2. $MnCo_2O_4$ has very low activity due to the presence of $Co^{2+}$and Mn^{3+}. Propylene oxidation was studied on $CoMn_2O_4$[182, 183]. The rate of adsorption of O_2 as well as surface coverage of O_2 was found to decrease by addition of Li_2O or TiO_2. Activation energy for O_2 chemisorption increases as also the surface oxygen bond strength. In $MnCo_2O_4$ addition of TiO_2 increases the rate of oxidation due to higher frequency factor.

Methane oxidation over MFe_2O_4 exhibits[184] the following order of activity for various spinels Co > Ni > Cu > Zn > Mn > Mg. Catalytic activity of spinels $Zn_{1-x}Cd_xCr_2O_4$ ($1 >= x >= 0$) was studied by Tulenin[185] in the temperature interval 773 - 1023 K. They showed that all the spinels studied catalyse total methane oxidation and their catalytic activity passes through a minimum with increase of cadmium content, it was further

noticed that individual chromites were found to exhibit higher activity than that of their mixtures, which is a rare case of antisynergism in catalysis. Krishnaswamy and chokkalingam[186] observed higher selectivity of MCr_2O_4 (M = Co, Cu, Zn) for dehydrogenation reaction with order of activity Co > Zn > Cu. Litchner and Szalek[187] correlated the electronic factors with catalytic activity of MFe_2O_4 (M = Zn, Fe, Co or Ni). The n-type ferrites were found to exhibit high activity than p-type ferrites. Narsimhan and Swamy[188] investigated that mechanism of dehydrogenation and dehydration over $MgAl_{2-x}Fe_xO_4$ changes with 'x', further, the variation of selectivity with 'x' is related to the type and symmetry of Fe^{3+} ion which is crucial in influencing the solid state as well as the catalytic properties. Massoth and Scarpiello[189] observed that the ease of surface reducibility decreases with increase in chromium concentration $ZnFe_2O_4 > ZnCrFeO_4 > ZnCr_2O_4$. The catalyst remains in the oxidised state when a mixture of butene and air are passed. A surface reaction sequence for the oxidation of butene to butadiene over $ZnCrFeO_4$ involving an iron-oxygen radical centre is proposed. Identification of structure of active sites for catalytic hydrogenation of dienes over $CuCr_2O_4$ and $CuAl_2O_4$ was undertaken by Jalolwiecki et al[190], which showed the critical importance of the cuprous ion at octahedral site.

Kehl[191] studied $Mg_xCr_yFe_2O_4$ for dehydrogenation of butene and reported high activity and selectivity towards butene dehydrogenation. Rennard and kehl[192] were of the opinion that substitution of Cr^{3+} ion in $ZnCr_xFe_{2-x}O_4$, significantly increases the efficiency of catalyst for oxidative dehydrogenation and stabilizes the catalyst against bulk reduction in hydrocarbon atmosphere.

Cimino et al[193] noticed that high temperature quenched spinels are more active than low temperature spinels because of higher octahedral occupancy of Co^{2+} ions in $CoAl_2O_4$, and samples with higher Ni_{tetr}/Ni_{oh} ratio for $MgAl_2O_4$-$NiAl_2O_4$ were found[194] to exhibit less activity. Magnetic susceptibility measurements in conjunction with ESR studies of $MgAl_2O_4$-$MgCr_2O_4$ were made use of by Egerton and Vickermann[195] to study the correlation between the catalytic activity and the electronic interactions in the solid solutions. Cimino et al[196] studied decomposition of N_2O over $Ni_xZn_{1-x}Al_2O_4$ and $CoGa_xAl_{2-x}O_4$ and came to the conclusion that the local configuration of ions are important then collective solid state properties, further according to him the neighbourhood of the active centre play an important role in the reaction. The reaction of CO with oxides of nitrogen on Co_3O_4 is found[197] to proceed via the formation of carbonate species and its reaction with gas phase N_2O. Thermoelectric power measurements were utilized[198] for initiating the reaction on $CoFe_2O_4$. The reaction was found to undergo through redox mechanism of the catalyst. Shelef and Otto[199] carried out NO + CO reaction over Co_3O_4 and $CuCr_2O_4$ in which N_2O is produced during the reaction and $CuCr_2O_4$ is found to possess higher activity for this reaction.

CHAPTER 3

EXPERIMENTAL TECHNIQUES

EXPERIMENTAL TECHNIQUES

Oxides with spinel structure have been reported to possess interesting structural, solid state and catalytic properties. The usual method for the preparation of spinel involves the use of ceramic technique, in which oxides, hydroxides, nitrates, carbonates or oxalates are used as starting material. Besides, spinels can also be prepared by combustion method, sol gel method, freeze drying and spray drying.

The thermal decomposition of co-precipitation derived precursors in order to obtain oxides with homogenous composition, though it is the old non conventional powder preparation technique is still an extensively used and a powerful method. The technique of co-precipitation has been fully exploited in the present contest for the preparation of series of spinels for their physical and catalytic studies.

3.1 MATERIAL PREPARATION

The solid solutions of compositions $Ni_{1-x}Cu_xMn_2O_4$, $Zn_{1-x}Cu_xMn_2O_4$, $Co_{1-x}Cu_xMn_2O_4$, and $Ni_{1-x}Co_xMn_2O_4$ (where x = 0.0, 0.3, 0.5, 0.7, and 1.0) were prepared by co-precipitation technique [63,200 - 204], a step wise process is shown in flow diagram (fig. 3.1). The respective metal nitrates and acetates of A. R. grade quality supplied by S.D. fine and LOBA chemicals were taken in stoichiometric proportion, by weighing requisite quantities on calculating the final composition desired and dissolved in about 150-200 ml of distilled water. The solution was heated at 333-353 K with stirring in order to obtain a clear homogenous solution. Sodium hydroxide solution was prepared by dissolving NaOH (A.R. grade LOBA chemical) in a distilled water to obtain a solution of approximately equimolar concentration and is taken in a burette. Solution of metallic salts and Sodium hydroxide were then mixed by drop wise addition of NaOH from burette to the solution of metal ions in the beaker. Solution in the beaker was constantly and uniformly stirred on a magnetic stirrer till the precipitation was complete, the pH of the solution was maintain between 9-10. The precipitate was then digested on a water bath at 363 K for three hours. The completion of precipitate was checked, by adding the precipitating agent along the sides of the beaker containing the precipitate. The precipitated hydroxides along with its parent solution was subjected to a process of oxidation by dropwise addition of 30% Hydrogen peroxide from a burette with continuously stirring the precipitated

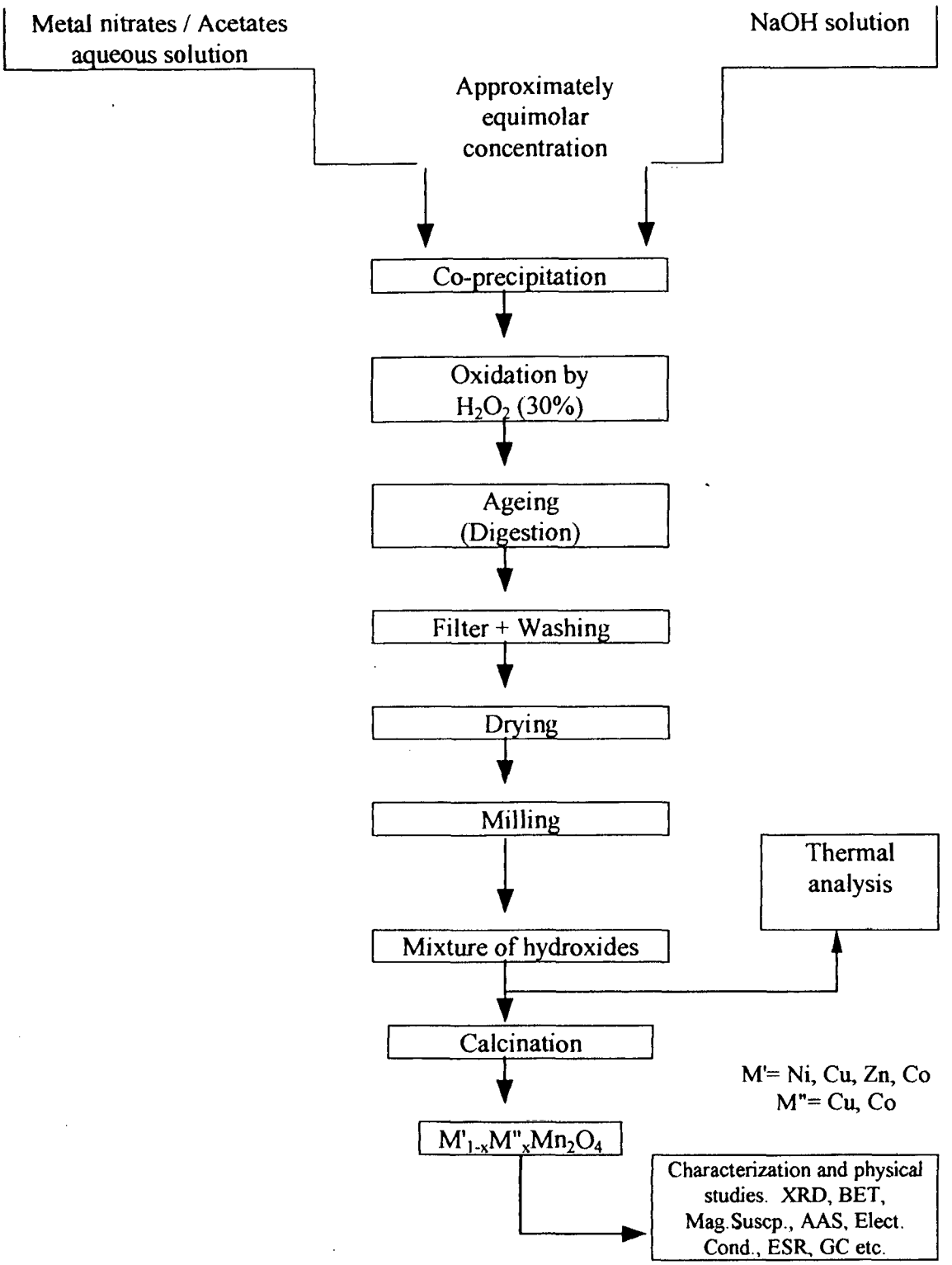

Fig. 3.1. Flow diagram of preparative method.

mixture on a magnetic stirrer. The precipitate was then washed and filtered using minimum amounts of water and dried in an oven at 353 K $\pm$5 K for 15-20 hours. The dried precipitate was ground well in a mortar and then heated in a muffle furnace at 973-1073 K for 7-10 hours in order to form the required oxides. If x-ray showed the presence of biphasic character, then further heating is done to obtain a monophasic compound. The composition obtained finally after characterisation was designated as a spinel catalyst.

3.2 CHARACTERIZATION

Materials prepared by co-precipitation method were characterised employing X-Ray Diffraction technique, Atomic Absorption Spectroscopy and BET liquid N_2 adsorption method.

3.2.1 X-Ray technique

Spinels prepared by co-precipitation method were characterised by examining powder x-ray diffractograms. The diffraction patterns were recorded on a Philips X-ray diffractometer (PW 1820) using CuKα or FeKα radiation as per the requirements, filtered through nickel or chromium absorber at a scanning rate of 2°/min. The compounds were identified by comparing the observed interplanar d-spacing and relative peak intensities with those reported in the JCPDS data file.

3.2.2 Atomic Absorption Spectroscopy (AAS)

The sodium contamination in the spinels prepared by co-precipitation method using $NaOH$, was found out using an Atomic absorption spectrometer. Approximately 200 mg of sample was dissolved using 20 ml of pure HCl, it was then further diluted to the required concentration. By comparing the standard, the total amount of sodium was determined.

3.2.3 B.E.T. Method (Surface Area Measurement)

Surface Area of the catalysts were measured using BET, nitrogen adsorption method on ANYGAS Version 2.10 using Quantachrome Autosorb Automated Gas Adsorption system. Specific surface areas of the catalysts are calculated with the help of well known Brunauer, Emmet and Teller (BET) expression.

$$\frac{P}{V(P_o-P)} = \frac{1}{V_m C} + \frac{(C-1)}{V_m C} \times \frac{P}{P_o} \quad \ldots\ldots\ldots\ldots\ldots (1)$$

Here 'P' is the equilibrium pressure, 'P_o' the saturated vapour pressure of the gas at the temperature of the adsorption, 'V' is the volume of the adsorbed gas at S.T.P.,C is a constant related to the heat of adsorption and V_m the volume of gas at S.T.P. required to form a monolayer. Various

quantities from the above equation like P, P_o and V could be determined experimentally. V_m and C can be obtained by plotting $P/V(P_o-P)$ versus P/P_o. Plot should give a straight line with slope (S) = C-1 / V_mC, and intercept (I) = $1/V_mC$, which proves the validity of equation -(1)

It can be shown from equation -(1) that V_m = 1/S+I and C = S/I+1. Since V_m is the volume of the gas at 273 K and 1 atm. pressure necessary to cover the surface with one layer of the gas, it is easy to convert it to the number of molecules involved.

Assuming 16.2 A° as the value of the cross sectional area of single nitrogen molecule at liquid nitrogen temperature, Brunauer, Emmet and Teller have shown that

$$\text{Surface Area} = 4.38V_m \text{ (C.C., S.T.P.) } m^2/g \quad \text{.....(2)}$$

Surface area for various catalyst were observed in the range of 1.46-8.9 m^2/g.

3.3 ELECTRICAL CONDUCTIVITY MEASUREMENT

Electrical conductivity measurements were carried out using a two probe conductivity cell in the temperature range of 300 K - 723 K as shown in fig. 3.2. For the measurement of electrical conductivity, sample pellets were made using a pressure of 5000 kg/cm^2. Prepared pellets were then

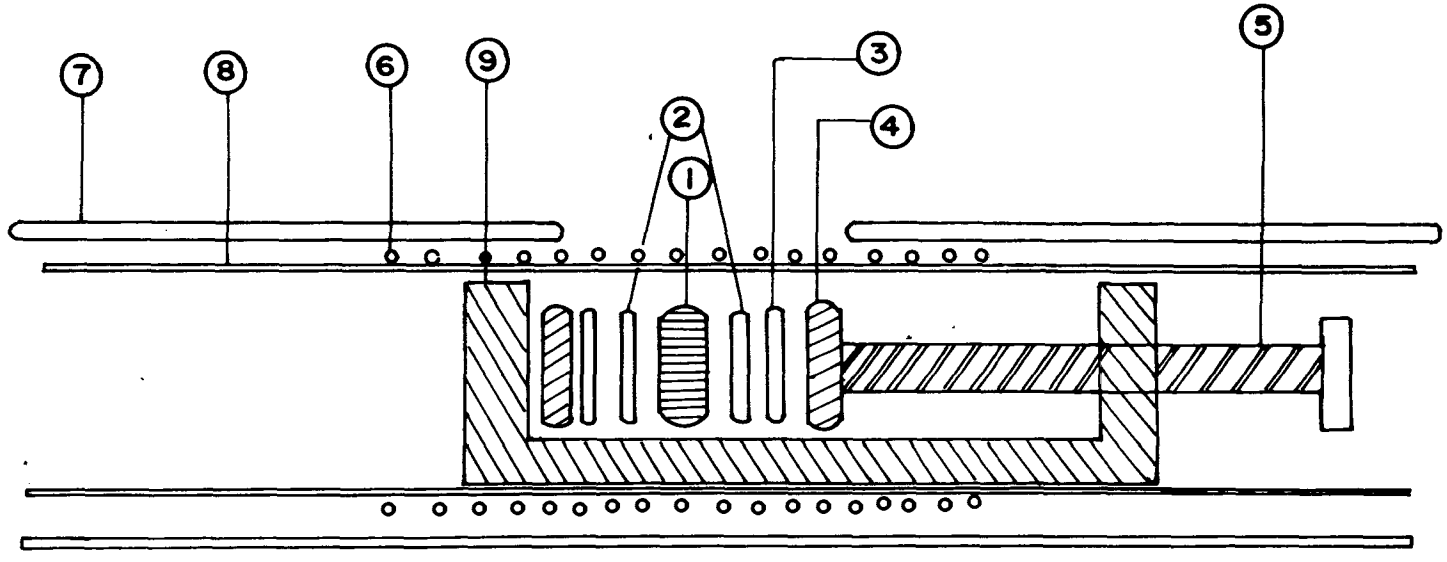

Fig. 3.2. Assembly used for Thermoelectric measurement of samples. 1. Pellet, 2. Silver electrodes, 3. Mica sheets, 4. Adjustable screw, 5. Rotating shaft, 6. Heating element, 7. Furnace outline, 8. Inner ceramic tube, 9. Brass assembly holder.

subjected to heat treatment at 1048 $\pm$ 10 K for 15-20 hours. The pellet was tightly held between two polished and cleaned silver electrodes by adjustable screw type assembly and the resistivity measurements were carried out from room temperature(R.T.) to 723 K.

3.4 MAGNETIC SUSCEPTIBILITY MEASUREMENT

The magnetic susceptibility χ_g in air of the spinels were determined by Guoy method at R.T. A field of the order of 5000 gauss was employed. A sensitive analytical balance was used to measure the difference in weights. Mercury tetrathiocynatocobaltate (Hg $[Co(SCN)_4]$) was used as the standard material. The sample tube was washed, dried and filled with the standard substance Mercury tetrathiocynatocobaltate up to the mark and hanged between the electromagnets of the Guoy balance. The weight was recorded before applying the field and after applying the appropriate field. The procedure is repeated for the samples whose χg is to be determined. The magnetic susceptibility of the sample was calculated by using the following relation

$$\chi_{g\,(sm)} = \chi_{g\,(st)} \propto \frac{W_2 - W_1}{W_4 - W_3} \times \frac{W_3}{W_1} \quad (\text{where } \chi_{g\,(st)} = 16.44\times10^{-6} \text{ constant})$$

χg_{sm} is the susceptibility per gram of the sample, χg_{st} is the susceptibility per gram of the standard, W_1 and W_2 are the weights of sample in absence and presence of field respectively, where as W_3 and W_4 are the weights of standard in absence and presence of field.

3.5 ELECTRON SPIN RESONANCE (ESR) STUDY

Electron spin resonance occurs when a spinning electron in an externally applied magnetic field absorbs sufficient electromagnetic radiation to cause the inversion of the spin state of the electron, which is also known as electron paramagnetic resonance and as electron magnetic resonance.

ESR study was carried out for the spinels containing paramagnetic species and for the identification of the catalytically active species for the reaction. In ESR spectroscopy a magnetic field strength of 3220 gauss (≅3300 gauss a field strength which is commonly employed) was employed. The energy level difference due to electron spin was 6.1×10^{-17} ergs (or about 1.5×10^{-24} cal) and frequency 'ν' is 9.2 GC (giga cycles or 10^9 cycles per sec.), this frequency lies in the microwave region of the electromagnetic radiation spectrum. The ESR spectra were taken at the X-band on a varian E-112 spectrometer at 298 ± 2K. The sample was mounted in a quartz tube and TCNE was used as a field calibrant taking its g-value as 2.00277.

Spectroscopic splitting factor (g) or gyromagnetic ratio was obtained from the following relation ,

$$\mu = -g\beta s$$

where 'μ' is the magnetic moment, 'β'the Bohr magneton (ergs/gauss), 'g' the gyromagnetic ratio and 's' is the spin of electron +1/2 or -1/2

3.6 THERMAL STUDIES (TGA/DTG/DSC)

The thermal technique of TGA/DTG/DSC was used to study the heat effects, associated with physical and chemical changes of the substances. The thermal effects, exothermic or endothermic associated with preceeding physical and chemical changes were studied by a differential method in which the sample temperature is continuously compared against the temperature of a thermally inert reference material. TGA was recorded to study the behaviour of weight loss of the sample. Sample was continuously weighed as it was heated at a constant preferably linear rate 5-10 K/min with a constant flow of nitrogen.

TGA analysis was carried out on General V_2. 2A DuPont 9900 in the temperature range of 300 K-723 K in the atmosphere of nitrogen at the rate of 5-10 K/min with a sample size of 10.00 to 13.00 mg. DSC scans were also recorded of some representative samples over a relevant temperature range using a model General V4. 1C DuPont 200.

3.7 CATALYTIC STUDIES

Spinel catalysts were tested for the model reaction of CO oxidation by using AMIL-NUCON series 5700 Gas Chromatograph on-line for the analysis of reactants and products. Experimental set up for on-line analysis is shown in fig. 3.3. High purity H_2 gas was used as a carrier gas with a constant flow rate of 40 ml/min. Two types of columns were used for sample analysis, molecular sieve 13X and reference column Porapak Q. Injector and Detector were operated at a temperature of 323 K and oven at 338 K. Constant current flow of 150 mA was supplied to Thermal Conductivity Detector (TCD) through out the reaction studies. Gas Chromatograph was equipped with eight port valve to inject the gaseous samples to be analysed. Analysed data were recorded on a Omniscribe® recorder at a chart speed of 2 cm/min to obtain the quantitative information of reaction study.

Carbon monoxide required for the reaction studies was prepared in laboratory by warming Formic acid (AR) and Sulphuric acid (AR) in a specially designed glass reactor. It was purified by passing through NaOH and Molecular sieve, it was finally dried over Calcium chloride. CO so prepared, was found to be highly pure, as confirmed by Gas Chromatography. Standard O_2 and N_2 were used from commercial cylinders.

Reaction study was carried out in a continuous flow, fixed bed glass reactor, in which 1.0 g of powdered catalyst was supported between glass beats and glass wool plugs on either side. The catalytic activity was

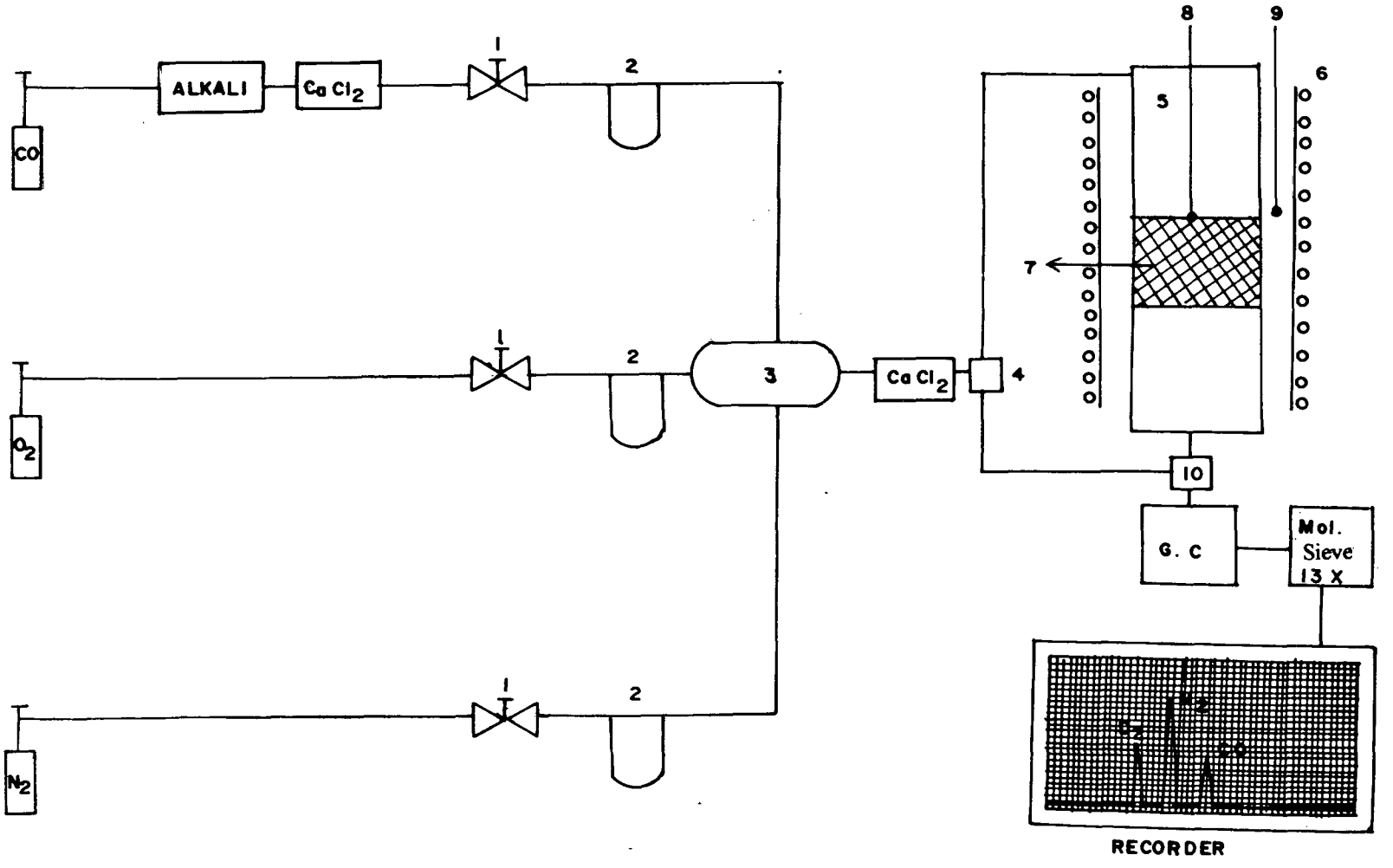

Fig. 3.3. Schematic diagram of the experimental reaction set up.
1. Fine control needle valve, 2. Flow meter, 3. Mixing bulb, 4. Two way valve, 5. Glass reactor, 6. Electric furnace, 7. Catalyst bed, 8. Thermocouple T_1, 9. Thermocouple T_2, 10. Eight port valve.

determined using a feed gas composition of 5% CO, 5% O_2 and 90% N_2. The individual gas flow rates were controlled using flow meters and precision needle valves. CO conversion was checked at a various catalyst temperature point by point measurements from low temperature to elevated temperature. The total flow rates used were between 5000 to 10000 ml/hr. The reactants could be taken straight to the G.C without passing through the catalyst bed, by using a bypass. The products were injected at a regular intervals into the G.C. and analysed using molecular sieve 13X. The TCD was used for detecting the reactants and products. The kinetic parameters such as rate of reaction, activation energy and frequency factors were evaluated by carrying out kinetic studies under steady state conditions over these catalysts. Partial pressure studies were carried out over the various catalyst by passing variable flow rates of O_2 at constant CO flow and vice-versa.

CHAPTER 4

SOLID STATE STUDIES

SOLID STATE STUDIES

The various solid state experimental studies such as structural characterization, thermal analysis, electrical resistivity, magnetic susceptibility and electron spin resonance were carried out. The comparison of different results were made and discussed on the basis of experimental data.

4.1 X-RAY DIFFRACTION ANALYSIS

The formation of monophasic spinels were checked by recording the x-ray powder diffractogrammes of all the samples such as $Ni_{1-x}Cu_xMn_2O_4$, $Zn_{1-x}Cu_xMn_2O_4$, $Co_{1-x}Cu_xMn_2O_4$ and $Ni_{1-x}Co_xMn_2O_4$. The d-spacing and intensities corresponding to 2θ obtained from the diffractogrammes were compared with the values reported in the literature (JCPDS data file) and found to be monophasic. Since the d-spacing of the intermediate

compositions are not reported in literature, the values were compared with the end members namely $NiMn_2O_4$, $CuMn_2O_4$ and $ZnMn_2O_4$, $CoMn_2O_4$, respectively. Among these, $NiMn_2O_4$ forms an inverse spinel, $CoMn_2O_4$ and $ZnMn_2O_4$ forms normal spinel. Figures 4.1, 4,2, 4.3, 4.4 and 4.5 shows x-ray diffraction patterns of some of the representative samples.

It is well known that $CuMn_2O_4$ is sensitive to thermal treatment during its preparation. Some of the authors[43, 48, 205] could not obtain a pure sample of this compound. However a number of workers[36, 47, 206, 207] claimed to have obtained it in a cubic phase. On the other hand only Buhl[25] could synthesise it only as a tetragonal phase by calcining at 1213 K and quenching from temperature above 1023 K. Below 1023 K $CuMn_2O_4$ progressively gets transformed into a cubic phase. However our results of x-ray analysis after comparison with the values reported in JCPDS data file has indicated that $CuMn_2O_4$ is a cubic spinel, $NiMn_2O_4$ crystallizes in cubic form and $ZnMn_2O_4$ into a tetragonal form, where as $CoMn_2O_4$ crystallizes in a tetragonal form as per the earlier reports [204, 208-210].

Among all the metals in first transition series, Cu^{2+} has the strongest square (dsp^2) bond forming power, it is expected to occupy an octahedral (Oh) site which is also reported by Goodenough and Loeb[211]. The results of an x-ray powder study by Zaslavaski et al[39] showed that $CuMn_2O_4$ is not a normal spinel but partially inverted with inversion parameter λ within the

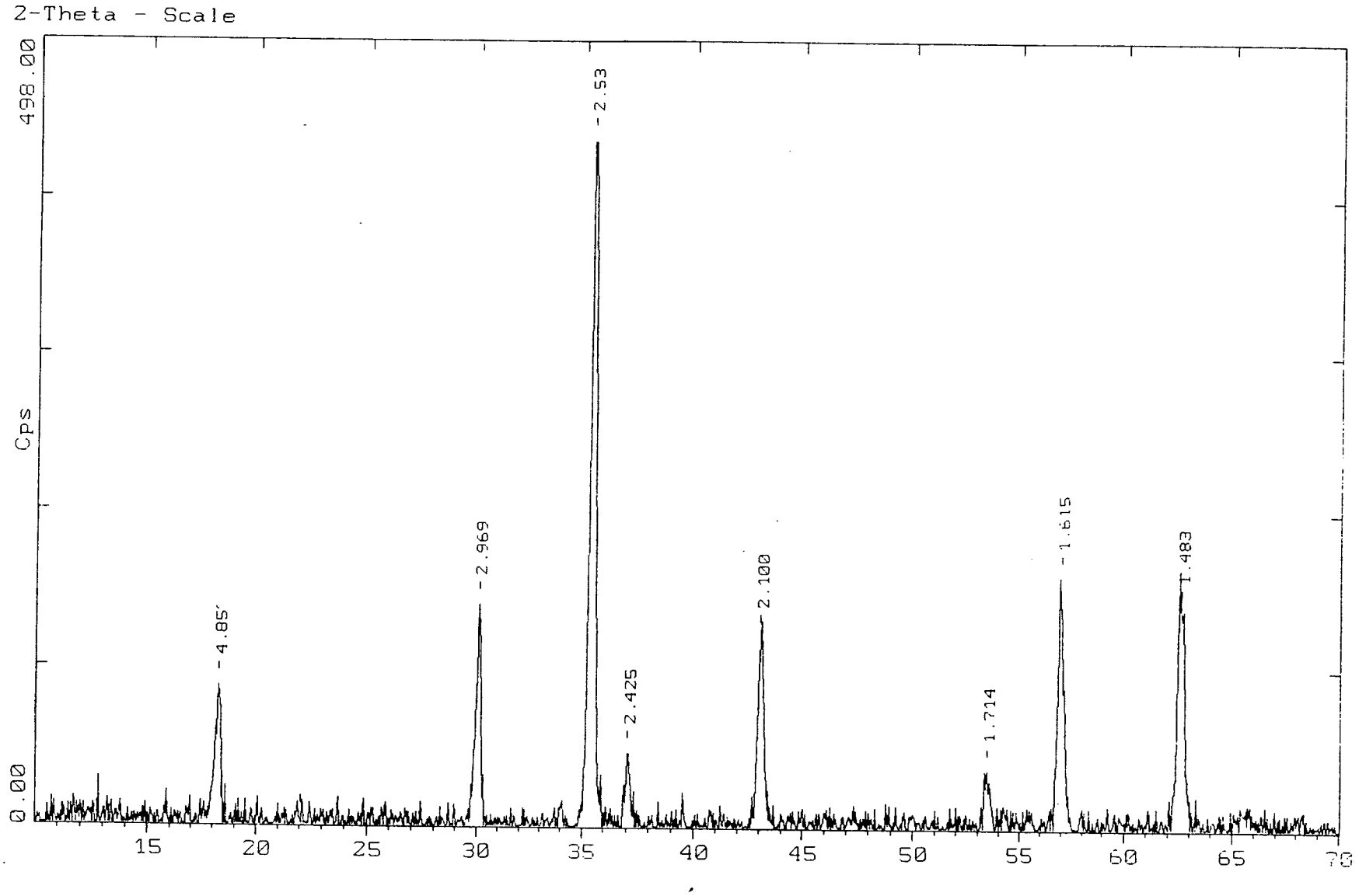

Fig. 4.1. X-ray powder diffraction pattern of $NiMn_2O_4$

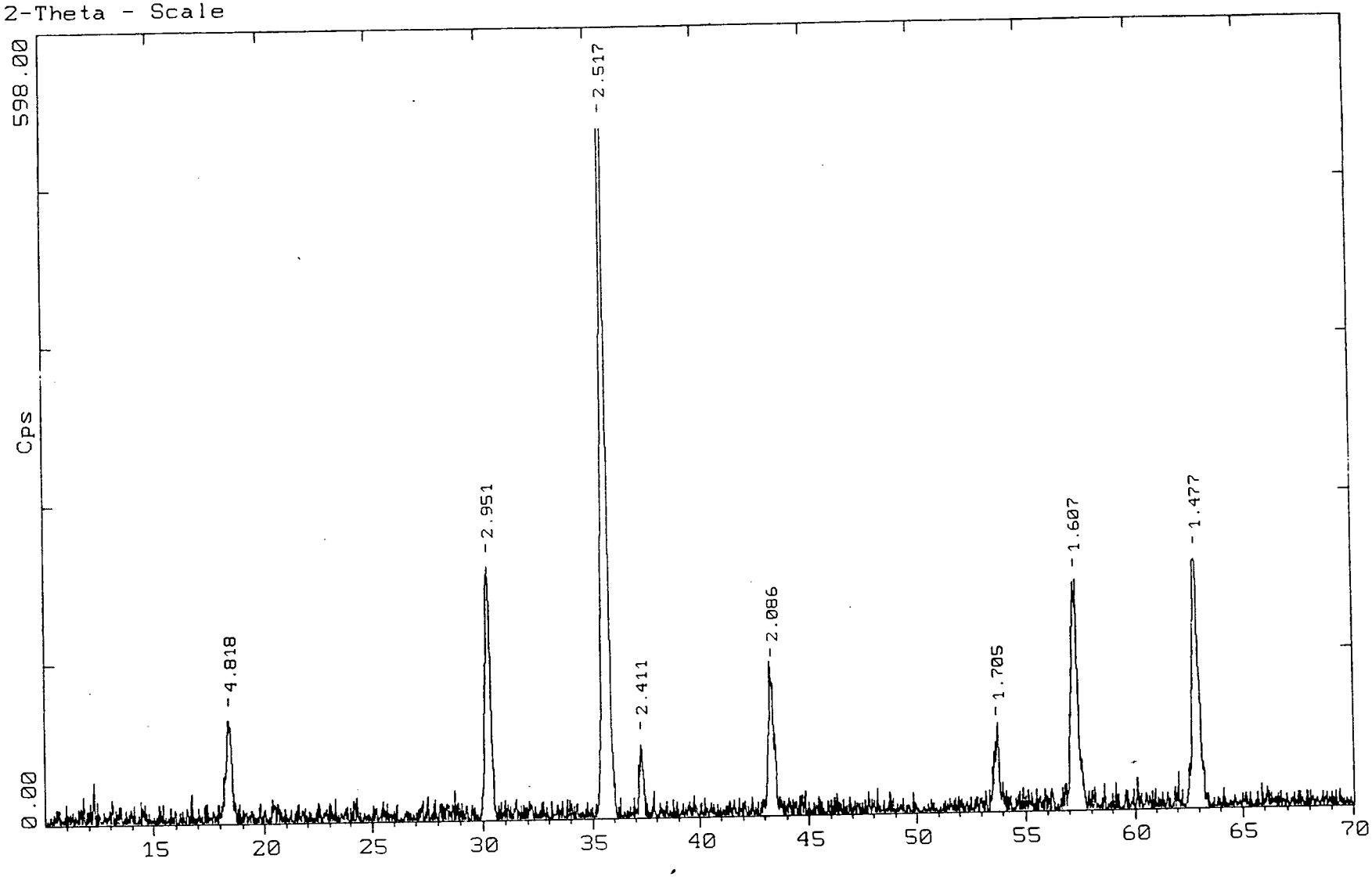

Fig. 4.2. X-ray powder diffraction pattern of $Ni_{0.5}Cu_{0.5}Mn_2O_4$

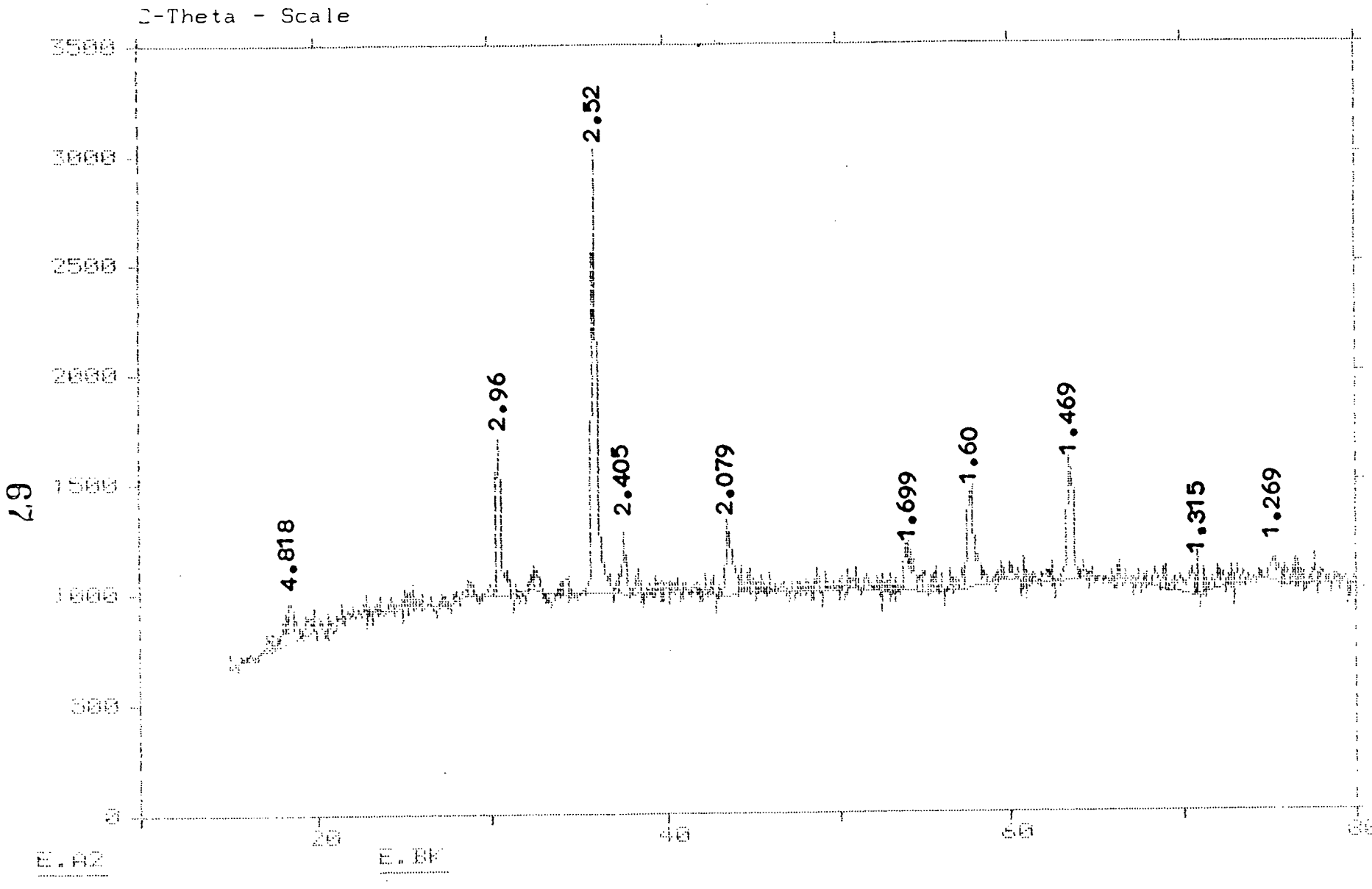

Fig. 4.3. X-ray powder diffraction pattern of $CuMn_2O_4$

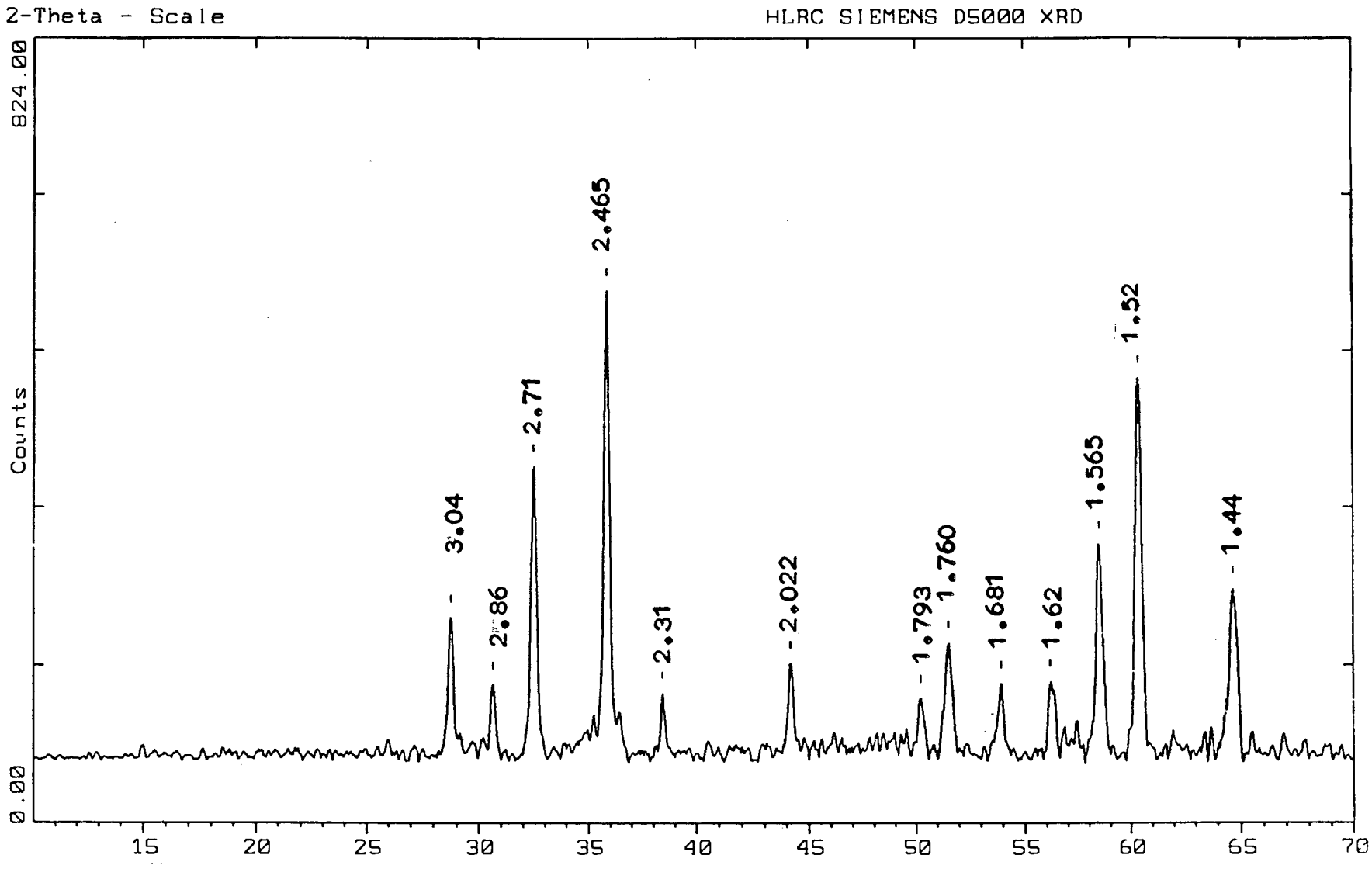

Fig. 4.4. X-ray powder diffraction pattern of $ZnMn_2O_4$

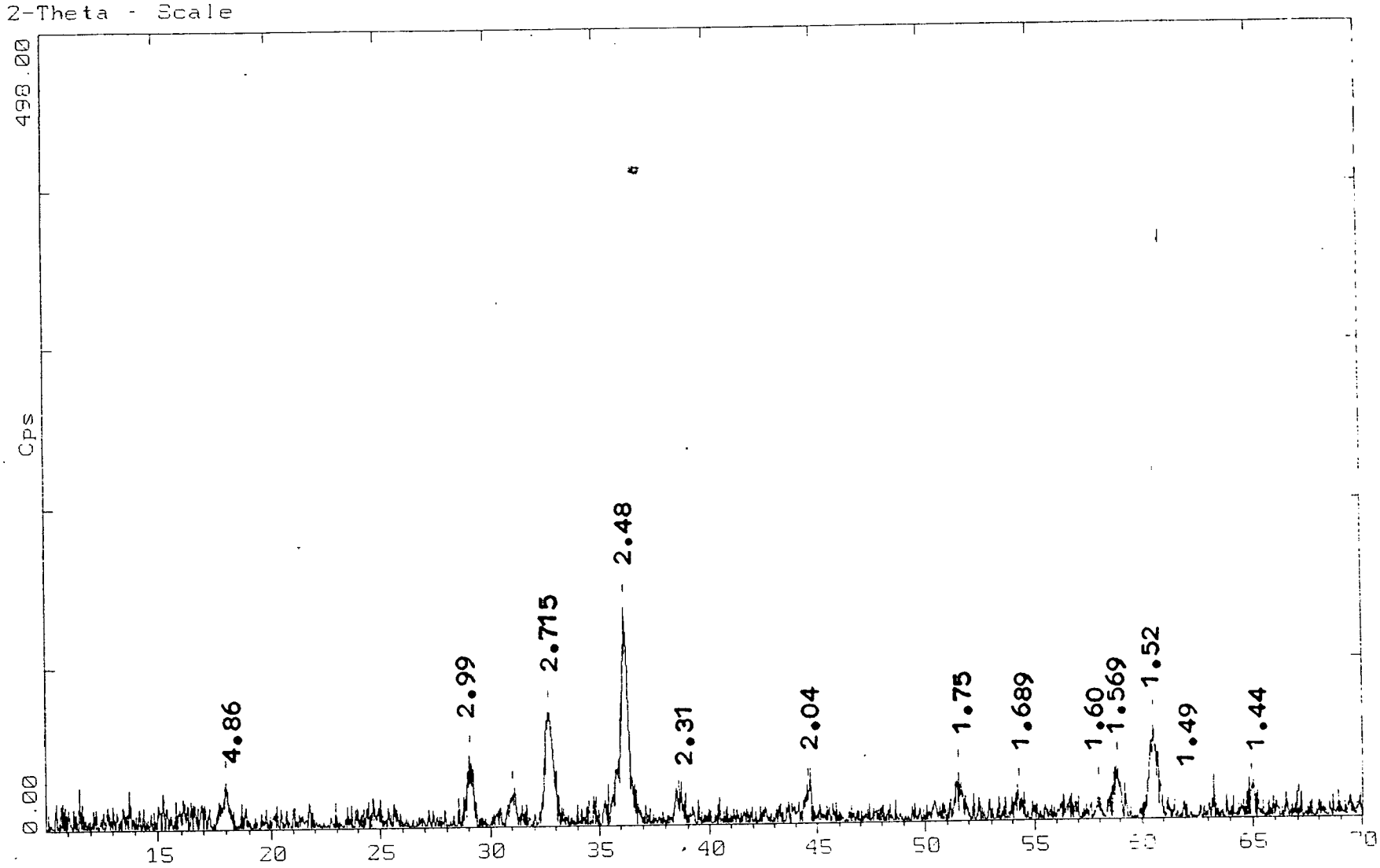

Fig. 4.5. X-ray powder diffraction pattern of $CoMn_2O_4$

limits $0.67 \leq \lambda \leq 1$. Inverse structure of $NiMn_2O_4$ from crystallographic data obtained by Sinha et al[29] was supported by the fact that Ni^{2+} ions show strong tendency to occupy Oh sites and suggested a structure as $Mn^{2+}[Ni^{2+}Mn^{4+}]O_4^{2-}$. In $Ni_{1-x}Cu_xMn_2O_4$ symmetry is cubic throughout the system according to Kshirsagar[47]. The observed cubic symmetry over the entire range of composition is explained by Bhandage and Keer[31], as due to the absence of Jahn-Teller distortion on account of mutual neutralization of ions like Cu^{2+} and Mn^{3+} having tendency to distort the structure. It was observed by Kshirsagar and Biswas[37] that for $ZnMn_2O_4$: $CuMn_2O_4$ system there is a transition from tetragonal to cubic form at 83% $CuMn_2O_4$ and for $CoMn_2O_4$: $CuMn_2O_4$ system this transition was observed at 53% $CuMn_2O_4$.

4.2 THERMAL ANALYSIS

Co-precipitated samples of manganites before decomposition were subjected to thermal studies, to find out the decomposition temperature of hydroxides and then initiation of solid state diffusion reaction. TGA/DTG patterns of representative samples are shown in figures 4.6, 4.7 and 4.8.

Thermal studies show that there are two major steps in the decomposition process, the probable reactions are, 1. Dehydration and 2. Decomposition of hydroxides to corresponding oxides.

TGA/DTG pattern of $NiMn_2O_4$ hydroxides composition show a weight loss between 453 - 598 K due to decomposition of hydroxides of the

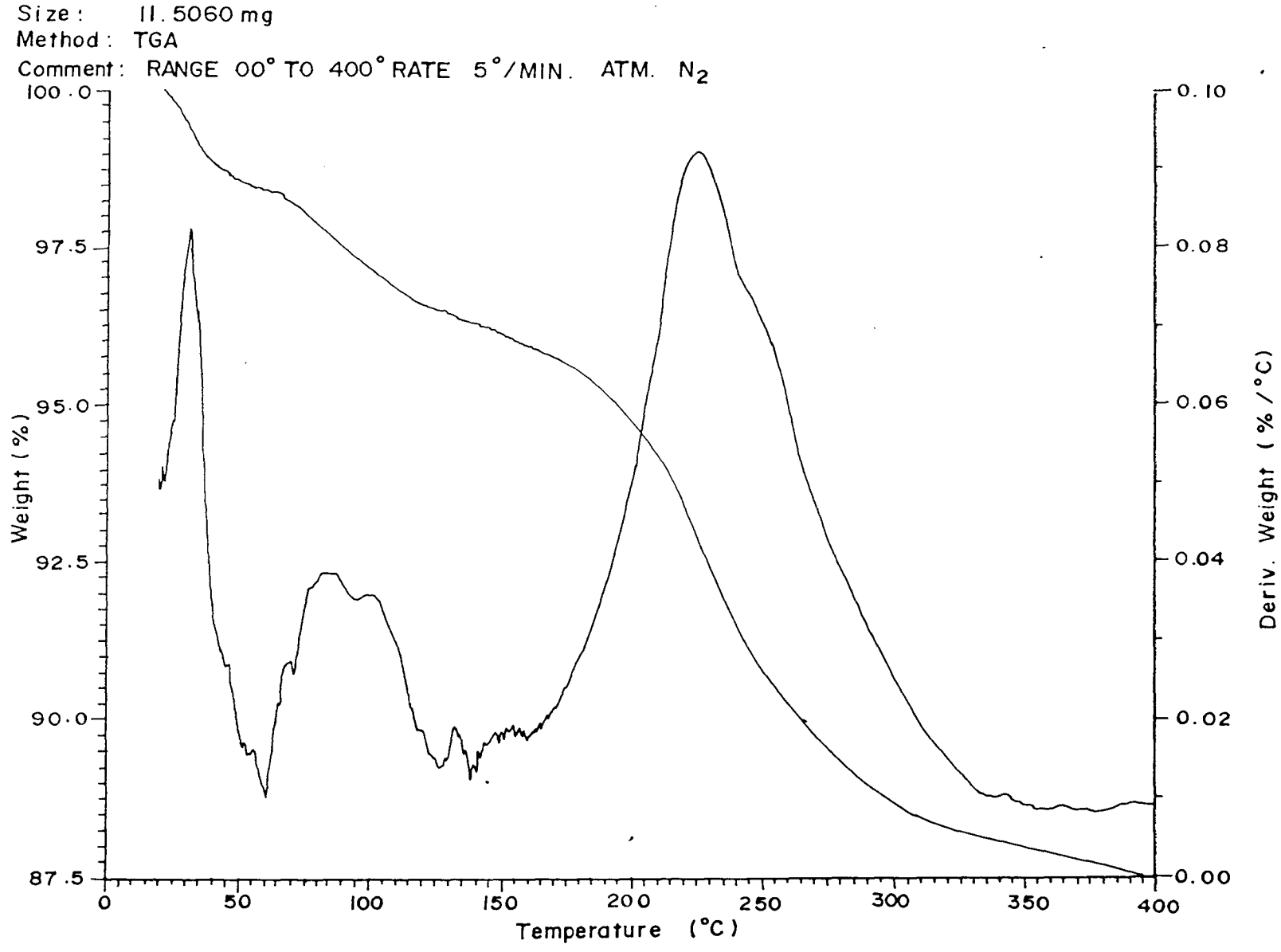

Fig. 4.6. TGA/DTG curves of $NiMn_2O_4$

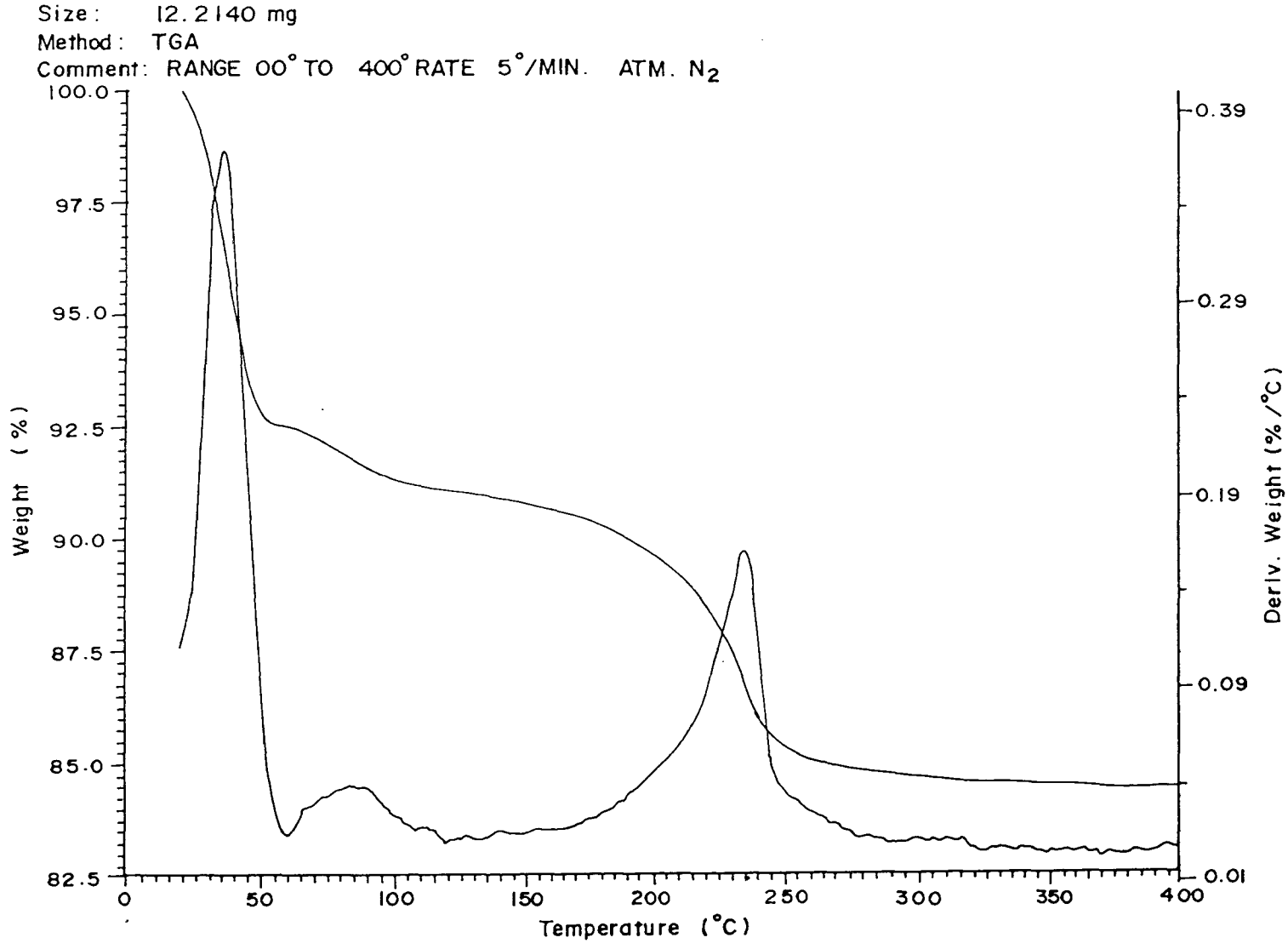

Fig. 4.7. TGA/DTG curves of $Ni_{0.5}Cu_{0.5}Mn_2O_4$

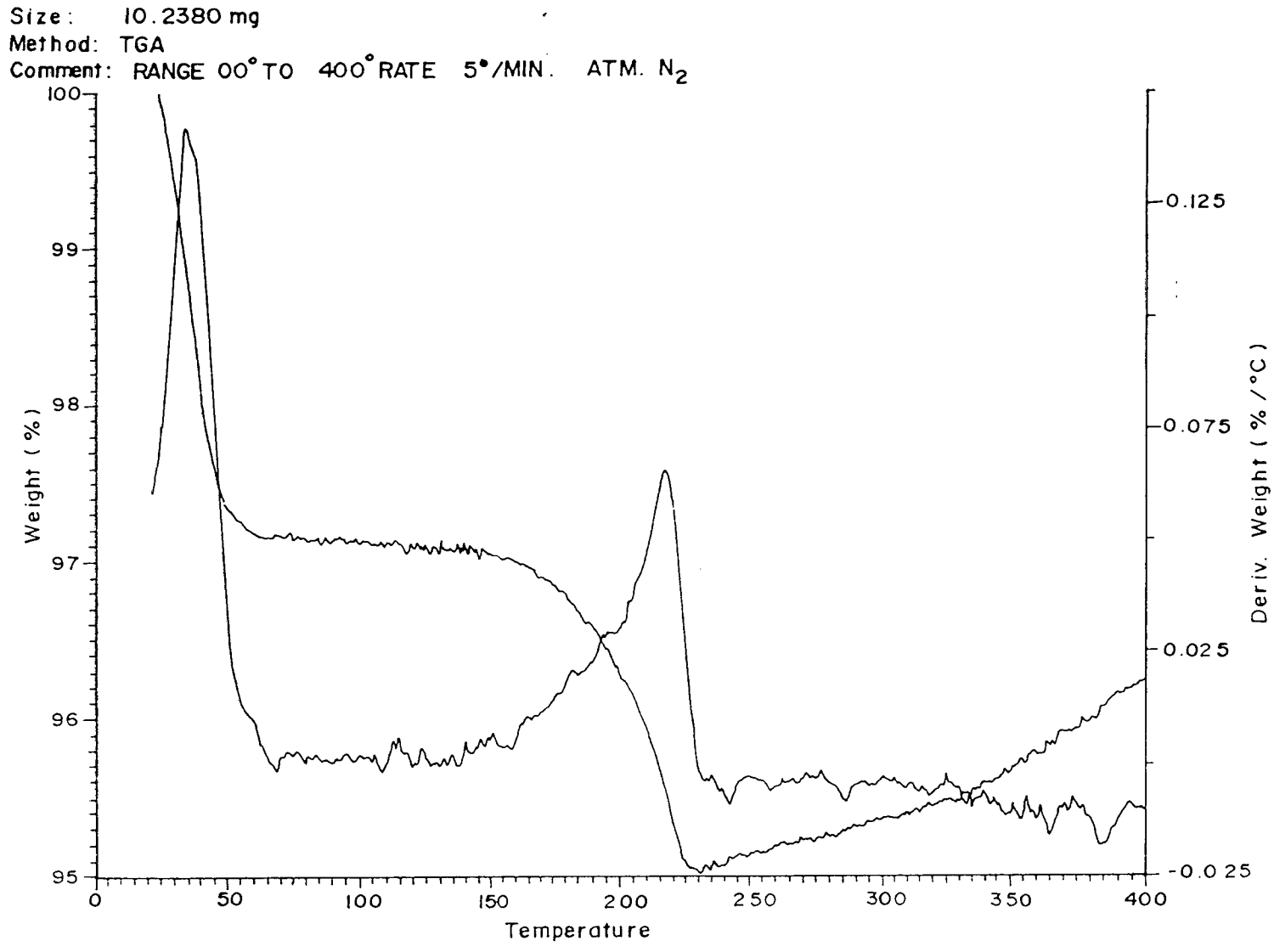

Fig. 4.8. TGA/DTG curves of $CuMn_2O_4$

constituent metals. The maximum weight loss of ≅ 9.0 % occurred at around 498 K. The decomposition of hydroxides is followed by a solid state diffusion reaction leading to spinel formation. In the case of $CuMn_2O_4$ and $Ni_{0.5}Cu_{0.5}Mn_2O_4$ hydroxides composition showed maximum weight loss at 490 K and 509 K respectively. DSC of representative samples were recorded employing V4. 1C DuPont 2000, gave exothermic peaks at 478 K and 466 K for $ZnMn_2O_4$ and $Zn_{0.3}Cu_{0.7}Mn_2O_4$ hydroxide composition respectively. Change in enthalpy were found out to be 24.6 and 32.8 J/g respectively for the above compositions, (fig. 4.9 - 4.10)

4.3 ELECTRICAL RESISTIVITY MEASUREMENT

Electrical resistivity of the different prepared samples were measured using two probe method at various temperature from R.T. to 723 K. The conductivities of manganites found to vary in the range 10^2 to 10^{-11} ohm^{-1} cm^{-1} at R.T. as expected for semiconductors. Plot of resistivity (ρ) versus Temperature (T) are shown in figures 4.11 and 4.12 for $Ni_{1-x}Cu_xMn_2O_4$ and $Zn_{1-x}Cu_xMn_2O_4$ respectively. Resistivity is found to decrease with increase in temperature for all the compositions that were studied for sries-I and series-II.

Resistivity decreases with the increase in copper content in $Ni_{1-x}Cu_xMn_2O_4$ system. The improvement in conductivity is attributed to the

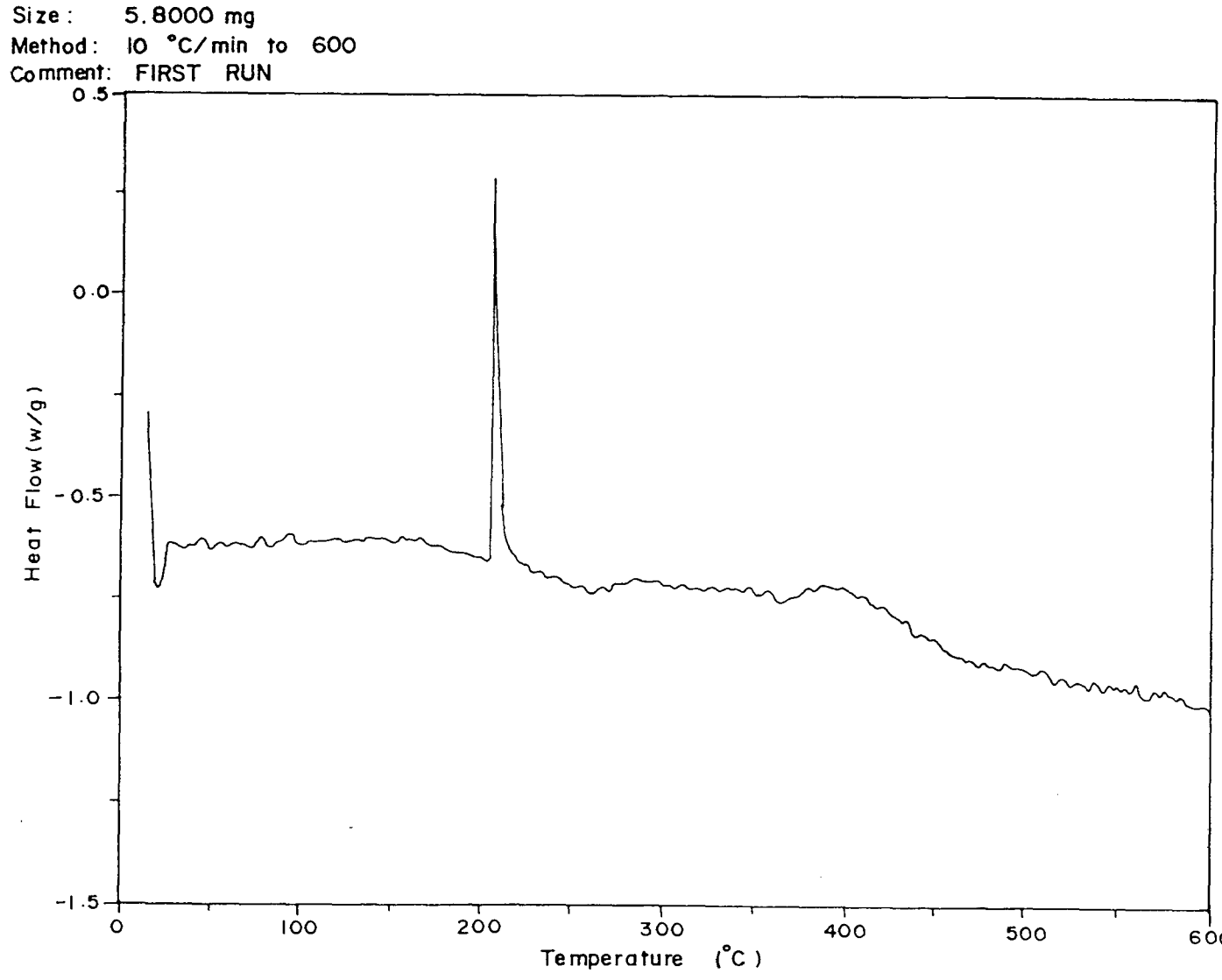

Fig. 4.9. DSC scan for $ZnMn_2O_4$

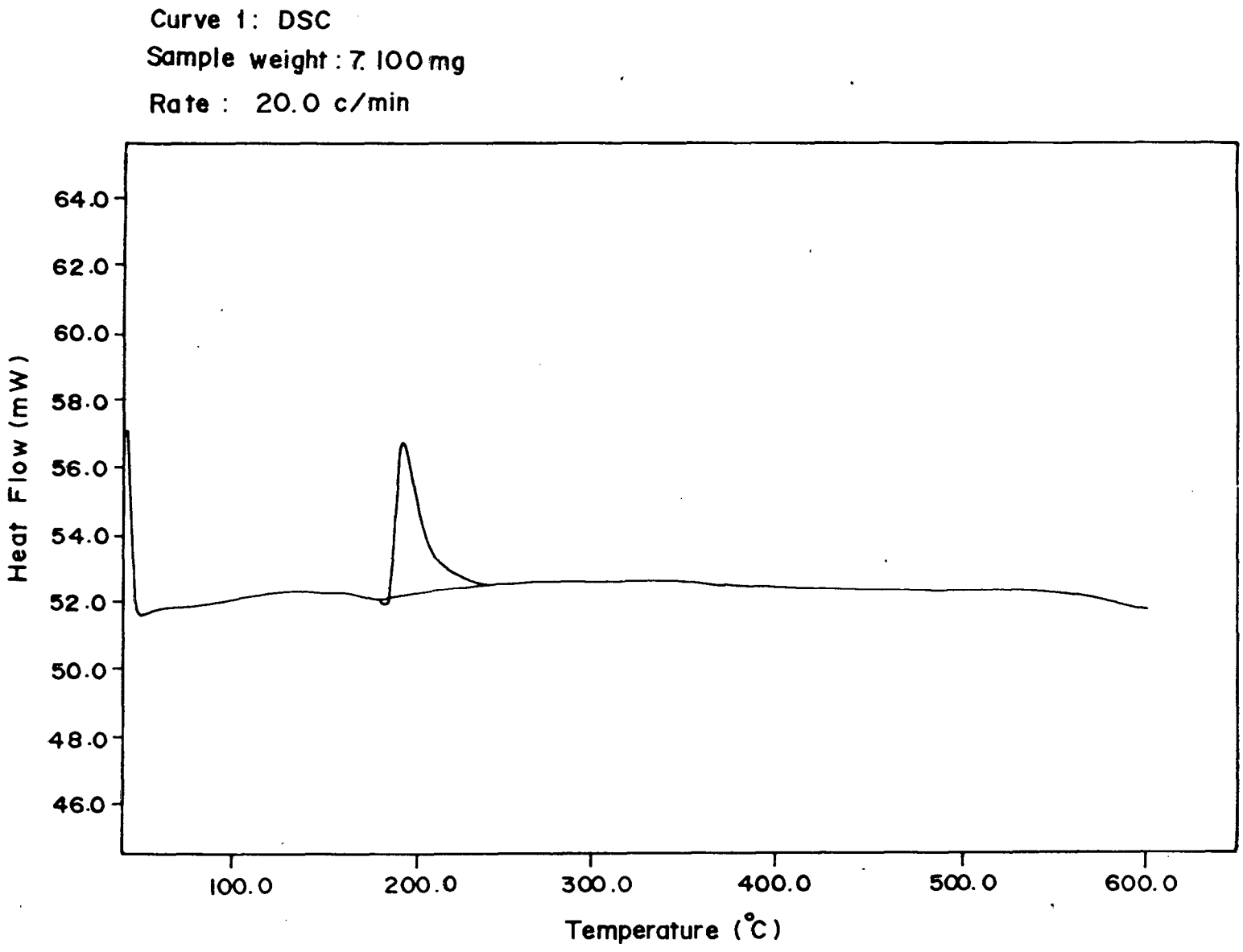

Fig. 4.10. DSC scan for $Zn_{0.3}Cu_{0.7}Mn_2O_4$

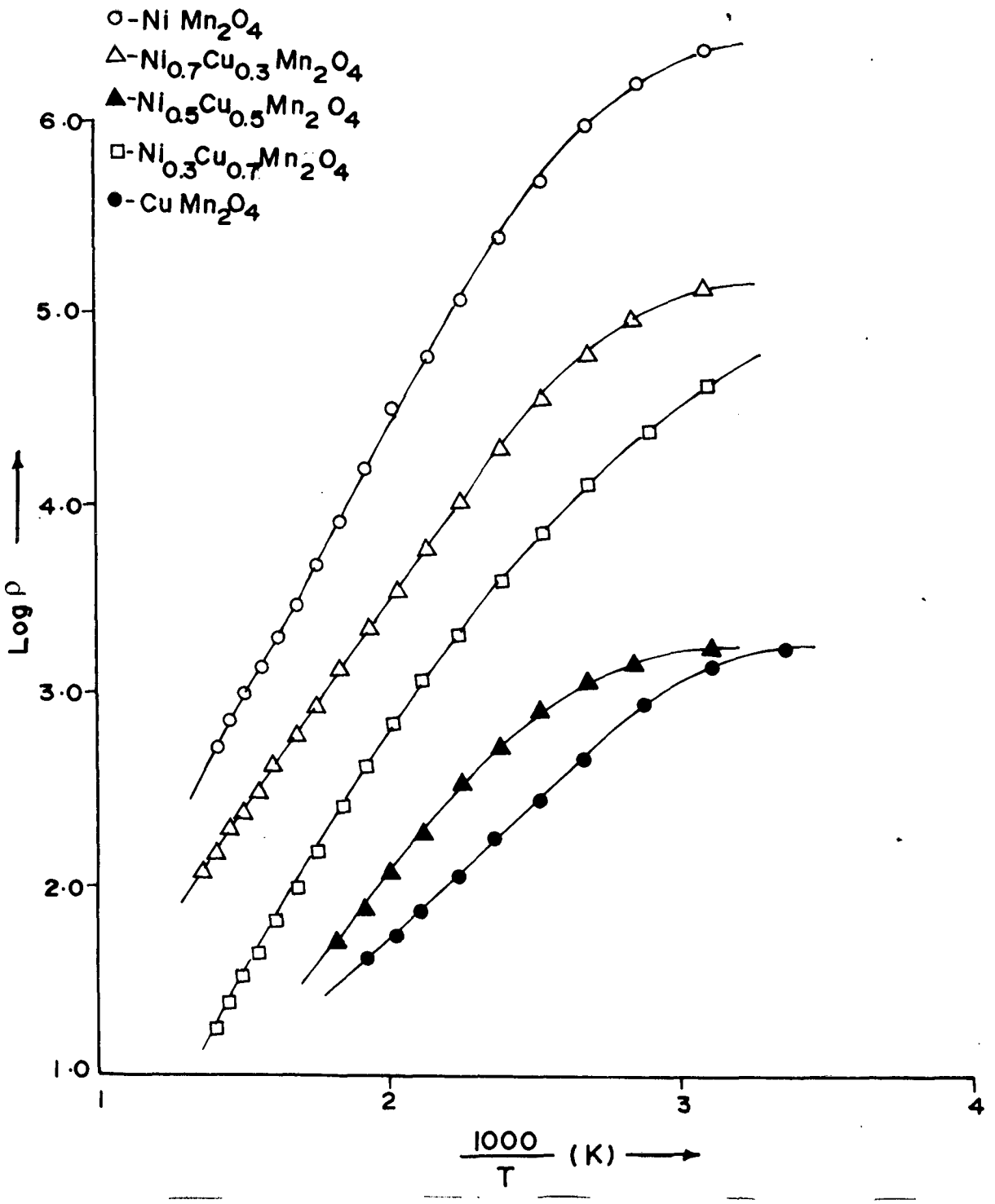

Fig. 4.11. Variation of electrical resistivity of $Ni_{1-x}Cu_xMn_2O_4$ with temperature

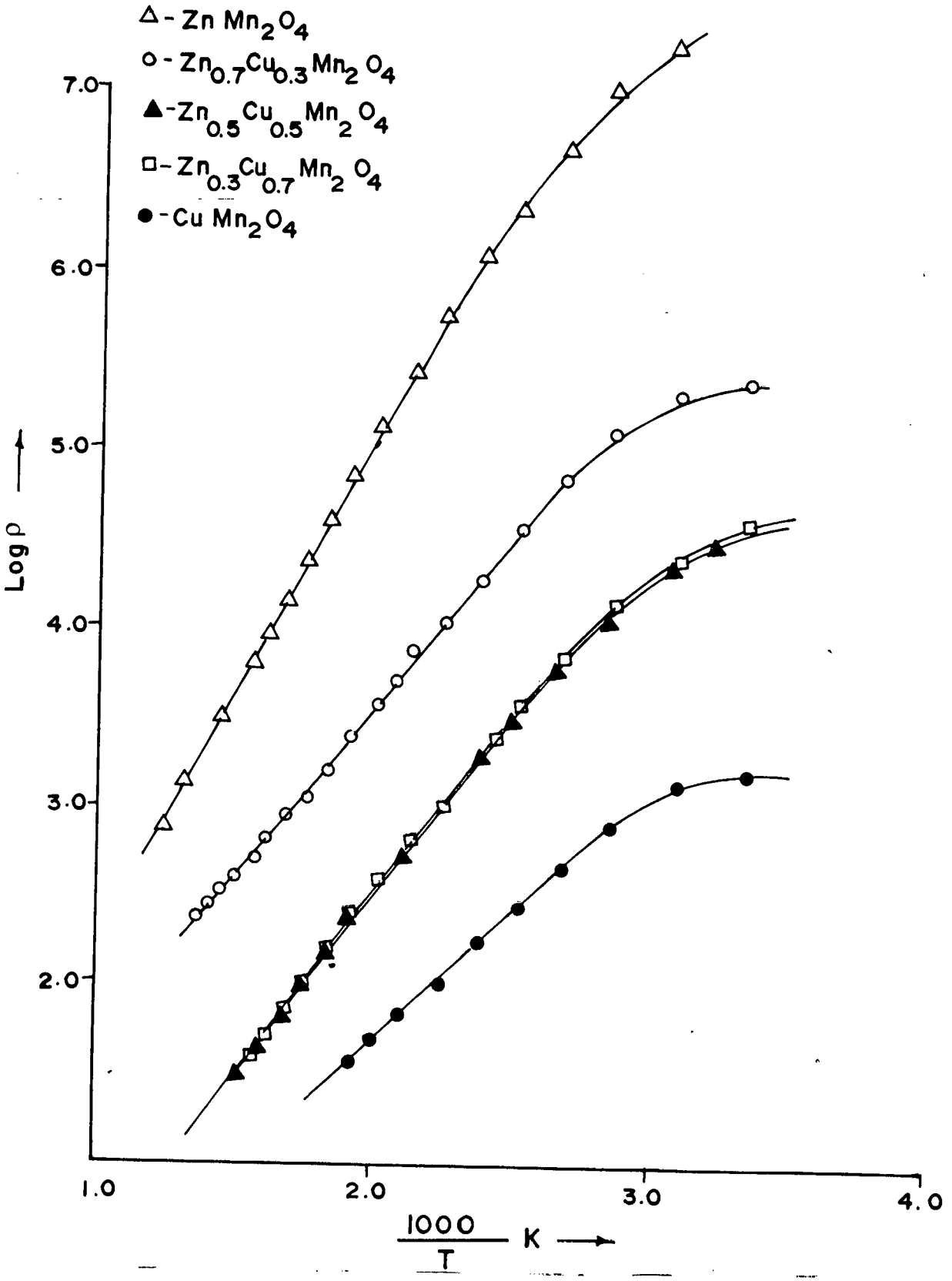

Fig. 4.12. Variation of electrical resistivity of $Zn_{1-x}Cu_xMn_2O_4$ with temperature

copper content rather than nickel at a given temperature. From the literature it is seen that B-site cations are responsible for electrical conduction in spinels by virtue of symmetry. Thus more significant B-B interactions determines the electrical conduction. From this it is tempted to conclude that a conductivity in manganite spinels is due to manganese ions present on the Oh site of the lattice, it is also found to depend on site symmetry from earlier reports[59, 60].

According to Verwey and co-workers[212] for high electrical conductivity in transition metal oxides is that, the material must contain cations of the same element with oxidation number differing by unity situated at a similar site in crystal structure which were called as mixed valence semiconductors. The electrical conductivity cannot be explained in copper manganite with ionic structure $Cu^{2+}[Mn_2^{3+}]O_4^{2-}$, since electron cannot be transferred from Mn^{3+} ion to another Mn^{3+} ion. In $Ni_{1-x}Cu_xMn_2O_4$, p-type conductivity was observed by many investigators for all the compositions except at x = 0. However, Mulla and Darshane[63] reported that in $NiMn_2O_4$, when $Mn^{3+} < Mn^{4+}$ it exhibits n-type conductivity and when $Mn^{3+} > Mn^{4+}$ it was observed to be p-type.

In series -II, ($Zn_{1-x}Cu_xMn_2O_4$) only p-type conductivity is likely to be observed throughout the series, since $ZnMn_2O_4$ is being reported as p-type and $CuMn_2O_4$ which is also a p-type. Resistivity versus Temperature behaviour plot show a linear variation for all the compositions as observed

by Kshirsagar[47] as well as Bhandage and Keer[31]. An unexpected improvement in the value of conductivity was observed at x = 0.5 over x = 0.7. Similar observations were also made by Larson and Arnot[59] for n-p type semiconductors. Such phenomena is also observed in series-II, however it is not that prominent as in series-I.

Rosenberg[60] observed that gradual increase of Mn^{4+} quantity in Oh sublattice causes the decrease of resistivity and energy of activation for conduction. Thus the observed conductivity in manganites could be explained on the basis of Mn^{4+}-Mn^{3+} ion pair association which is in agreement with many authors[36, 42, 213 - 215]. The result can be easily explained on the basis of an electron transfer process shown by Sinha et al[29] as

$$Cu^{2+} + Mn^{3+} \longrightarrow Cu^{1+} + Mn^{4+}.$$

comparatively high resistivity was observed for compositions with small x-value which may be due to low concentration of Mn^{3+}-Mn^{4+} ion pairs resulting in the large average distance between equivalent sites available for hopping. With increase in copper content in solid solution the number of Mn^{3+}-Mn^{4+} ion pairs, at B-site increases, resulting in the corresponding decrease of resistivity which is an inverse function of Mn^{4+} ion concentration.

Nickel manganite is known to have cubic inverse spinel structure with Ni^{2+} occupying octahedral B-site. Following are the ionic structures for $NiMn_2O_4$ which are supported by many investigators[45, 48, 59, 216, 217].

1) $Mn^{2+}[Ni^{2+}Mn^{4+}]O_4^{2-}$ 2) $Mn^{3+}[Ni^{2+}Mn^{3+}]O_4^{2-}$

However, according to Laberty[65] occupation of Oh site by Ni^{2+} reduces Mn^{3+}/Mn^{4+} redox couples on the same lattice site which are the cause for good electrical conductivity of nickel manganites. $Mn^{2+}[Ni^{2+}Mn^{4+}]O_4^{2-}$ does not account for good electrical conductivity, which implies that a part of Ni^{2+} cations must be in tetrahedral (Td) site.

According to the recent studies carried out by Asbrink[218] the distribution of cations in $NiMn_2O_4$ can be represented as $(Ni_{1-v}^{2+}Mn_{v/2}^{2+})[Ni_v^{2+}Mn_{2-v}^{3+}Mn_{v/2}^{4+}]O_4^{2-}$ (where $v = 0.87$ at 115 K and 0.8 at R.T.). Thus the observed low conductivity in $NiMn_2O_4$ could be explained due to Mn^{3+}-Mn^{4+} ion pair association on the basis of above ionic distribution. Higher conductivity in $CuMn_2O_4$ can be attributed to the tetrahedrally located Cu^{2+} and Cu^{1+} ions besides Mn^{3+}-Mn^{4+} ion pairs which have been considered by Kshirsagar[47] with the ionic structure conveniently represented as

$$Cu_{1-z}^{2+}Cu_z^{1+}[Mn_{2-z}^{3+}Mn_z^{4+}]O_4^{2-} \quad (0 < z < 0.1)$$

Bhandage and Keer[23] have proposed the following configuration for $CuMn_2O_4$ based on structural, electrical and magnetic behaviour.

$$(Cu_{1-y-z}^{+}Cu_z^{2+}Mn_y^{3+})[Cu_y^{2+}Mn_{1+z}^{3+}Mn_{1-y-z}^{4+}]O_4^{2-} \quad (\text{where } y = 0.3, z = 0.1)$$

Resistivity versus Temperature plot for series -II also shows similar behaviour as in series-I. With the increase in x-value resistivity is found to decrease for variable compositions at constant temperature. Decrease in resistivity with increase in copper content is known due to Mn^{3+}-Mn^{4+} ion pairs. $ZnMn_2O_4$ is expected to exhibit relatively higher resistivity on account of its normal symmetry and strong tendency to occupy tetrahedral site, further Zn cannot be so easily reduced unlike copper in $CuMn_2O_4$. Thus the observed high resistivity of $ZnMn_2O_4$ can be explained as due to tetragonal symmetry, which is in agreement with the earlier reports[59].

4.4 MAGNETIC SUSCEPTIBILITY MEASUREMENT

The magnetic susceptibility of different compounds were determined by Guoy balance at room temperature, using a field strength of 10,000 gauss. The magnetic moments in Bohr magneton were calculated using an expression μ_{eff} (B.M) = $2.84\sqrt{\chi_m}.T$. where $\sqrt{\chi_m}$ is the molar magnetic susceptibility at room temperature .

The observed gram susceptibility values at room temperature are presented in table 4.1 for series -I, II and III. Gram susceptibility values for

Table 4.1 Magnetic Susceptibility data of different spinels

Sr. No.	Catalysts	χ_g	μ_{eff} (B.M.)
1	$NiMn_2O_4$	5.906×10^{-5}	5.7652
2	$Ni_{0.7}Cu_{0.3}Mn_2O_4$	6.123×10^{-5}	5.8884
3	$Ni_{0.5}Cu_{0.5}Mn_2O_4$	5.637×10^{-5}	5.6615
4	$Ni_{0.3}Cu_{0.7}Mn_2O_4$	5.785×10^{-5}	5.7472
5	$CuMn_2O_4$	6.084×10^{-5}	5.9119
6	$ZnMn_2O_4$	3.988×10^{-5}	4.8048
7	$Zn_{0.7}Cu_{0.3}Mn_2O_4$	4.552×10^{-5}	5.1274
8	$Zn_{0.5}Cu_{0.5}Mn_2O_4$	5.0623×10^{-5}	5.4031
9	$Zn_{0.3}Cu_{0.7}Mn_2O_4$	5.446×10^{-5}	5.5998
10	$CoMn_2O_4$	4.454×10^{-5}	5.0090
11	$Co_{0.7}Cu_{0.3}Mn_2O_4$	4.675×10^{-5}	5.1470
12	$Co_{0.5}Cu_{0.5}Mn_2O_4$	5.130×10^{-5}	5.4022
13	$Co_{0.3}Cu_{0.7}Mn_2O_4$	5.540×10^{-5}	5.6249

$Ni_{1-x}Cu_xMn_2O_4$ are in the range of 5.637×10^{-5} to 6.123×10^{-5}. Susceptibility values increase gradually with increase in x-values for $Zn_{1-x}Cu_xMn_2O_4$ and $Co_{1-x}Cu_xMn_2O_4$.

The higher value of magnetic susceptibility for $CuMn_2O_4$ may be due to copper ions present in the system. The presence of Cu^{2+} and Mn^{3+} ions in the spinel which have substantial additional Jahn-Teller stabilisation on interaction, results in the formation of ion pairs Mn^{3+}-Mn^{4+} along with Cu^{1+} or Cu^{1+} and Cu^{2+}. Formation of Mn^{3+}-Mn^{4+} accounts for the higher magnetic susceptibility which is observed for different compositions containing higher copper content. With the increase in concentration of $CuMn_2O_4$, B-B interaction becomes more stronger with increasing Mn^{3+}-Mn^{4+} ion pairs, there by resulting in a increase of susceptibility. Relative strength of A-sited ions in stabilizing tetragonal distortion of the lattice by B-sited Mn^{3+} ion is given by Kshirsagar and Biswas[37] as $Zn^{2+}>Mn^{2+}>Co^{2+}>Cd^{2+}>Mg^{2+}$. A-sited Zn^{2+} stabilizes the tetragonal distortion much strongly than Co^{2+}. Thus lower values of magnetic susceptibility for $ZnMn_2O_4$ and $CoMn_2O_4$ can be explained on the basis of tetragonal stabilisation.

In series $Zn_{1-x}Cu_xMn_2O_4$ and $Co_{1-x}Cu_xMn_2O_4$ as x-value increases, symmetry changes from tetragonal to cubic form, which gets reflected into their magnetic susceptibility values. This explains higher magnetic susceptibilities for cubic systems like $CuMn_2O_4$ and $NiMn_2O_4$ and lower values for $ZnMn_2O_4$ and $CoMn_2O_4$ which are tetragonal. In $Ni_{1-x}Cu_xMn_2O_4$

the symmetry is cubic throughout the system thus showing a small variation in the susceptibility values.

4.5 ESR STUDIES

ESR studies carried out for various samples gave an insight about the catalytically active and paramagnetic species. The technique was used as qualitative tool to ascertain the presence of Cu^{2+} ions on B-site. ESR data of different spinels is presented in table 4.2. The g-values of ESR spectra for $Ni_{1-x}Cu_xMn_2O_4$ gradually increases with increase in x-value. As the manganese content is constant throughout the series the variation in g-value may be due to copper. Similar phenomena was also observed for series-II ($Zn_{1-x}Cu_xMn_2O_4$). A very weak ESR signal for $CoMn_2O_4$ is recorded. However at x = 0.5 ($Co_{0.5}Cu_{0.5}Mn_2O_4$) a peak was recorded with g-value of 2.2876. ESR spectra of representative samples are shown in fig. 4.13 - 4.15

In a series of $Ni_{1-x}Cu_xMn_2O_4$ decrease in g-value of ESR with increase in x indicates that there is improvement in the activity of spinels which could be due to Cu^{2+} ions. Since Cu^{2+} ions have a strong octahedral site preference, it is expected to occupy B-site in AB_2O_4 spinel system. Ni^{2+} ions also have a strong Oh site preference thus more of Ni^{2+} is expected to occupy B-site. Our results of ESR show that copper is the active species in the series-I, in which g-value observed for $NiMn_2O_4$ is 2.3288 and for $CuMn_2O_4$ it is 1.9570. Results of ESR carried out for $Ni_{1-x}Cu_xMn_2O_4$ are in

Scan Range : 4000 G, Time Constant : 0.128 sec, Modulation Amplitude : 0.5 G
Field Set : 3220 G, Temperature : R.T., Modulation Frequency : 100 KHz
Microwave Power : 0.1 mW, Microwave Frequency : 49.08 Ghz.

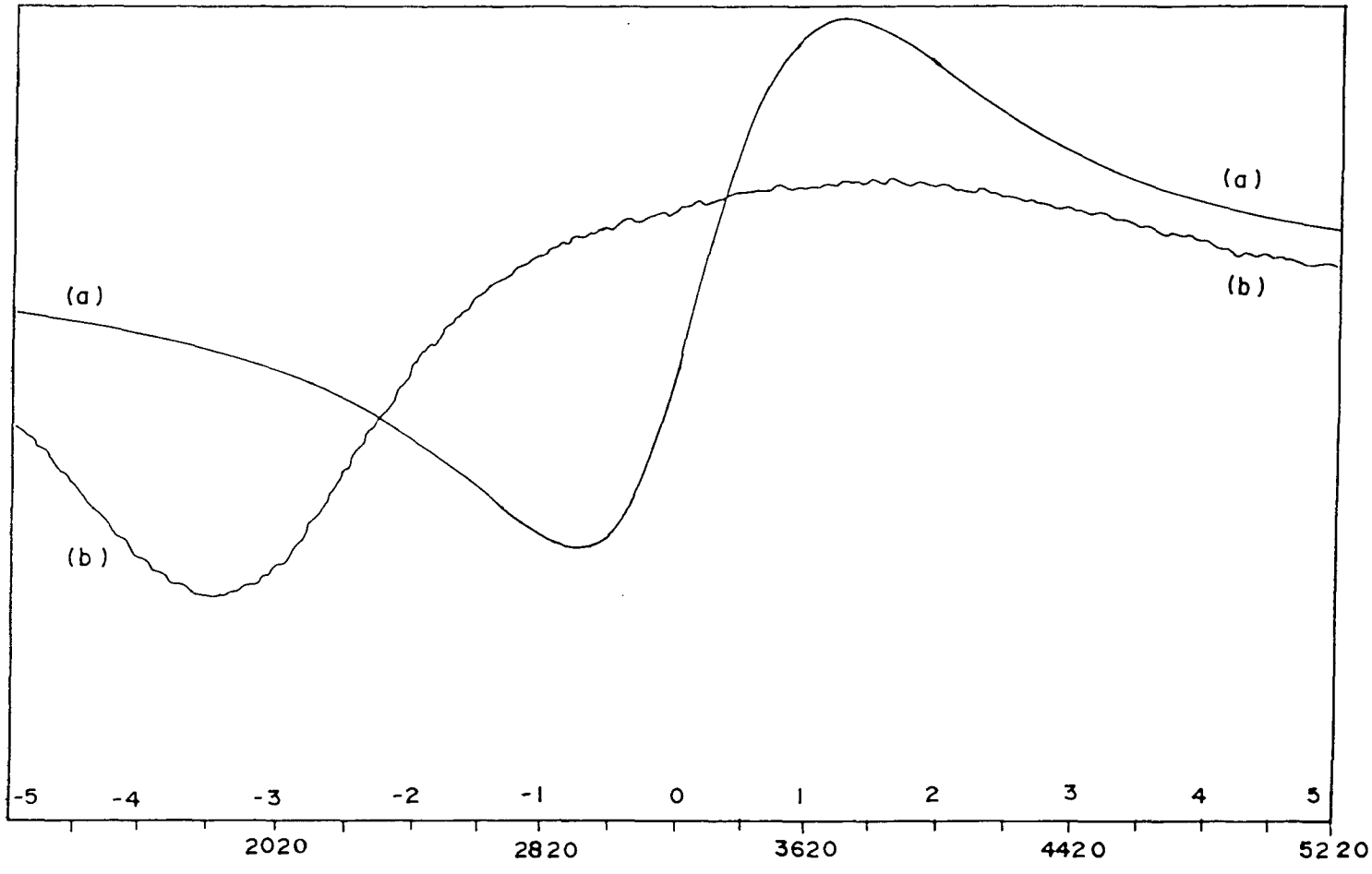

Fig. 4.13. ESR spectra of (a) $CuMn_2O_4$ and (b) $ZnMn_2O_4$

Scan Range : 4000 G, Receiver Gain : 5 x 10^2 x 10, Modulation Amplitude : 0.5 G
Field Set : 3220 G, Temperature : R.T., Modulation Frequency : 100 KHz
Microwave Power : 1.0 mW, Microwave Frequency : 49.08 GHz

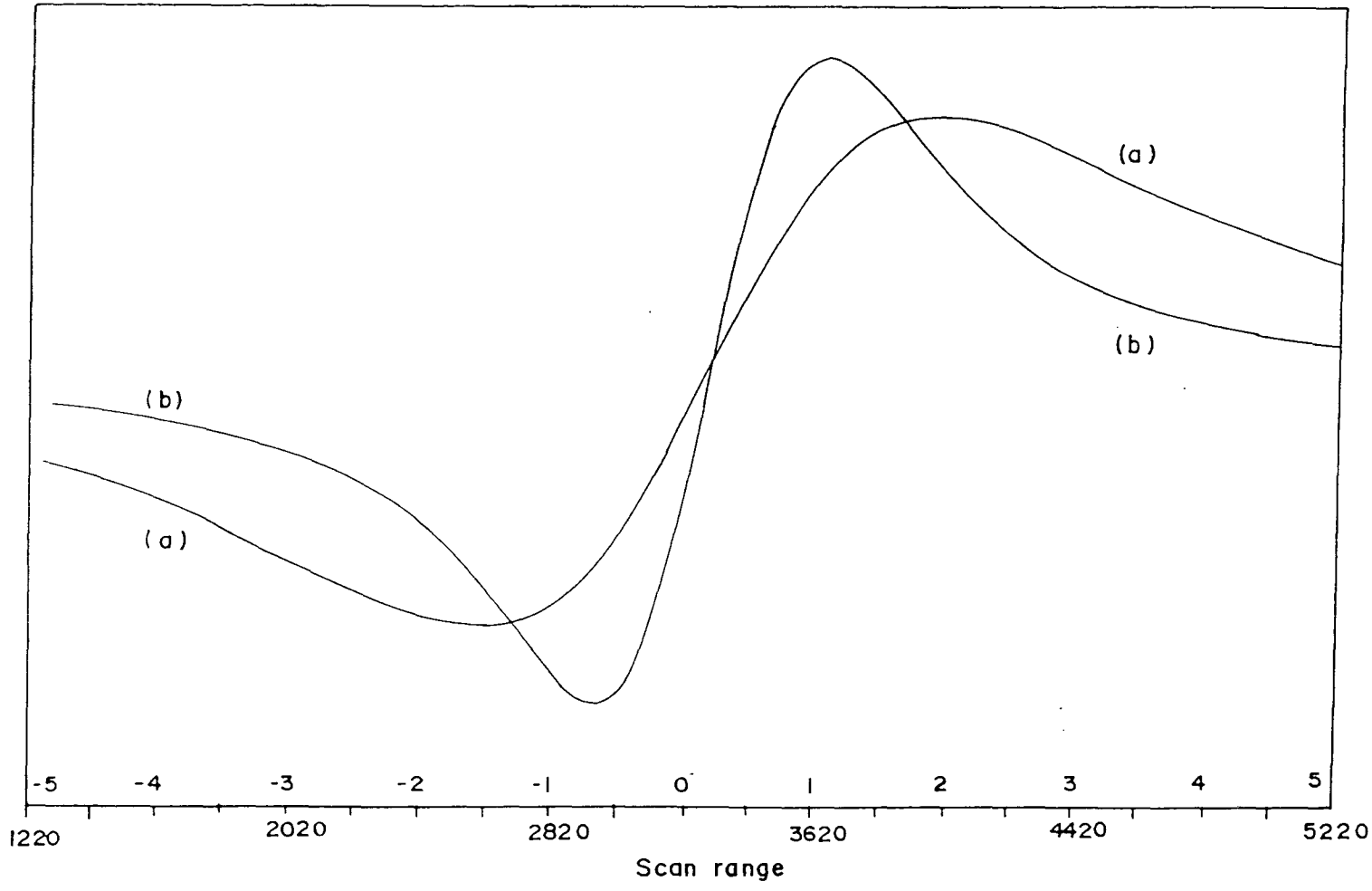

Fig. 4.14. ESR spectra of (a) $Zn_{0.5}Cu_{0.5}Mn_2O_4$ and (b) $Zn_{0.3}Cu_{0.7}Mn_2O_4$

Scan Range : 4000 G, Receiver Gain : $3.2 \times 10^2 \times 10$ Modulation Amplitude : 0.5 G
Field Set : 3220 G, Temperature : R.T., Modulation Frequency : 100 KHz
Microwave Power : 5 mW, Microwave Frequency : ~ 9.07 GHz

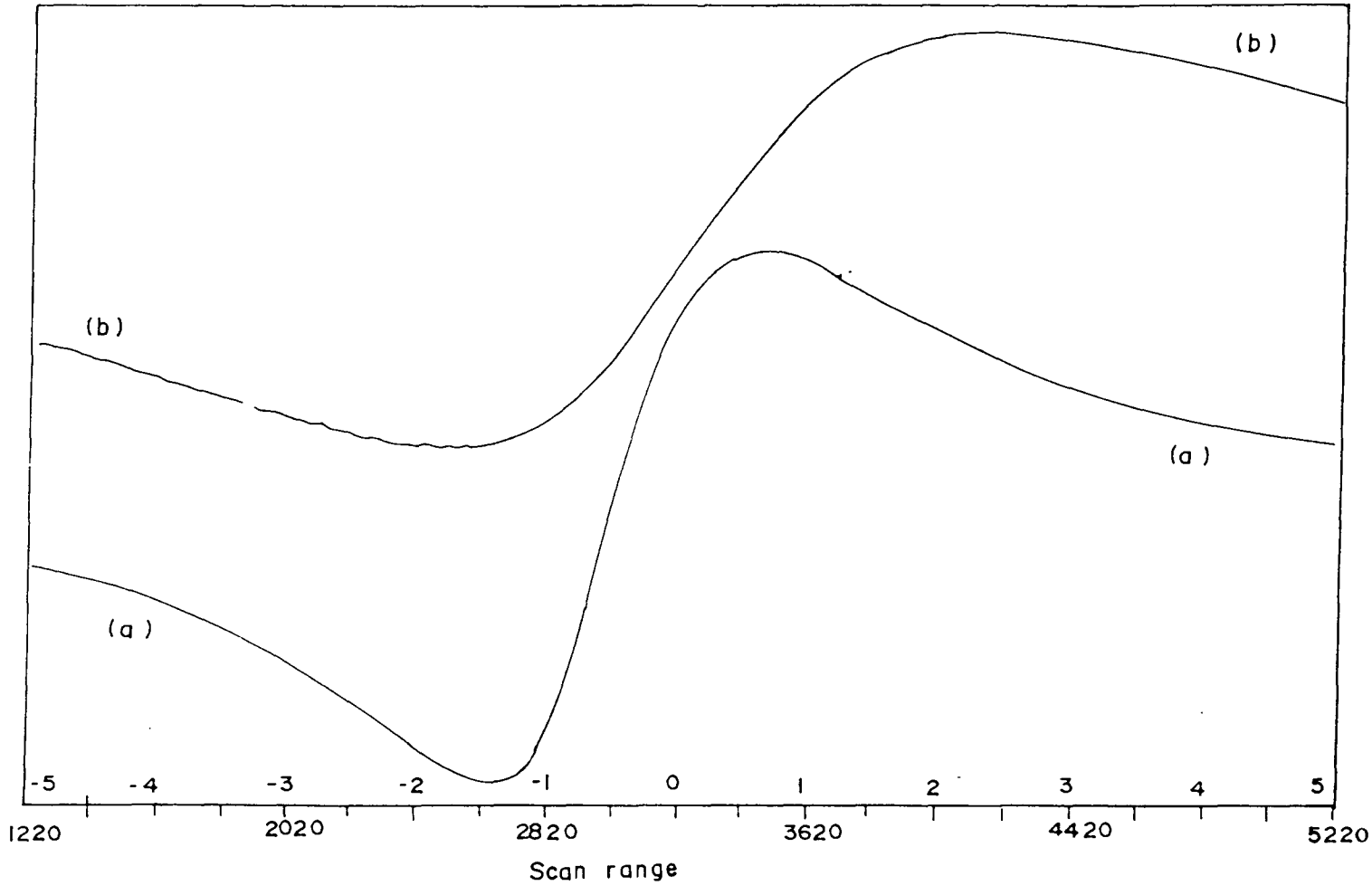

Fig. 4.15. ESR spectra of (a) $Ni_{0.7}Cu_{0.3}Mn_2O_4$ and (b) $Ni_{0.5}Cu_{0.5}Mn_2O_4$

Table 4.2 ESR data of different spinels

Sr. No.	Catalysts	g-Value	Line width (gauss)
1	$NiMn_2O_4$	2.3288	1070
2	$Ni_{0.7}Cu_{0.3}Mn_2O_4$	2.1173	800
3	$Ni_{0.5}Cu_{0.5}Mn_2O_4$	1.9808	1484
4	$Ni_{0.3}Cu_{0.7}Mn_2O_4$	1.9604	1950
5	$CuMn_2O_4$	1.9570	780
6	$ZnMn_2O_4$	2.7231	1080
7	$Zn_{0.7}Cu_{0.3}Mn_2O_4$	1.9889	1015
8	$Zn_{0.5}Cu_{0.5}Mn_2O_4$	1.9723	1310
9	$Zn_{0.3}Cu_{0.7}Mn_2O_4$	1.9675	660
10	$CoMn_2O_4$	v. w signal	---
11	$Co_{0.5}Cu_{0.5}Mn_2O_4$	2.2876	1440

consistent with the earlier reports of Bhandage and Keer[31]. From ESR studies they have confirmed that Ni is present at B-site only, where as part of divalent Cu occupies an Oh site. Results of ESR obtained for series -II ($Zn_{1-x}Cu_xMn_2O_4$) are also in consistent with reports[23]. There is a large variation in g-value from 2.7231 for $ZnMn_2O_4$ to 1.9889 for $Zn_{0.7}Cu_{0.3}Mn_2O_4$, with partial substitution of Zn by Cu, indicating that copper manganite is relatively more ESR active among the different compositions within the series and $ZnMn_2O_4$ is least active. In series-III. ($Co_{1-x}Cu_xMn_2O_4$) g = 2.2876 for x = 0.5 was found to be higher than g = 1.9570 for x = 1.0. Substitution of Co by Cu show an improvement in ESR activity which may be due to large number of free electrons from copper. Presence of a considerable amount of Cu^{2+} ions observed on B-site tempted Bhandage and Keer[23] to arrive at the following ionic configuration for $CuMn_2O_4$

$$Cu_{1-y-z}^{+}Cu_z^{2+}Mn_y^{3+}[Cu_y^{2+}Mn_{1+z}^{3+}Mn_{1-y-z}^{4+}]O_4^{2-}.$$

Our results of ESR and electrical conductivity are fully in agreement with the above ionic structure.

From the overall study of ESR spectroscopy it can be inferred that the substitution of Ni, Zn, or Co by Cu enhances ESR signal. The activity may be attributed to the catalytically active copper species in the lattice which exhibits paramagnetism in its divalent oxidation.

CHAPTER 5

CATALYTIC CARBON MONOXIDE OXIDATION

CATALYTIC CARBON MONOXIDE OXIDATION

The transition metal oxide spinels provide an excellent base for correlating catalytic and solid state properties, because they can be well characterised by different techniques. In this chapter the catalytic activity of series of manganite spinels with effect of A-site substitution is being discussed with respect to CO oxidation, separately for series-I ($Ni_{1-x}Cu_xMn_2O_4$), series-II ($Zn_{1-x}Cu_xMn_2O_4$), series-III ($Co_{1-x}Cu_xMn_2O_4$) and series-IV ($Ni_{1-x}Co_xMn_2O_4$). Though this reaction is extensively studied over noble metal oxides and other oxide catalyst, it is not well studied over manganite spinels. This reaction is also significant from the point of automobile exhaust pollution control.

5.1 SURFACE AREA

The surface area of the samples were measured by BET nitrogen adsorption at the boiling liquid nitrogen temperature employing an instrument ANY GAS VERSION 2.10 using Quantachrome Autosorb Automated Gas Adsorption system, the results are summarised in table 5.1. The compounds prepared by co-precipitation technique possessed the surface area as low as 1.46 m^2/g and as high as 8.9 m^2/g. The low surface area of some of the compounds may be due to more sintering. The nitrogen adsorption is not quite a satisfactory method for absolute measurement of low surface area and as such the variation seen among the different compositions are within the experimental errors.

5.2 CATALYTIC ACTIVITY

The catalytic oxidation of CO was studied in a fixed bed flow reactor of which detail has been described in chapter-3. One gram of the catalyst was placed between glass wool plugs. Catalyst is initially heated at 523 K in O_2 atmosphere for about half an hour to remove any moisture present. To check CO conversion, reaction is started at room temperature with requisite quantity of CO, O_2 and N_2. At each temperature the catalyst was maintained for about half an hour with the flowing reaction mixture and then the series of injection were made in the gas chromatograph at an interval of ten minutes. The increase in activity is expressed in terms of the percentage

Table 5.1 Specific surface area of the prepared catalysts

Sr. No	Catalysts	Surface area (m^2/gm)
1	$NiMn_2O_4$	5.60
2	$Ni_{0.7}Cu_{0.3}Mn_2O_4$	5.40
3	$Ni_{0.5}Cu_{0.5}Mn_2O_4$	3.20
4	$Ni_{0.3}Cu_{0.7}Mn_2O_4$	5.40
5	$CuMn_2O_4$	4.32
6	$ZnMn_2O_4$	1.46
7	$Zn_{0.7}Cu_{0.3}Mn_2O_4$	2.97
8	$Zn_{0.5}Cu_{0.5}Mn_2O_4$	6.42
9	$Zn_{0.3}Cu_{0.7}Mn_2O_4$	4.95
10	$CoMn_2O_4$	7.76
11	$Co_{0.7}Cu_{0.3}Mn_2O_4$	6.00
12	$Co_{0.5}Cu_{0.5}Mn_2O_4$	6.69
13	$Co_{0.3}Cu_{0.7}Mn_2O_4$	6.50
14	$Ni_{0.7}Co_{0.3}Mn_2O_4$	8.90
15	$Ni_{0.5}Co_{0.5}Mn_2O_4$	7.60
16	$Ni_{0.3}Co_{0.7}Mn_2O_4$	8.40

conversion of CO with temperature for different compositions. Kinetic data were also evaluated on some of the catalyst.

5.2.1 Series-I : Nickel copper manganite ($Ni_{1-x}Cu_xMn_2O_4$)

The temperature dependence of CO conversion studied over different compositions of $Ni_{1-x}Cu_xMn_2O_4$ (x = 0.0, 0.3, 0.5, 0.7, 1.0) is shown in fig. 5.1. The rate of CO conversion increases with increase in 'x' value till x = 0.5, further increase in 'x' value declines the CO conversion rate. Thus $Ni_{0.5}Cu_{0.5}Mn_2O_4$ exhibits relatively higher CO oxidation efficiency among the different compositions within the series-I. For arriving at any correlation between catalytic behaviour and other properties the kinetic measurements of different compositions were carried out at low conversion rate and in the low temperature region. Fractional conversion of CO (X_{co}) versus W/F_{CO} where 'W' is the mass of the catalyst taken and F_{CO} is the number of moles of CO flowing per hour, at different temperatures is shown for a representative sample in fig. 5.2 and 5.3 A linear variation of the conversion was observed with decreasing flow rate. The rates calculated from such plots are shown as Arrhenius plots in fig. 5.4. The kinetic parameters such as the reaction rates, the activation energy (E_a) and frequency factor (A) were evaluated from the Arrhenius plots and are summarised in table 5.2.

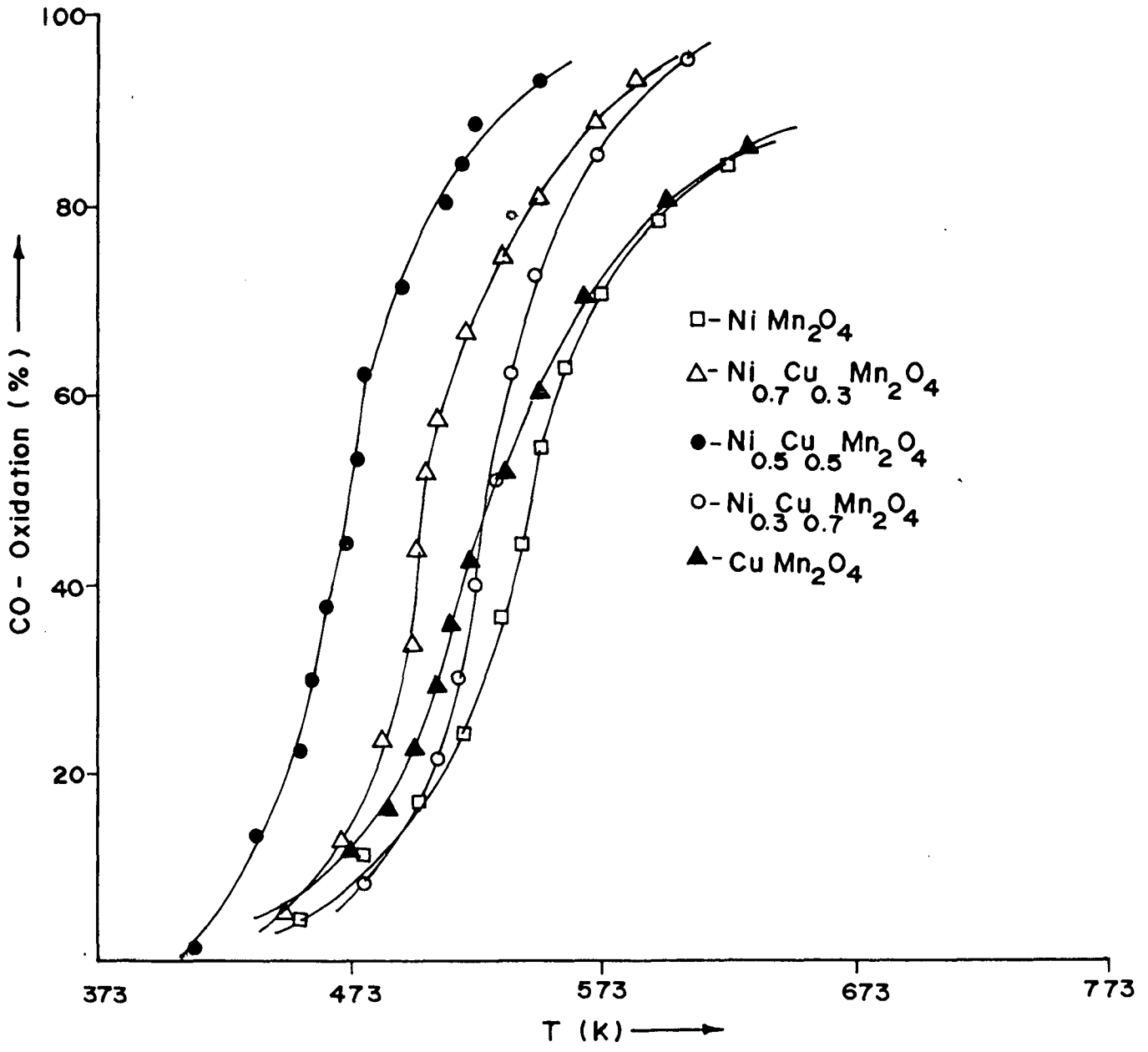

Fig. 5.1. CO conversion as a function of catalyst temperature for $Ni_{1-x}Cu_xMn_2O_4$

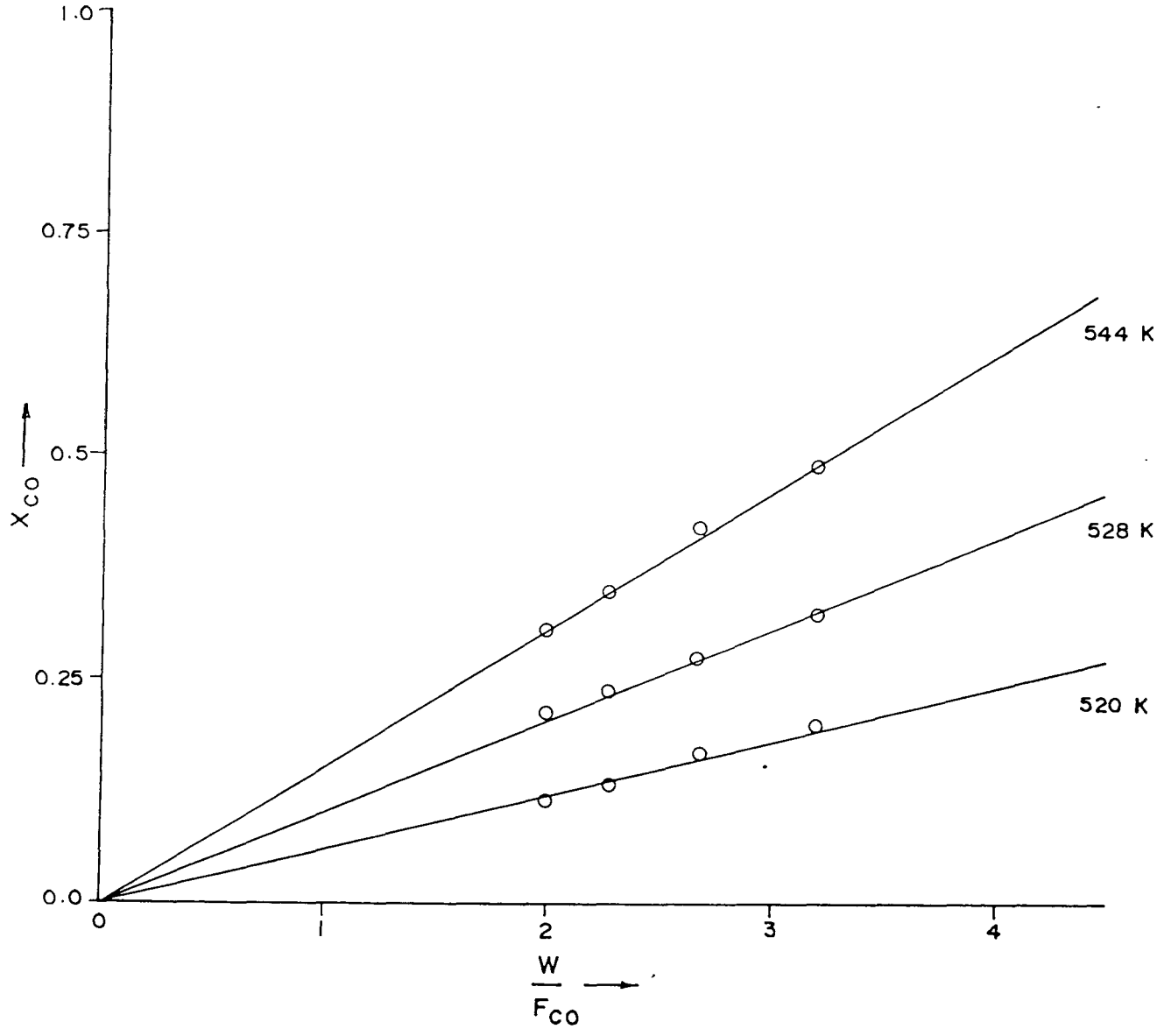

Fig. 5.2. Resident time plot for the representative sample of $NiMn_2O_4$

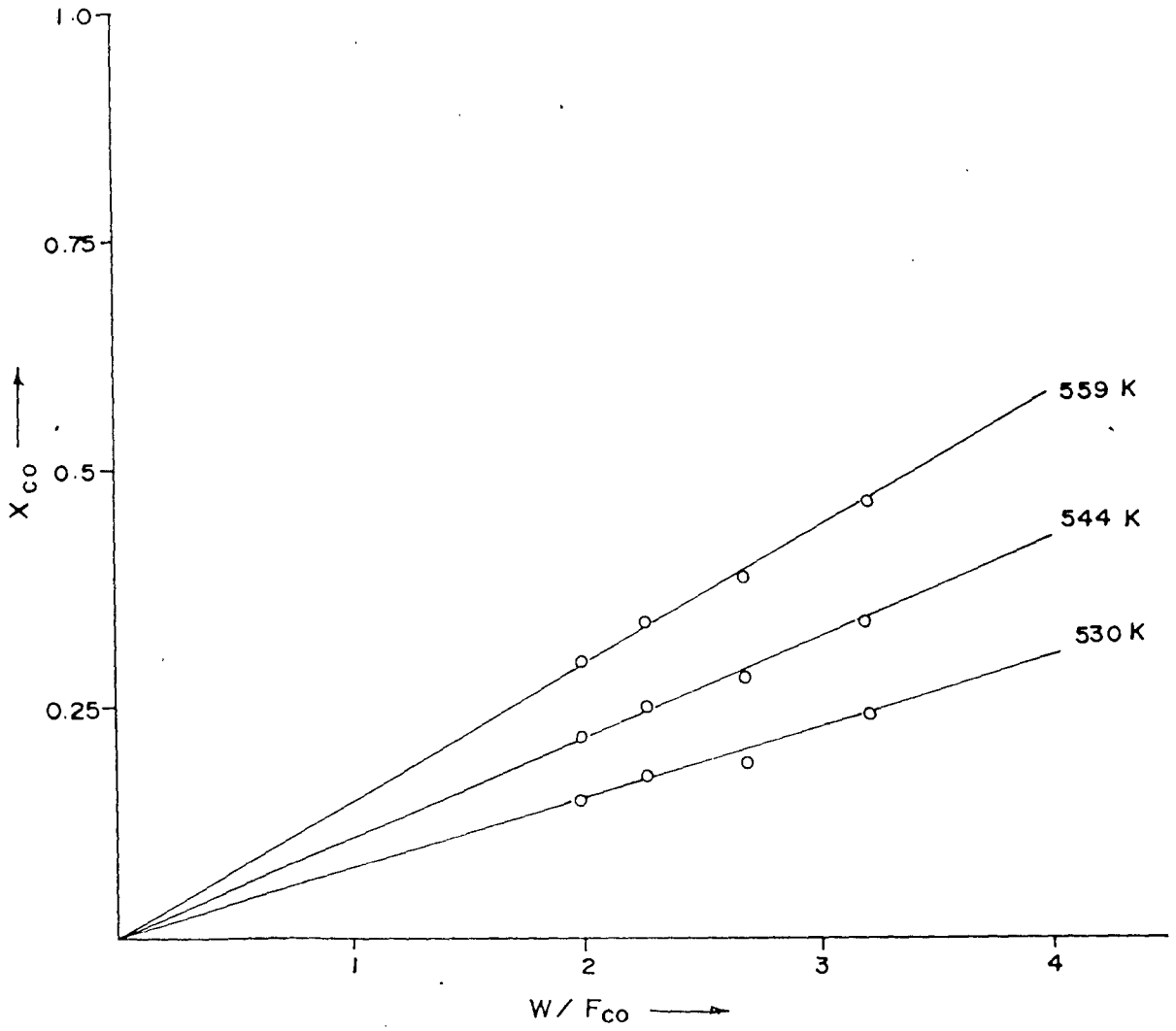

Fig. 5.3. Resident time plot for the representative sample of $Ni_{0.3}Cu_{0.7}Mn_2O_4$

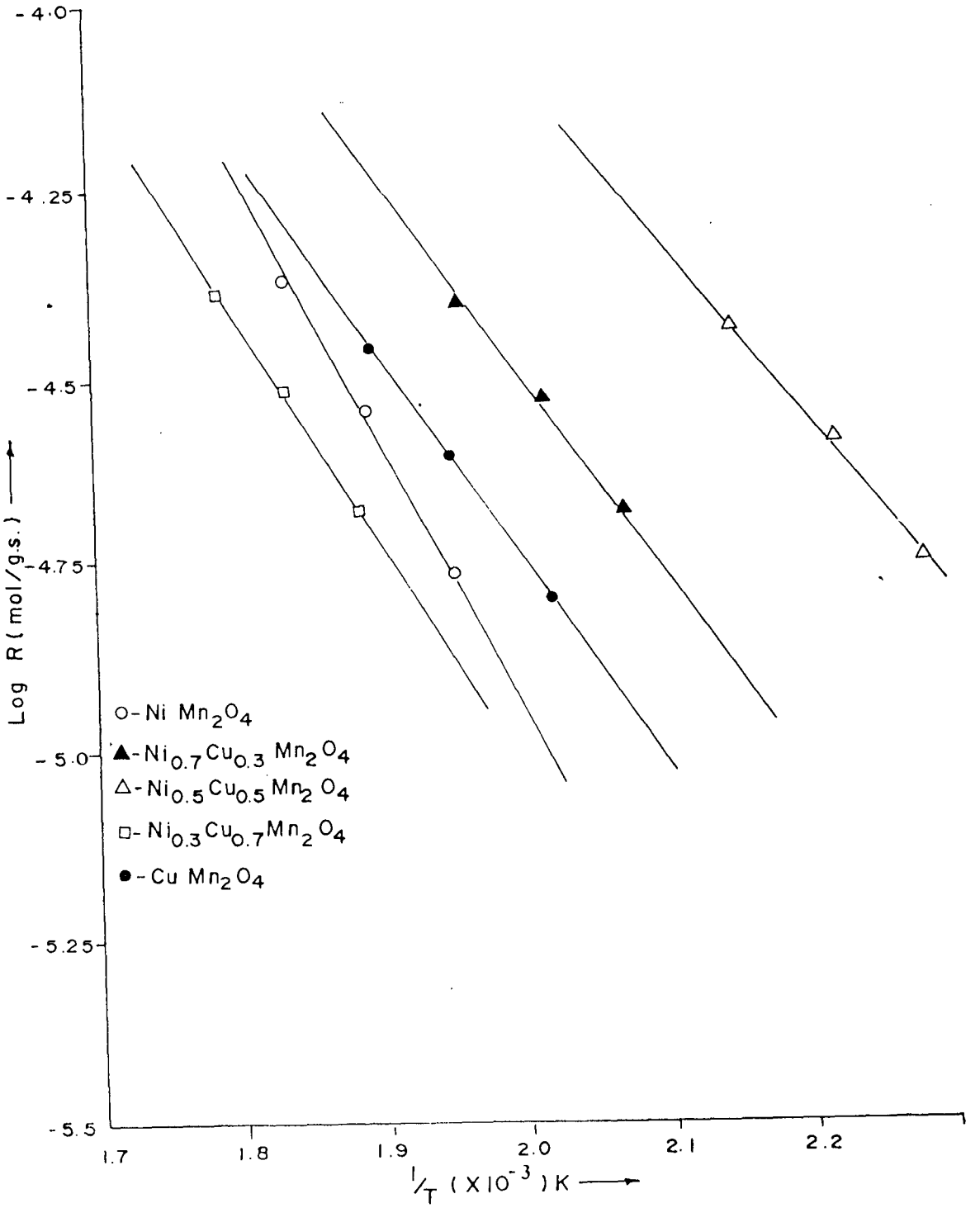

Fig. 5.4. Arrhenius plot for $Ni_{1-x}Cu_xMn_2O_4$

Table 5.2 Kinetic parameters of CO oxidation over different catalysts

Sr. No.	Catalysts	Surf. area (m^2/g)	Temp (°K)	Rate (Molec./m^2.s)	Ea (kcal/mol)	Freq. factor (Molec./m^2.s)
1	$NiMn_2O_4$	5.6	512	$1.8284x10^{18}$	16.510	$1.8585x10^{18}$
2	$Ni_{0.7}Cu_{0.3}Mn_2O_4$	5.4	483	$2.3236x10^{18}$	12.254	$2.3537x10^{18}$
3	$Ni_{0.5}Cu_{0.5}Mn_2O_4$	3.2	440	$3.5136x10^{18}$	11.014	$3.5582x10^{18}$
4	$Ni_{0.3}Cu_{0.7}Mn_2O_4$	5.4	530	$2.3236x10^{18}$	13.769	$2.3544x10^{18}$
5	$CuMn_2O_4$	4.32	495	$2.1920x10^{18}$	12.593	$2.2202x10^{18}$

Discussion

In a series of $Ni_{1-x}Cu_xMn_2O_4$, composition with x = 0.5 exhibits highest activity in terms of CO oxidation followed by 0.3 > 0.7 > 1.0 > 0.0. The end compositions i.e. $NiMn_2O_4$ and $CuMn_2O_4$ showed lower activities. The CO conversion shown by intermediate compositions are relatively much higher than the end compositions. The higher activities can be attributed to the phenomena of synergism[164], which results from the co-operative effect of two different metal ions i.e. nickel and copper in their divalent state placed on A-site of AB_2O_4 spinel.

The interpretation of trend in catalytic activity of intermediate compositions towards CO oxidation is quite complicated due to presence of three different metal ions, as also large number of factors such as thermodynamic and kinetic parameters, site preference energies, preferential surface enrichment etc. play significant role in deciding the overall performance of such catalysts.

Some recent studies on mixed catalyst of manganese and copper have shown that at the surface of the catalyst copper ions are partially reduced by manganese ions and this cause low activities of Mn containing mixed oxides[165, 219]. However, partial replacement of copper by nickel creates a large number of Ni^{2+} and Mn^{4+} ions on the octahedral site due to their site preference energies, thus displacing Mn^{3+} ions on tetrahedral site, which is in agreement with earlier reports[18, 31].

Thus the observed catalytic activity may be due to Ni^{2+} ions besides Cu^{2+} ions. Though copper is active in its dipositive oxidation state for CO oxidation, but unexpectedly the activity is found to be lower inspite of large copper content as observed for x = 0.7, this may be due to the surface enrichment of manganese over copper as reported by Yang et al[219]. This also explains the low rate of CO oxidation over $CuMn_2O_4$ compared to the intermediate compositions.

Substitution of nickel in the lattice of $NiMn_2O_4$ by copper which shows a continuous rise in CO conversion till x = 0.5 clearly indicates that the substitution is much effective and significant, and the observed rise in CO conversion can be said to be due to increase in Cu content in $NiMn_2O_4$. Considering the composition $Ni_{0.3}Cu_{0.7}Mn_2O_4$, low activity was observed at temperatures below 523 K. Effect of copper at this composition becomes prominent at high temperature above 523 K. This suggests that there may be transformation of Cu^{1+} + Mn^{4+} to Cu^{2+} + Mn^{3+} occurring at high temperature, creating more number of active sites, which is in agreement with earlier reports[215]. Further the higher activity of $Ni_{0.3}Cu_{0.7}Mn_2O_4$ in comparison with lower activity of $CuMn_2O_4$ at 548 K reveals that the increased CO conversion is due to Ni^{2+} ions. Thus the low temperature CO conversion can be attributed to nickel rather than copper which is partly in its reduced state as Cu^{1+}. The presence of manganese which is constant throughout the series also affects the overall activity to some extent, since

the presence of nickel and copper in their different oxidation state give rise to manganese species in oxidation state such as Mn^{2+}, Mn^{3+} and Mn^{4+}. Therefore, though not significant, variable contribution of Mn ions towards CO oxidation for different compositions is also to be considered. Study reveals that it is a co-operative effect of two metals which give pronounced change in CO conversion at x = 0.5 at all the temperatures, thus indicating the typical phenomena of synergism which occurs by breaking the activation energy barrier of both limiting steps.

Our data of electrical conductivity , electron spin resonance and magnetic susceptibility is in agreement with the ionic structure arrived earlier for $CuMn_2O_4$ and $NiMn_2O_4$ i.e.

I $\quad Cu_{0.6}^{+}Cu_{0.1}^{2+}Mn_{0.3}^{3+}[Cu_{0.3}^{2+}Mn_{1.1}^{3+}Mn_{0.6}^{4+}]O_4^{2-}$

II $\quad Ni_{1-v}^{2+}Mn_{v/2}^{2+}[Ni_{v}^{2+}Mn_{2-v}^{3+}Mn_{v/2}^{4+}]O_4^{2-}$ (where $v = 0.8$ at R.T.)

Based on these ionic structures the catalytic oxidation of CO can be attributed to more active Cu species in their divalent state which have occupied octahedral sites. This is in accordance with the reports[220], that octahedral sites are exposed exclusively at the surface of the spinel oxide and only these sites participates in reaction. Similarly CO conversion over $NiMn_2O_4$ can be explained due to octahedrally exposed Ni^{2+} ions. In the

above ionic structure some of the copper ions (Cu^{2+}) are also seen on the tetrahedral sites. Some of the investigators[166] have reported that activity of Cu^{2+} ions on tetrahedral site is more than octahedral sites on account of their large susceptibility for reduction. The above ionic structure explains the contribution of Cu^{2+} ions from tetrahedral site also towards CO oxidation. The presence of manganese in either of the oxidation states also helps to explain oxidation reaction via adsorption.

Activation energy for $Ni_{0.5}Cu_{0.5}Mn_2O_4$ is found to be lowest i.e. 11.014 kcal/mol in this series with highest rate of reaction. Also the highest value of frequency factor explains the exposure of large number of active sites on the surface of the catalyst. The lowest frequency factor for $NiMn_2O_4$ i.e. 1.8585×10^{18} molec/m^2s with its low catalytic activity is attributed to nickel ions (Ni^{2+}). Further the improvement in the activity of $NiMn_2O_4$ by addition of little quantity of copper indicates that the activity rise is due to available copper and nickel sites for the reaction. Approximately same frequency factor for composition with x = 0.3 and 0.7 confirms that Ni^{2+} as well as Cu^{2+} ions participates in surface oxidation reaction. However, minor contribution from Cu^{1+}, Mn^{2+}, Mn^{3+} and Mn^{4+} cannot be neglected which could directly or indirectly affect the CO conversion.

5.2.2 Series-II : Zinc copper manganite ($Zn_{1-x}Cu_xMn_2O_4$)

The spinel $Zn_{1-x}Cu_xMn_2O_4$ is tested for CO oxidation and the role of $Zn^{2+}$and Cu^{2+} are attempted to explain the catalytic activity. The temperature dependence of CO conversion studied for different compositions is shown in fig. 5.5. The fractional conversion of CO (X_{CO}) v/s W/F_{CO} plot for representative samples are presented in fig. 5.6 and 5.7. Kinetic parameters derived from Arrhenius plot are summarised in detail in table 5.3.

Discussion

In $Zn_{1-x}Cu_xMn_2O_4$ with the increase in copper content the activity of zinc substituted manganite is increased to a marked extent which is quite expected on account of higher activity of Cu^{2+} species. Relatively low activity is exhibited by the end compositions. However, a observed rapid rise of CO conversion in the region of x = 0.3 to 0.7, suggests that combination of both the metals must have created a synergistic effect breaking the activation energy barrier of both the limiting steps. According to Sinha et al[29] in the zinc manganites, the normal arrangement is stabilised by the strong tendency of these ions to form sp^3 bonds (regular or distorted) in the tetrahedral site $Zn^{2+}[Mn^{3+}]_2O_4$. However, a large quantity of $CuMn_2O_4$ (83%) is required to remove the distortion in $ZnMn_2O_4$ as reported by Kshirsagar and Biswas[37]. Thus a pronounced change in catalytic activity near x = 0.7 is attributed to crystallographic phase transition from tetragonal

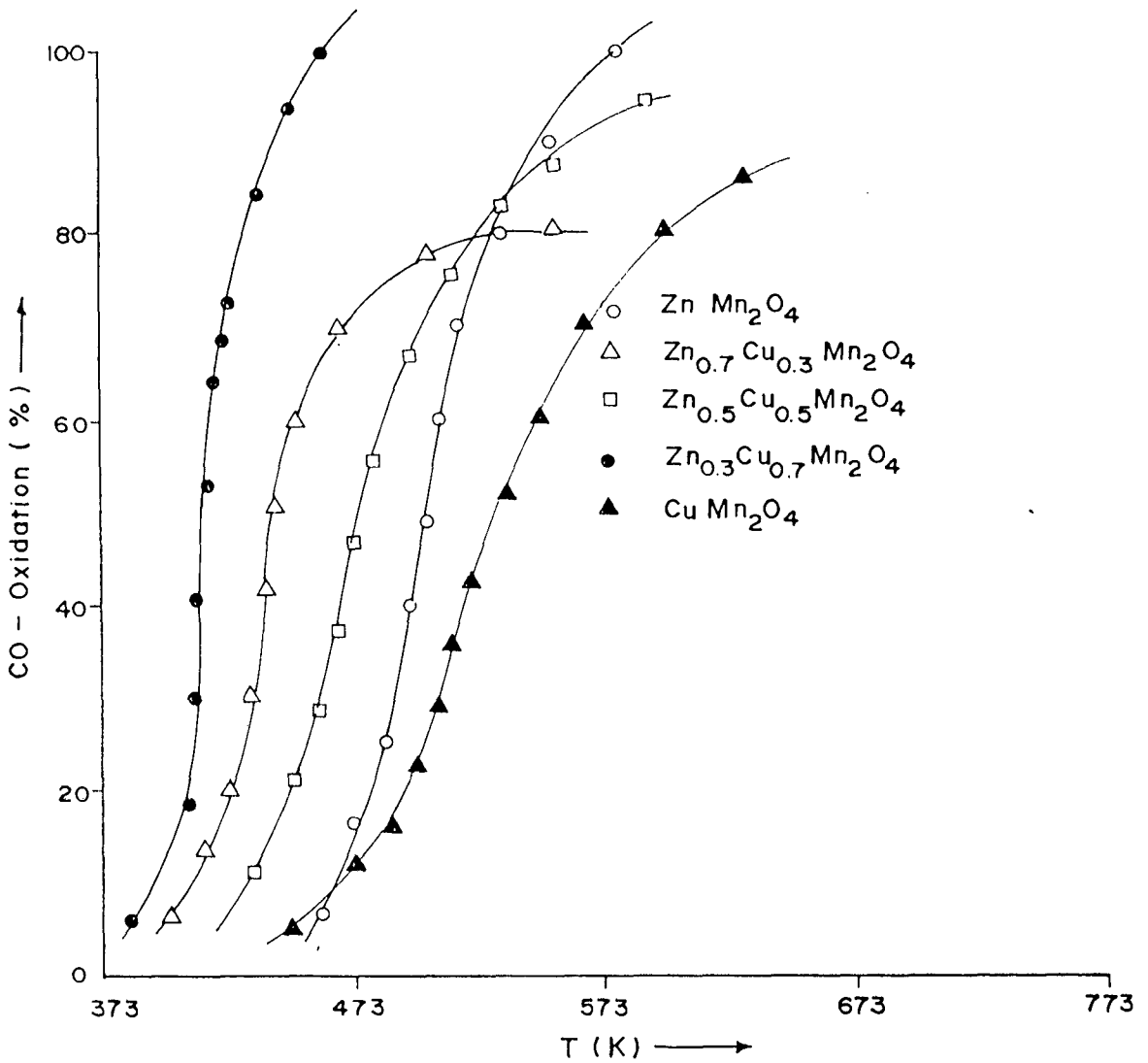

Fig. 5.5. CO conversion as a function of catalyst temperature for $Zn_{1-x}Cu_xMn_2O_4$

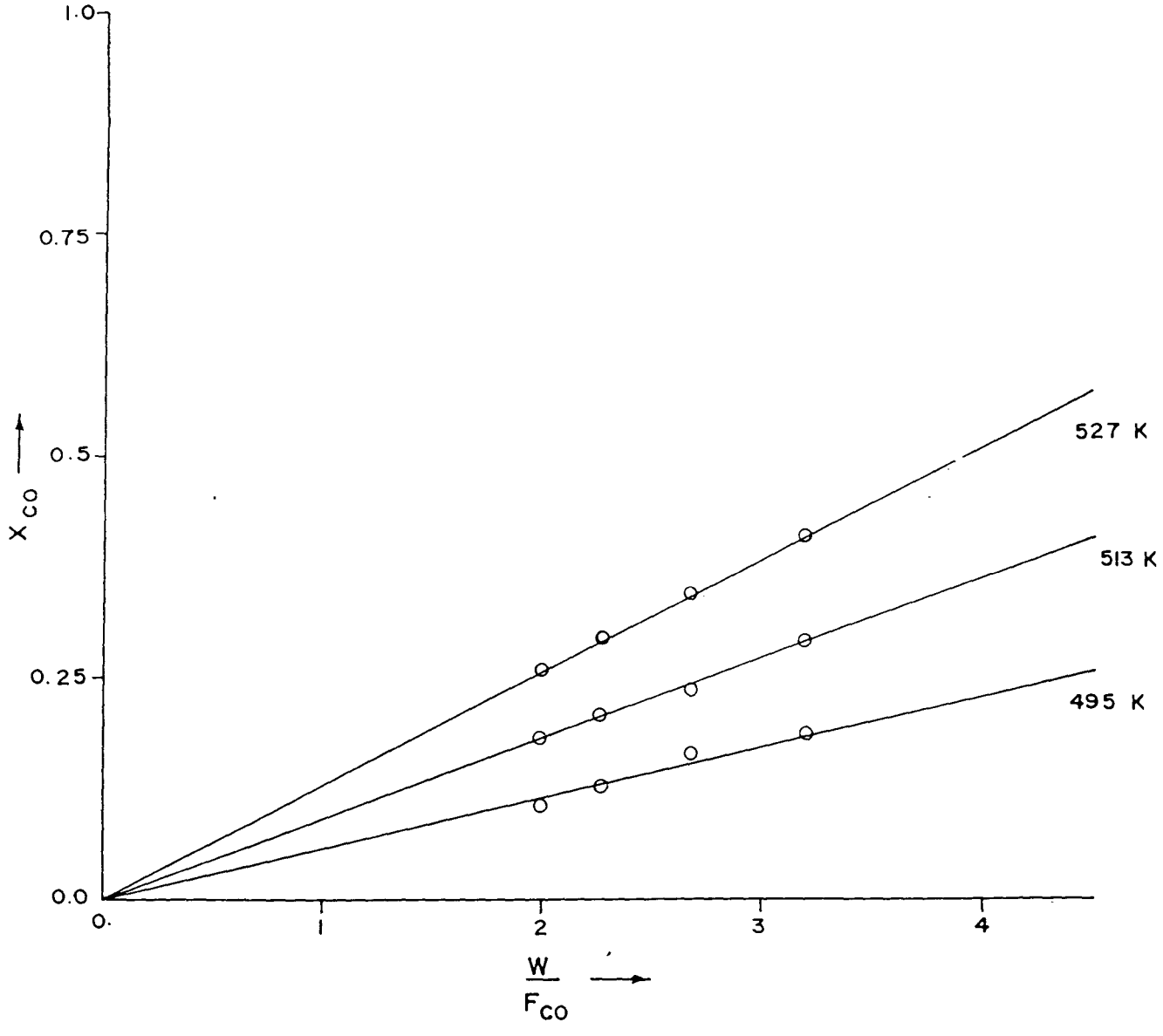

Fig. 5.6. Resident time plot for the representative sample of $CuMn_2O_4$

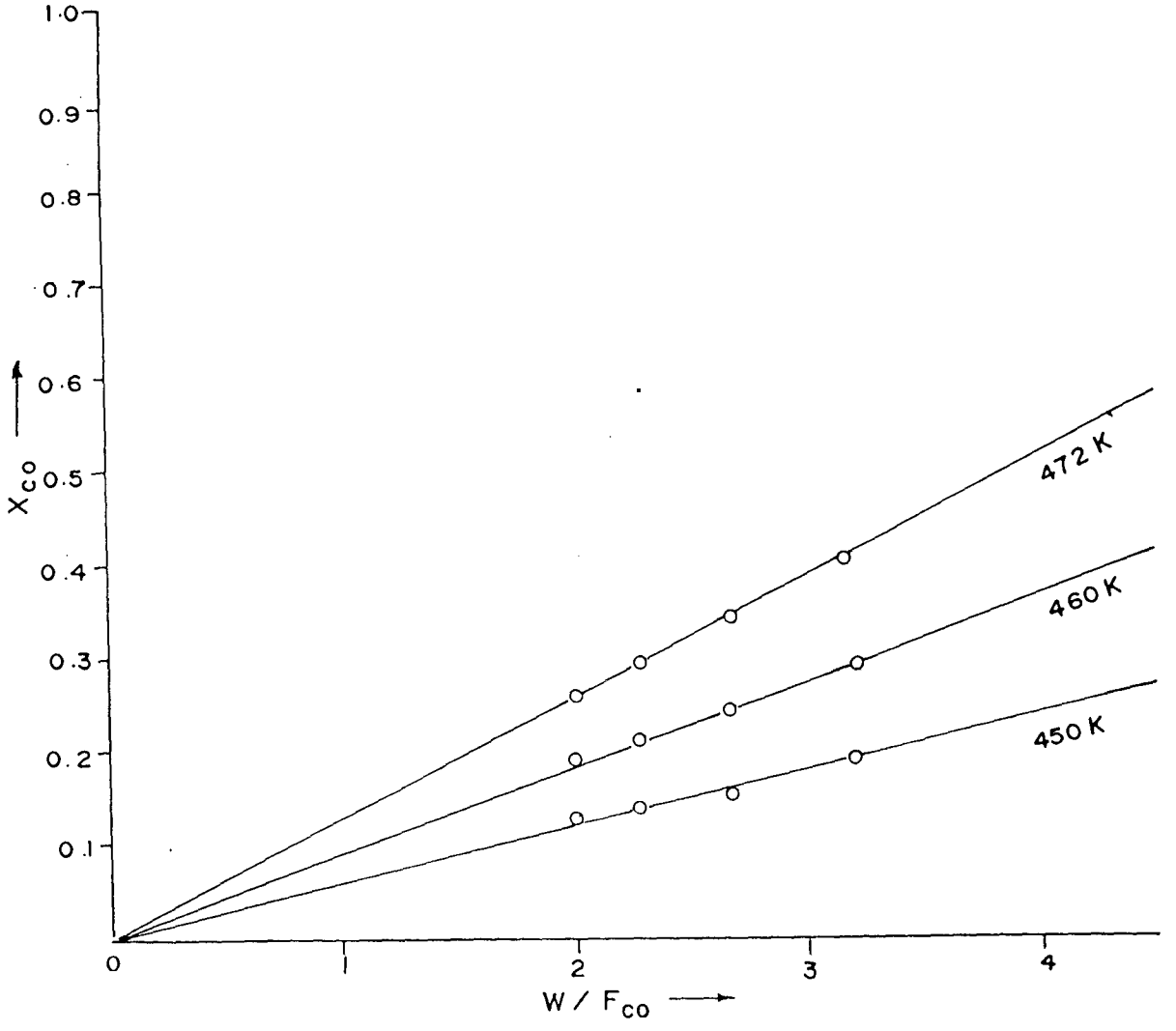

Fig. 5.7. Resident time plot for the representative sample of $Zn_{0.5}Cu_{0.5}Mn_2O_4$

Table 5.3 Kinetic parameters of CO oxidation over different catalysts

Sr. No.	Catalysts	Surf. area (m^2/g)	Temp (°K)	Rate (Molec./m^2.s)	Ea (kcal/mol)	Freq. factor (Molec/m^2.s)
1	$ZnMn_2O_4$	1.46	486	$7.0080x10^{18}$	10.6080	$7.0864x10^{18}$
2	$Zn_{0.7}Cu_{0.3}Mn_2O_4$	2.97	422	$3.6000x10^{18}$	9.1741	$3.6400x10^{18}$
3	$Zn_{0.5}Cu_{0.5}Mn_2O_4$	6.42	450	$1.5742x10^{18}$	9.8332	$1.5917x10^{18}$
4	$Zn_{0.3}Cu_{0.7}Mn_2O_4$	4.95	408	$2.1124x10^{18}$	8.8878	$2.1358x10^{18}$
5	$CuMn_2O_4$	4.32	495	$2.1920x10^{18}$	12.593	$2.2202x10^{18}$

to cubic in the catalyst. Such improvement in the catalytic activity in the region of crystallographic phase transition have been reported in literature[165, 221]. This is in agreement with the studies made by Kanamori[46] and Rosenberg et al[60] that Jahn-Teller stabilization is dynamic above and static below the transition.

Unexpected decline in CO conversion at x = 0.5 can be explained on the basis of electrical conductivity data. The improvement in the conductivity at x = 0.5 , as explained in the previous chapter is attributed to the number of Mn^{3+}-Mn^{4+} ion pair associations in which the formation of Mn^{4+} ion reduces the number of active sites of copper ions (Cu^{2+}). The surface enrichment of manganese over copper as observed by Yang et al[219] and preferential exposure of Oh sites on the surface helps us to interpret that the overall activity is reduced to some extent either because active sites of Cu^{2+} are blocked by relatively less active manganese Mn^{3+}/Mn^{4+} or because of reduction of Cu^{2+} by Mn^{3+} giving rise to less active Cu^{1+} along with Mn^{4+}.

Goodenough and Loeb[20] suggested that if the cation at the A-site forms a strong covalent bond, the octahedrally co-ordinated bonds at B-site become weak correspondingly, the distortion from cubic symmetry to lower symmetry is further explained as due to formation of covalent bond. This explains the decrease of CO conversion as we go from cubic to tetragonal symmetry. Moreover Cu^{2+} and Mn^{3+} have according to some authors[18, 222], same ratio of energetic stabilization in Oh and Td site. Since the partial

substitution of $CuMn_2O_4$ by $ZnMn_2O_4$ is likely to produce more of Cu^{2+} on Oh site as Zn prefers Td site which is in accordance with Jacobs et al[220], such substitution should result in the stabilization of cubic type spinel as observed by Castiglioni et al[223], thus resulting in the improved catalytic activity towards CO oxidation. Studies by Moller et al[119] also showed that CO adsorbs on Cu/Cu_xO and migrate along the surface to the ZnO areas to form CO_2^- complex on ZnO i.e. $ZnCO_2^-$, ultimately desorption of CO_2 molecule occurs from ZnO. The study reveals that the existence of Zn^{2+} and Cu^{1+} ion (as seen from the ionic structure) play a significant role of adsorption-desorption phenomena in the oxidation reaction of CO. From kinetic studies the energy of activation is found to be lowest for $x = 0.7$ (i.e. 8.8878 kcal/mol) followed by $x = 0.3$ and 0.5 respectively, thus indicating that they possess good catalytic activity for CO oxidation. Relatively higher activation energies observed for $ZnMn_2O_4$ and $CuMn_2O_4$ clearly shows that they are catalytically less active. Rate of reaction and frequency factor which are directly proportional to each other cannot be correlated with activation energy, since other parameters such as surface area, temperature etc. also affects the rate and frequency factor.

5.2.3 Series-III : Cobalt copper manganite ($Co_{1-x}Cu_xMn_2O_4$)

CO oxidation over $CoMn_2O_4$ and $CuMn_2O_4$ are well studied by many investigators[64, 224]. Studies have shown that among the non noble metal containing catalyst Co^{2+} and Cu^{2+} are chemically active species for CO oxidation. Here an attempt has been made to understand the effect of A-site substitution by copper in the lattice of $CoMn_2O_4$. The temperature dependence of CO conversion for different compositions are shown in fig. 5.6. Table 5.4 presents CO conversion data of various catalyst compositions.

Discussion

Substitution of Co in $CoMn_2O_4$ by copper showed a pronounced change in catalytic activity for CO oxidation. In this series of $Co_{1-x}Cu_xMn_2O_4$, x = 0.7 composition exhibits maximum catalytic activity followed by x = 0.3 > 0.5 > 1.0 > 0.0 respectively. However, the improvement in the activity of the intermediate compositions between $CoMn_2O_4$ and $CuMn_2O_4$ is on account of the co-operative effect of two mixed transition metal oxides as discussed before. Besides, the presence of manganese indirectly affects the activities of catalyst on account of its reducing action on Cu^{2+}, thus the overall performance of catalyst depends on the interaction of manganese with divalent ion, as observed in the earlier studies in series-I and series-II. According to Brabers and Setten[225] the

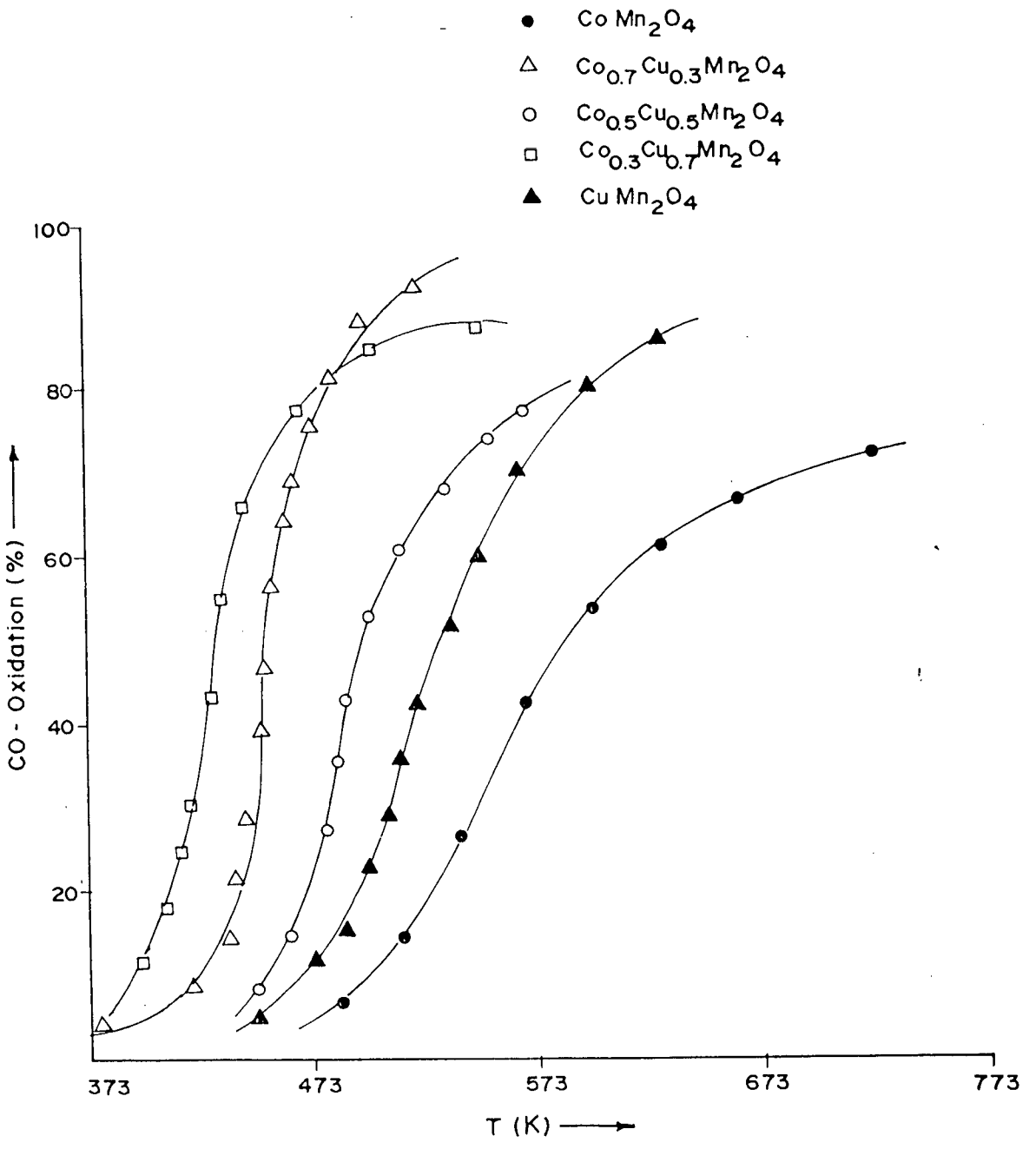

Fig. 5.8. CO conversion as a function of catalyst temperature for $Co_{1-x}Cu_xMn_2O_4$

Table 5.4 The reaction rate and the % conversion data at a given temperature for $Co_{1-x}Cu_xMn_2O_4$

Sr. No.	Catalysts	Surf. area m^2/g	Reaction temp. (°K)	% CO Conv^n	Rate (molec/m^2.s)
1	$CoMn_2O_4$	7.76	523	21	1.4148×10^{18}
2	$Co_{0.7}Cu_{0.3}Mn_2O_4$	6.00	443	27	2.3527×10^{18}
3	$Co_{0.5}Cu_{0.5}Mn_2O_4$	6.69	473	22	1.7193×10^{18}
4	$Co_{0.3}Cu_{0.7}Mn_2O_4$	6.5	413	24	1.9303×10^{18}
5	$CuMn_2O_4$	4.32	495	18	2.1920×10^{18}

octahedral sublattice is mainly occupied by Mn^{3+}(Jahn-Teller ion) which accounts for the tetrahedral deformation of the spinel $CoMn_2O_4$. The observed increase in catalytic activity at $x > 0.5$ can be partially attributed to crystallographic phase transition from tetragonal to cubic, which is in agreement with Kshirsagar and Biswas[37]. The activity at $x = 0.7$ is still expected to be higher but the surface enrichment of Mn over Cu and Cu over Co might have reduced the catalytic activity to certain extent by blocking the active sites of Cu as well as Co. The resultant activity can be due to preferential migration of Cu and Co from bulk to the surface of the catalyst.

According to the studies made by Sinha et al[29] Co^{2+} shows more or less equal affinity for both types of sites. However, according to some of the authors[18, 35] it is more stable on tetrahedral site. Since Co^{2+} can be partially oxidised to Co^{3+} in presence of Mn^{3+}, according to equation

$$Mn^{3+} + Co^{2+} \longrightarrow Mn^{2+} + Co^{3+}$$

the resultant Mn^{2+} and Co^{3+} will preferably occupy tetrahedral and octahedral sites respectively. These studies have tempted us to arrive at ionic structure close to that arrived at by yamamoto[209] from neutron diffraction studies, represented as $Co_{0.84}{}^{2+}Mn_{0.16}{}^{2+}[Co_{0.16}{}^{3+}Mn_{1.84}{}^{3+}]O_4{}^{2-}$ which could satisfactorily explain the low catalytic activity of $CoMn_2O_4$. Observed catalytic activity of $CoMn_2O_4$ can further be supported by

magnetic susceptibility data which show lower values of 5.009 BM for $CoMn_2O_4$ in comparison with highest value of 5.9119 BM for $CuMn_2O_4$ in this series. Substitution of cobalt by copper show a rapid rise in CO conversion at x = 0.7, whereas low CO conversion at x = 0.5 can be due to stoichiometric stabilization[31].

5.2.4 Series-IV : Nickel cobalt manganite ($Ni_{1-x}Co_xMn_2O_4$)

The studies of CO oxidation on various non noble metal oxide catalysts have shown that nickel and cobalt oxide are not the exceptions, they are chemically active species which can bring about CO conversion at varying degrees in different types of the system. In the present study the temperature dependence of CO conversion over the variable compositions highlights the effect of A-site substitution in $NiMn_2O_4$ by cobalt as depicted in fig.5.9 Table 5.5 presents CO conversion data over variable compositions.

Discussion

In a series $Ni_{1-x}Co_xMn_2O_4$ highest catalytic activity was observed for compositions with x = 0.3 which is followed by 0.7 > 0.5 > 0.0 > 1.0. Intermediate compositions show a prominent rise in CO conversion on account of higher activities due to co-operative effect of two different A-site cations. From the earlier studies it is observed that nickel and cobalt in

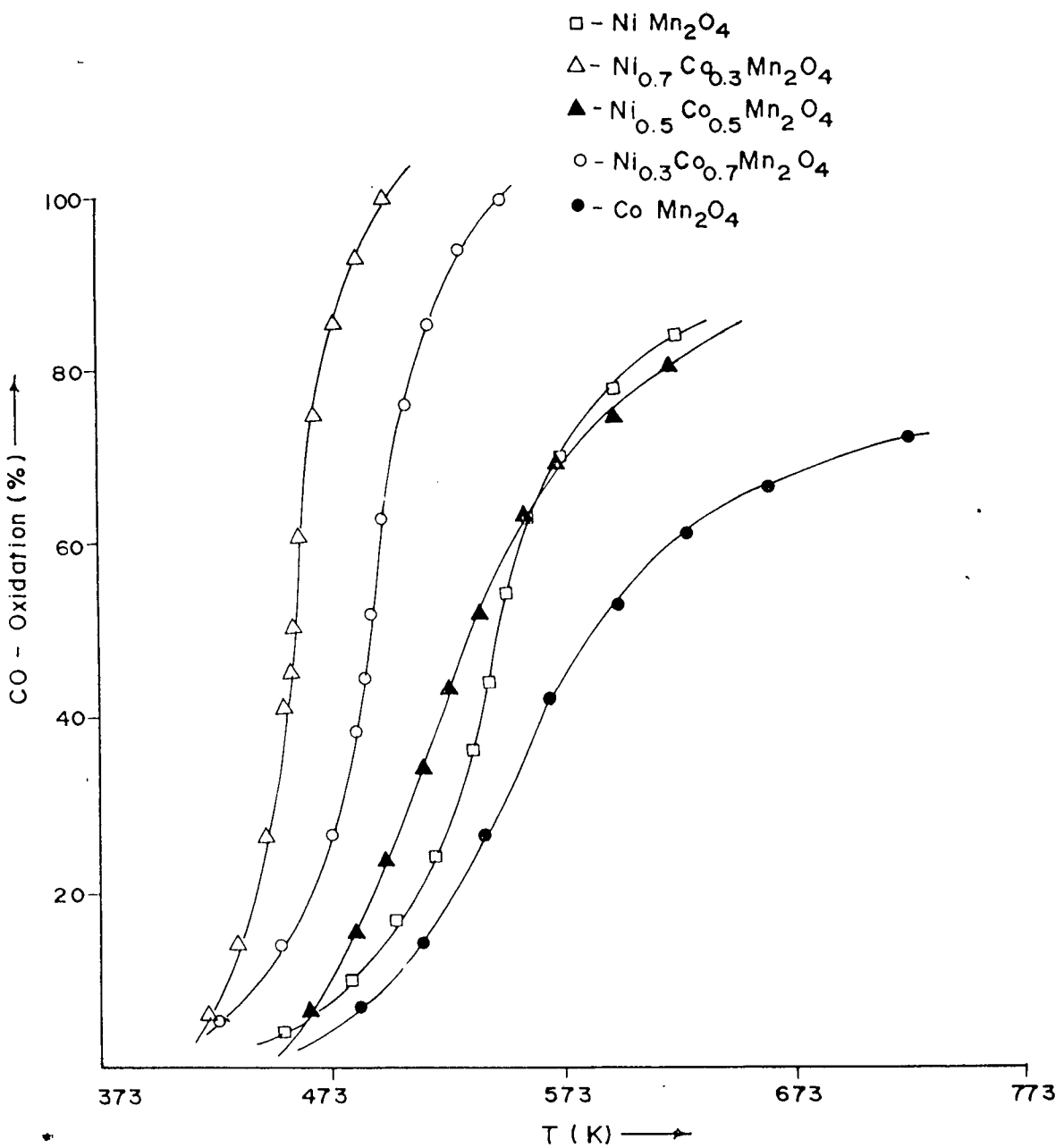

Fig. 5.9. CO conversion as a function of catalyst temperature for $Ni_{1-x}Co_xMn_2O_4$

Table 5.5 The reaction rate and the % conversion data at a given temperature for $Ni_{1-x}Co_xMn_2O_4$

Sr. No.	Catalysts	Surf.Area (m^2/g)	Reaction temp. (°K)	%CO Conv^n	Rate (molec/m^2.s)
1	$NiMn_2O_4$	5.6	523	27	2.5207×10^{18}
2	$Ni_{0.7}Co_{0.3}Mn_2O_4$	8.9	443	24	1.4098×10^{18}
3	$Ni_{0.5}Co_{0.5}Mn_2O_4$	7.6	498	26	1.7886×10^{18}
4	$Ni_{0.3}Co_{0.7}Mn_2O_4$	8.4	473	27	1.6805×10^{18}
5	$CoMn_2O_4$	7.76	523	21	1.4148×10^{18}

their divalent state have strong tendency to occupy octahedral and tetrahedral sites resulting in cubic and tetragonal symmetry respectively. Maximum catalytic activity at x = 0.3 might be due to tetragonal to cubic transition which is likely to occur at x < 0.5.

Partial substitution of Ni in $NiMn_2O_4$ by Co shows an enhancement in activity thus indicating that tetrahedrally located Co^{2+} are the active species for CO oxidation, however some contribution is likely to occur from Co^{3+} from an octahedral site.

5.3 COMPARATIVE STUDY OF ALL THE COMPOSITIONS

Comparative study of percentage conversion as a function of catalyst composition for all four series at different temperatures are made and following are the observations

In all the series that were studied for CO conversion, one common observation made is that the intermediate compositions were much more active than the end compositions. Such common observation was ascribed to a typical phenomena of synergism. Though intermediate compositions in all series displays better catalytic activity at different temperatures, the pattern of change in activity for intermediate compositions is not the same among these series as seen from figures 5.10 - 5.13.

Series-II, III and IV have analogy in the pattern of their activity unlike series-I, in which the maximum activity is observed at x = 0.5.

Series-II, III and IV show better activity at x=0.3 and 0.7. Such prominent change among the different series can be attributed to the phase transition as discussed earlier in this chapter. In series-I, there is no crystallographic phase change and cubic symmetry is observed throughout the series. In series-II, III and IV a phase transition is observed from tetragonal to cubic. Studies have shown that such transition leads to the improvement in the performance of the catalyst, and hence the catalytic activity.

In series-II, III and IV low activity at x = 0.5 compared to at x = 0.3 and 0.7 can be explained to be due to stoichiometric stability attained by incorporation of tetragonal and cubic phases. Further electrical conductivity data which were in consistent with the earlier reports led us to draw a conclusion that the improvement in conductivity at x = 0.5 produces more number of Mn^{4+} rather than Mn^{3+}, which means the reduction of one of the component from A-site of AB_2O_4 spinel, thereby lowering the activity of catalyst at x = 0.5.

Effect of partial substitution of A-site in either $ZnMn_2O_4$ or $CoMn_2O_4$ by copper is almost same, which is reverse of that in series-I. It can be interpreted that unlike in other three series, in series-I there is cubic symmetry throughout the series, where in the co-operative effect of two cubic spinels display their maximum activity at a point of intermediate composition of exactly x = 0.5. In series IV absence of copper does not show much variation, it resembles series-II and III from the fact that two different

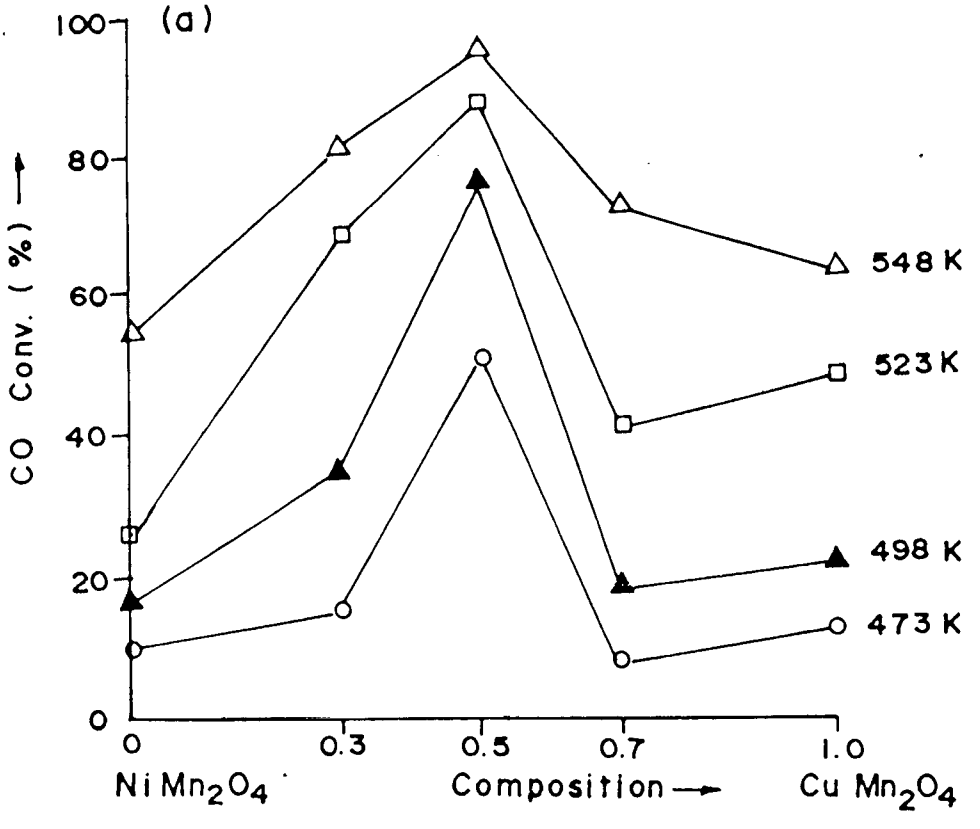

Fig. 5.10. Percentage conversion as a function of catalyst composition for the system

$Ni_{1-x}Cu_xMn_2O_4$

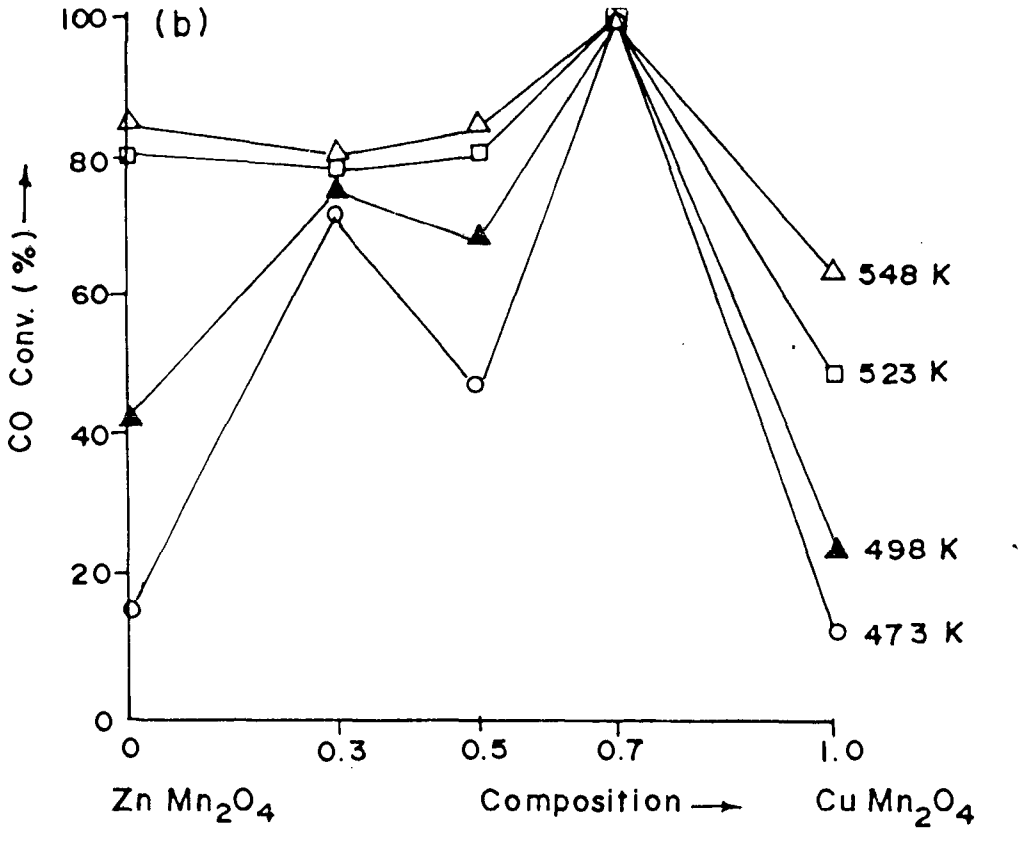

Fig. 5.11. Percentage conversion as a function of catalyst composition for the system $Zn_{1-x}Cu_xMn_2O_4$

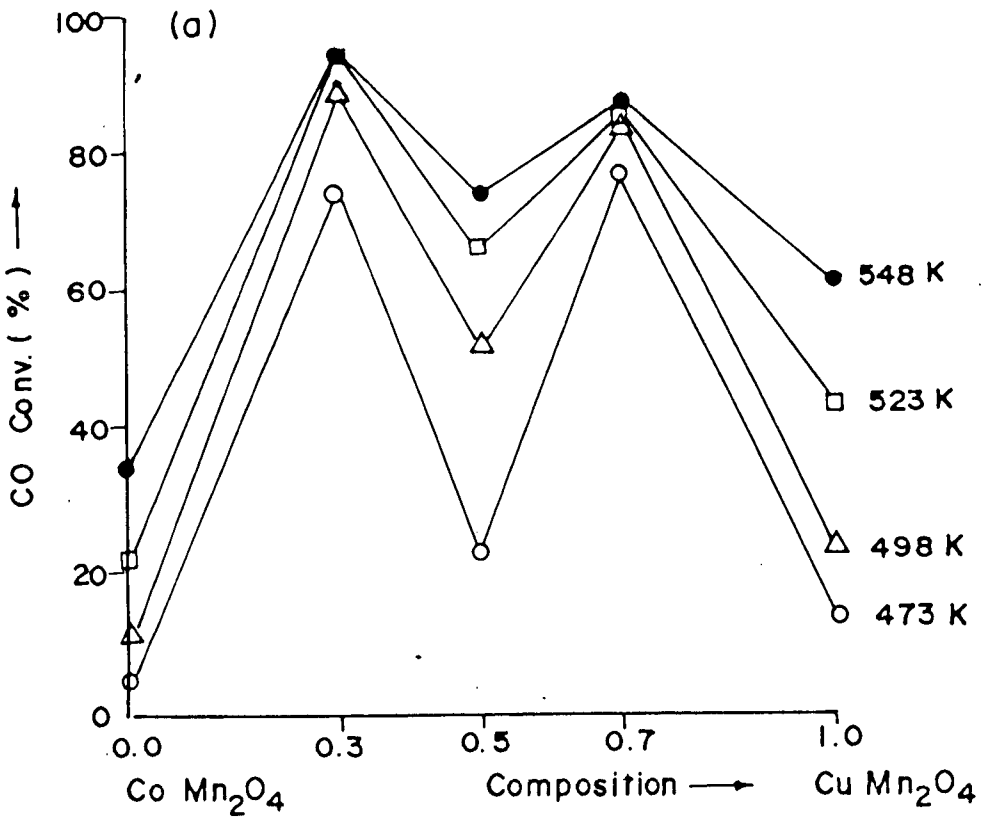

Fig. 5.12. Percentage conversion as a function of catalyst composition for the system $Co_{1-x}Cu_xMn_2O_4$

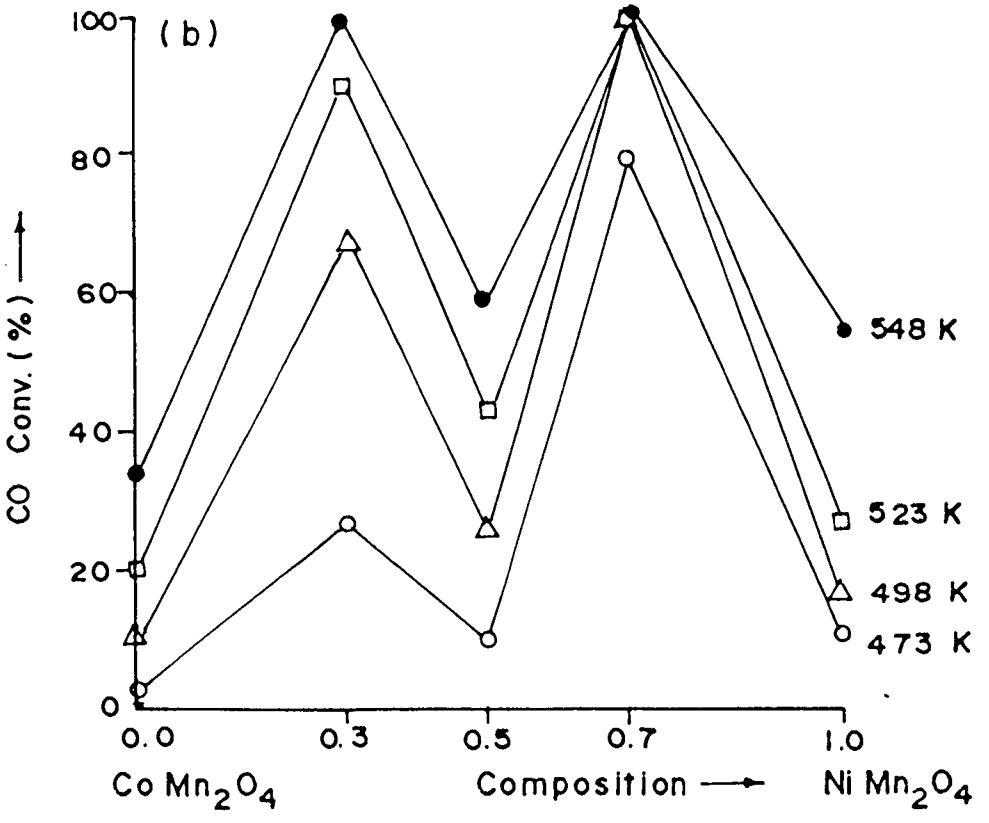

Fig. 5.13. Percentage conversion as a function of catalyst composition for the system $Ni_{1-x}Co_xMn_2O_4$

phases interact thus exhibiting similar activity pattern for intermediates. Comparative study of series-I and IV show that effect of partial substitution of Ni by Co in $NiMn_2O_4$ is much effective for CO conversion than the partial substitution of Ni by Cu in $NiMn_2O_4$.

The studies reveals that irrespective of the type of the metal ion on A-site, if the symmetry of one of the system is cubic and other is tetragonal then the similar pattern of activity is normally expected. From the overall study of CO oxidation over different catalyst compositions, 100% conversion is achieved for $Zn_{0.3}Cu_{0.7}Mn_2O_4$ and $Ni_{0.7}Cu_{0.3}Mn_2O_4$ at temperature as low as 468 K and 498 K respectively.

5.4 EFFECT OF PARTIAL PRESSURE OF THE REACTANTS AND REACTION MECHANISM

The effect of partial pressure of the reactants carbon monoxide and oxygen on the kinetics was studied on series of spinels, $Ni_{1-x}Cu_xMn_2O_4$ and $Zn_{1-x}Cu_xMn_2O_4$. The procedure followed was similar to that mentioned in the chapter - 3.

Partial pressure (logP) of CO and O_2 versus Rate (logR) plots are shown for the representative samples in fig. 5.14 and fig. 5.15 respectively. It is observed from the plot that reaction is observed to be first order with respect to CO and zero order dependence in O_2 as seen for all the compositions in the series.

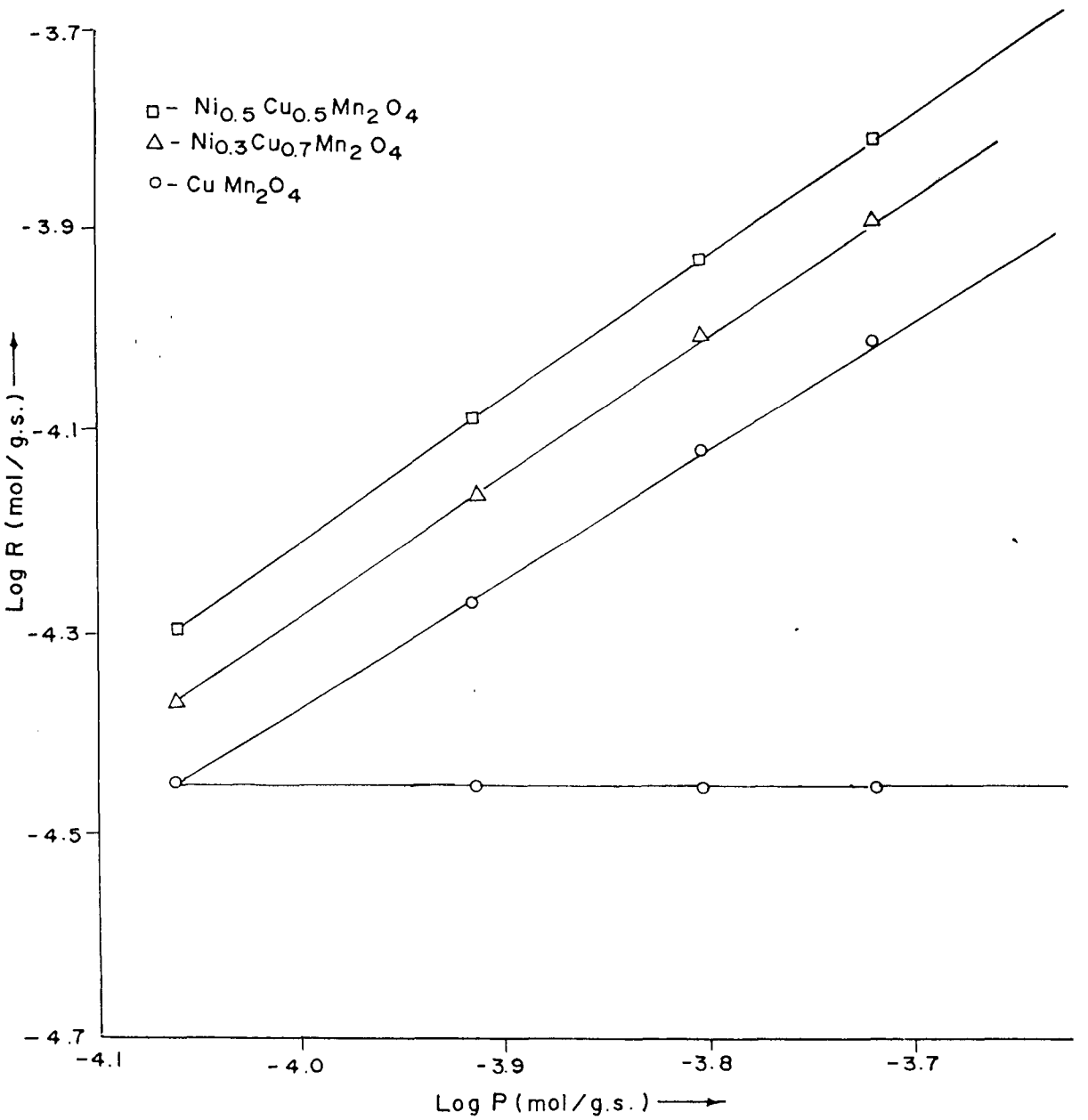

Fig. 5.14. Effect of reactant partial pressure on the rate of CO oxidation by O_2 for representative sample of $Ni_{1-x}Cu_xMn_2O_4$ (where x = 0.5, 0.7, 1.0)

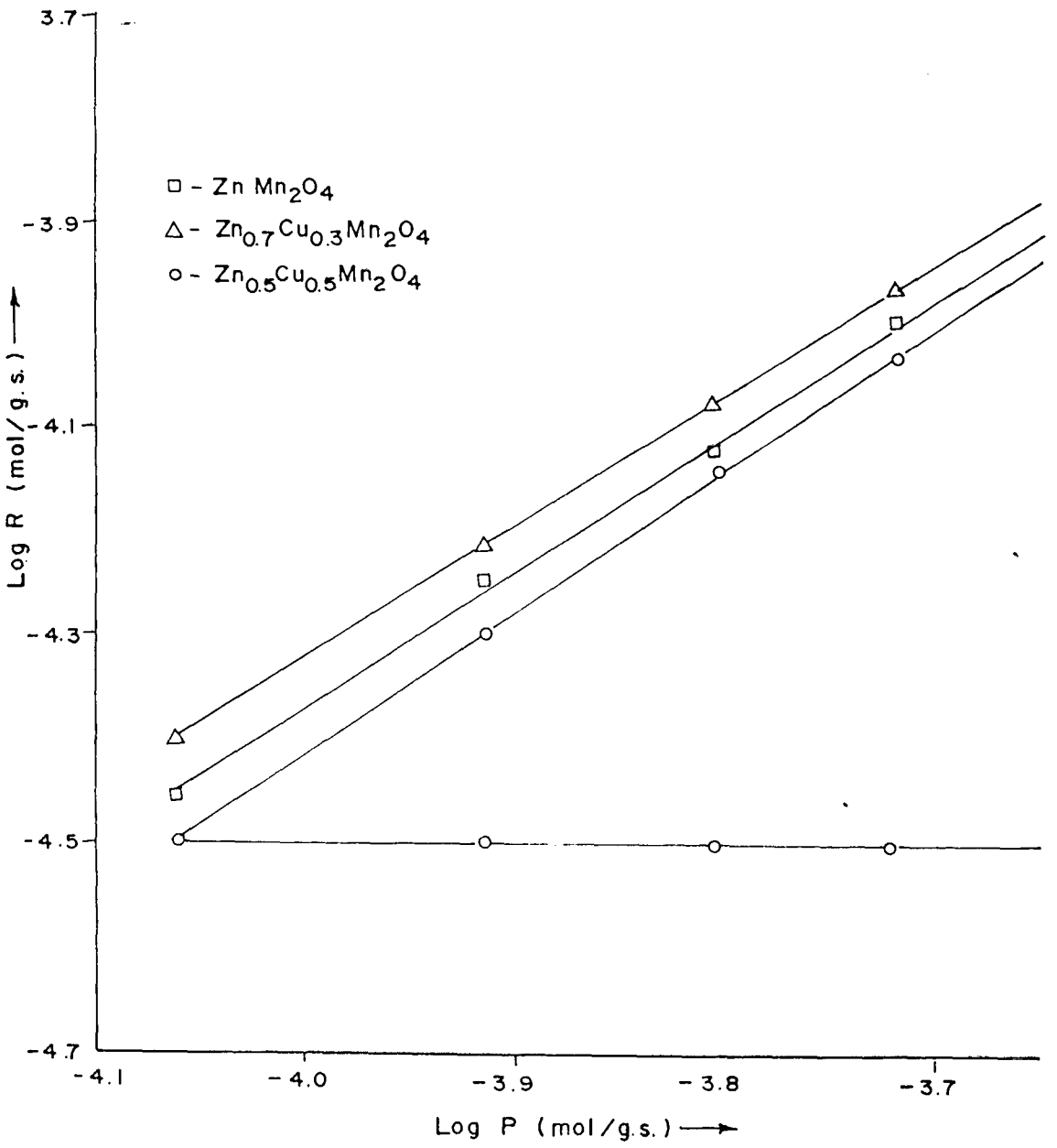

Fig. 5.15 Effect of reactant partial pressure on the rate of CO oxidation by O_2 for representative sample of $Zn_{1-x}Cu_xMn_2O_4$ (where x = 0.0, 0.3, 0.5)

The kinetic studies indicate that adsorption of CO is the rate limiting step. The electrical conductivity data suggests that oxygen adsorption as O^- species is fast and reversible. Such adsorption is found to occur far more extensively on p-type oxides than on n-type oxides[226]. Thus in series-I and series-II except $NiMn_2O_4$, all other compositions are expected to show oxygen adsorption phenomena on account of their p-type conductivity which is already reported by many investigators[31, 42, 47]. There are various possible ways by which O_2 can adsorb on the oxide surface.

(I) Adsorption of oxygen as anionic species may occur as follows.

$$O_{2(g)} \longrightarrow O_{2(ads)}$$

$$O_{2(ads)} + e^- \longrightarrow O_2^-{}_{(ads)}$$

$$O_2^-{}_{(ads)} + e^- \longrightarrow 2O_{(ads)}^-$$

$$O_{(ads)}^- + e^- \longrightarrow O_{(ads)}^{2-}$$

$$O_{(ads)}^{2-} \longrightarrow O_{(L)}^{2-}$$

$O_{(L)}^{2-}$ is then incorporated into the lattice.

(II) Adsorption of CO

Studies on Molecular Orbital Theory (MOT) suggests the formation of carbonyl species[106, 227]. The adsorbed CO may also form adsorbed surface carbonate species

$$CO_{(g)} \longrightarrow CO_{(ads)}^{+} + e^{-}$$

$$CO_{(ads)}^{+} + 2O^{2-} \longrightarrow CO_3^{2-} + e^{-}$$

(III) Interaction of CO with oxygen

Interaction of adsorbed CO with oxygen results in carbonate formation

$$CO_{(ads)}^{+} + 2O_{(ads)}^{-} \longrightarrow CO_3^{2-} + h$$

$$CO_{(ads)}^{+} + O_{(ads)}^{-} + O_{(L)}^{2-} \longrightarrow Co_3^{2-}$$

$$CO_{(ads)}^{+} + O_2^{-} \longrightarrow CO_{3(ads)}$$

(IV) Formation of CO_2 (Reaction of adsorbed species)

The adsorbed CO observed in step-II on interaction with adsorbed oxygen can directly result in the formation of CO_2 as also observed from earlier reports[130, 228, 230] or formation of CO_2 via carbonate formation as shown in step-III which is also reported by many investigators[229, 232].

$$CO_{(ads)}^{+} + O_{(ads)}^{-} \longrightarrow CO_{2(g)}$$

$$CO_{3(ads)}^{2-} \longrightarrow CO_{2(ads)} + O^{2-}$$

$$CO_{2(ads)} \longrightarrow CO_{2(g)}$$

$$CO_{3(ads)}^{2-} + CO_{(g)} \longrightarrow 2CO_{2(g)} + 2e^{-}$$

Many investigators have proposed the reaction mechanism for CO oxidation by oxygen. We propose the reaction mechanism in general for the above reactions based on our experimental data. Reaction proceeds by Langmuir-Hinshelwood type mechanism. However there are many reports that reaction also proceeds by Eley-Rideal type mechanism. The proposed mechanism is as follows.

$$MO + CO \longrightarrow MO...CO_{(ads)} \quad \cdots \quad (1)$$

$$MO...CO_{(ads)} \longrightarrow M[\ ]...CO_{2(ads)} \quad \cdots \quad (2)$$

$$M[\ ]...CO_{2(ads)} \longrightarrow M[\ ] + CO_{2(g)} \quad \cdots \quad (3)$$

$$M[\ ] + O_{2(g)} \longrightarrow MO...O_{(ads)} \quad \cdots \quad (4)$$

$$MO...O_{(ads)} + MO...CO_{(ads)} \longrightarrow MO + MO...CO_{2(ads)} \quad \cdots \quad (5)$$

$$MO...CO_{2(ads)} \longrightarrow MO + CO_{2(g)} \quad \ldots \quad (6)$$

$$MO...CO_{2(ads)} + MO...O_{(ads)} \longrightarrow MO + MO...CO_{3(ads)} \quad \ldots \quad (7)$$

$$MO...CO_{3(ads)} + M[\ ] \longrightarrow 2MO + CO_{2(g)} \quad \ldots \quad (8)$$

MO indicate oxidic spinel catalyst and M[ ] is the reduced catalyst site.

In reaction-(1) carbon monoxide gets adsorbed on metal oxide by transfer of electron from carbon atom of CO to metal atom M of oxide resulting in the formation of chemisorbed species. In the second step chemisorbed CO species give rise to chemisorbed CO_2 at reduced metal site with anion vacancy. Partially bonded CO_2 gets desorbed leaving reduced metal on the lattice, which subsequently takes up oxygen from the gas phase forming chemisorbed oxygen on MO as shown in the reaction-(4). Resultant chemisorbed species may interact with the reactive species produced in reaction-(1), forming normal metal oxide as well as metal oxide with adsorbed CO_2. Adsorbed CO_2 species on metal oxide being unstable at higher temperature, undergoes dissociation to regenerate MO and leaving CO_2 in the gas phase. Chemisorbed species produced in reaction-(4) and reaction-(5) may also interact to yield carbonate type adsorbed species at MO site which subsequently can react with reduced metal site to finally give metal oxide and carbon dioxide.

The different reactions that are discussed above are likely to occur during oxidation of CO on manganites, depending on the condition of oxidation as well as the nature of the catalyst surface. Of these the adsorption of CO may be rate limiting step in the oxidation of CO on transition metal manganites. In conclusion (I) The reaction is first order with respect to CO, (II) The oxygen uptake by manganite is fast and (III) The reaction of adsorbed CO with oxygen is also fast. The above reaction mechanism is in agreement with many investigations[64,106 230, 231, 233] in some form or the other.

CHAPTER 6

CONCLUSION

CONCLUSION

Transition metal oxides are well known for their solid state and catalytic properties. However, their complex oxides such as spinels and perovskites are being reported in literature to be much more active and exhibits better solid state and catalytic properties than TMO.

In the present investigations studies were carried out on transition metal manganite spinels with a view to investigate their solid state and catalytic properties.

The solid materials under present search were prepared by co-precipitation technique using Sodium hydroxide and hydrogen peroxide for homogenous formation of manganite spinels.

X-ray studies confirmed that the compounds prepared by co-precipitation were all in monophasic form, besides it was observed that $CuMn_2O_4$ and $NiMn_2O_4$ are cubic spinels, where as $ZnMn_2O_4$ and $CoMn_2O_4$

crystallised in tetragonal form. The studies have also shown that $ZnMn_2O_4$ and $CoMn_2O_4$ forms a normal spinel and $NiMn_2O_4$ forms an inverse spinel, however $CuMn_2O_4$ was found to exist as either normal or partially inverse spinel.

Spinels prepared by co-precipitation gave better surface area and higher activity for CO oxidation reaction. One obvious reason for higher activity, is the high surface area which was found to vary in the range of 1.46 - 8.9 m^2/g.

Thermal studies were carried out in order to study decomposition temperature behaviour of hydroxide compositions. It was noticed that the decomposition occurs at around 473-573 K which is subsequently followed by the solid state reaction progressing towards the spinel formation.

Magnetic susceptibility studies showed an increased in susceptibility values for cubic systems such as $NiMn_2O_4$ and $CuMn_2O_4$, however value decreases with the tetragonal stabilization of the lattice. Higher magnetic susceptibility of spinel is attributed to Mn^{4+}-Mn^{3+} ion pairs resulting from the Jahn-Teller stabilization of Cu^{2+} and Mn^{3+} ions.

Electrical resistivity versus Temperature behaviour showed that resistivity decreases linearly with rise in temperature, exhibiting the conductivity in the range of 10^2 -10^{-11} ohm^{-1}-cm^{-1} of typical semiconductors. Some spinels were found to exhibit n-type and some others p-type behaviour. Resistivity of different compounds were found to depend on the metal ions

occupying octahedral site of the spinel on account of B-B interaction. Resistivity is found to vary with the symmetry. Cubic spinels show better conductivity than those with tetragonal symmetry.

From ESR studies it is observed that some of the copper occupies B-site as Cu^{2+}. Substitution of Ni, Zn and Co by Cu in their respective manganites were found to enhance the ESR signal as observed from their g-values. ESR studies have confirmed that copper is the active species which accounts for the overall activity of mixed manganite spinels.

A significant rise in catalytic activity was observed by studying the effect of A-site substitution in the spinels (AB_2O_4). CO oxidation on various catalyst compositions in series of spinels showed that their end compositions are relatively less active than their intermediate compositions. Such property was attributed to the phenomena of synergism. The trend of catalytic activity within a series is interpreted to be due to the domination of large number of factors such as thermodynamic and kinetic parameters, tetrahedral and octahedral site preference energies, preferential surface enrichment of one metal ion over the other, crystallographic phase transition, stoichiometric stabilization of phase etc.

Comparative study of different series for catalytic CO oxidation showed that the pattern of their activity depends on site symmetry. In series-I, both the end compositions possess cubic symmetry, however series-II, III and IV are analogous with respect to activity on account of their

tetragonal to cubic transition and therefore differs from the series-I. The overall performance of the intermediatory compositions prepared and their variation in activity can be accounted for, either due to incorporation of copper in the spinel lattice or due to transition of spinel from tetragonal to cubic symmetry.

From partial pressure studies it can be concluded that CO oxidation reaction is first order with respect to CO and zero order dependence in O_2. Further from the experimental data we arrive at the Langmuir-Hinshellwood type mechanism of CO oxidation over different catalysts, which proceeds via carbonyl formation as explained by molecular orbital theory.

REFERENCES

1. W. F. Libby, science., **171**, 499 (1971).
2. R. J. H. Voorhoeve, J. P. Remeika and D. W. Johnson, Science.,**180**, 62 (1973).
3. M. Tsujimura, T. Furusava and D. Kunni, J. Chem. Engg. Japan, **16**, 132 (1983).
4. Idem, Ibid., **51**, 301 (1966).
5. A. K. Neyestanaki and L. E. Lindfors, Combust. Sci. Tenhnol., **97/(1/3)**, 121 (1994).
6. F. Severino and J. Laine, Proc. 1st Eur. Cong. Catal. Europacat 1, Mountphellier, **2,** 639 (1993).
7. V. Mathieu-Determince, J. B. Maggy, J. Verbust, Proc. 1st Eur. Cong. Catal. Europacat 1, Mountphellier, **2**, 789 (1993).
8. F. F. Volkenstein's, Electronic theory of catalysis on semiconductors, Pergamon press (1963).
9. B. Hannay, 'Treatise on solid state chemistry',**1,** Plenum, N.Y., (1975).
10. G. Blasse, Philips Res. Rept., Suppl., **3,** 1 (1964).
11. E. W. Gorter, Philips Res. Rept., **9**, 295 (1954).
12. J. Smith and H. P. J. Wijn, 'Ferrites', Cleaver Hume Press Ltd., N.Y. (1959)

13. N. N. Greenwood, 'Ionic crystals, lattice defects and non-stoichiometry', N.Y. Chemical Publishing Co. (1970).

14. H. Furuhashi, M. Inagaki and S. Naka, J. Inorg. Nucl. Chem. **35**, 3009(1973).

15. E. J. W. Verwey, E. C. Heilmann, J. Chem. Phys., **15**, 174 (1947).

16. E. W. Gorter, Philips Res. Rept., **18**, 383 (1963).

17. D. S. Mc Clure, J. Phys. Chem. Solids., **3**, 311 (1957).

18. J. D. Dunitz and L. E. Orgel, J. Phys. Chem. Solids, **3**, 318 (1957).

19. C. D. Spencer and D. Schroeer, Phys. Rev. B., **9**, 3658 (1974).

20. J. B. Goodenough and A. L. Loeb, Phys. Rev., **98**, 391 (1955.)

21. H. A. Jahn and E. Teller, Proc. Roy. Soc.A, **161**, 220 (1937).

22. K. S. Irani, A. P. B. Sinha and A. B. Biswas, J. Phys. Chem. Solids, **17**, 101 (1960).

23. G. T. Bhandage and H.V. Keer, J. Phys. C, **8**, 501 (1975).

24. M. Nogues and P. Poix, C. R. Acad. Sci. Ser. C, **272**, 1318 (1971).

25. R. Buhl, J. Phys. Chem. Solids, **30**, 805 (1969).

26. G. Filoti, A. Gelberg, V. Gomela and M. Rosenberg, Int. J. Magn., **2**, 65 (1972).

27. S. Miyahara, J. Phys. Soc. Japan, Suppl. B1, **17**, 181 (1962).

28. I. Aoki, J. Phys. Soc. Japan, **20** , 871 (1965).

29. A. P. B. Sinha, N. R. Sanjana and A. B. Biswas, Acta. cryst., **10**, 439 (1957).

30. N. K. Radhakrishnan and A. B. Biswas, Phys. Stat. Sol. A , **44**, 45 (1977).

31. G. T. Bhandage and H. V. Keer, J. Phys. C, **9** , 1325 (1976).

32. A. I. Zaslavskii, Kristallograffia, **7**, 835 (1962).

33. J. Jarrige and J. Mexmain, Bull. Soc. Chim. Fr., **3**, 405 (1976).

34. S. Asbrinc, Acta.Chem. Scand., **19**, 1766 (1965).

35. D. K. Kulkarni and Chintamani Mande, Ind. J. Pure. Appl. Phys., **12**, 60 (1974).

36. A. P. B. Sinha, N. R. Sanjana and A. B. Biswas., J. Phys. Chem., **62**, 191 (1958).

37. S. T. Kshirsagar and A. B. Biswas, J. Phys. Chem. Solids., **28**, 1493 (1967).

38. C. Delrome, Bull. Soc. France Mineral Cryst., **81**, 79 (1958).

39. A. I. Zaslavskii, Z. V. Karachentsva and A. I. Zharinova, Soviet phys. Crystallogr., **7**, 680 (1963).

40. I. T. Sheftal and Pavlotskii, Soviet Phys. Solid St., **7**, 2781 (1964).

41. A. Millar, J. Phys. Chem. Solids, **29**, 633 (1968).

42. C. D. Sabane, A. P. B. Sinha and A. B. Biswas, Ind. J. Pure Appl. Phys., **4**, 187 (1966).

43. G. Blasse, J. Phys. Chem. Solids, **27**, 383 (1966).

44. P. P. Jogalekar and A. P. B. Sinha, Indian J. Pure Appl. Phys., **5**, 9 (1967).

45. M. O'Keeffe, J. Phys. Chem. Solids, **21**, 172 (1961).

46. J. J. Kanamori, J. Appl. Phys., **31**, Suppl. 14 (1960).

47. S. T. Kshirsagar, J. Phys. Soc. Japan, **27**, 1164 (1969).

48. P. F. Bongers, Ph.D. Thesis, Leiden University, Leiden (1957).

49. B. N. Naik and A. P. B. Sinha, Indian J. Pure Appl. Phys., **7**, 1706 (1969).

50. I. T. Sheftal, A. I. Zaslavskii, E. V. Kurlina and G. N. Tekster, Proc. Sburyakova, Soviet Phys. Solid State, 3, 1979 (1962).

51. A. Bhaduri, H. V. Keer and A. B. Biswas, Indian J. Pure Appl. Phys. **12**, 745 (1974).

52. A. Meenakshisundaram, N. Gunasekaran and V. Srinivasan, Phys. Stat. Sol. (a) **69**, K 15 (1982).

53. E. J. W. Verwey, P. W. Heayman and F. C. Romejin, J. Chem. Phys., **15**, 181 (1947).

54. J. B. Goodenough, 'Magnetism and Chemical Bond', Interscience Publishers Inc. and John-Wiley Inc. N.Y.(1963).

55. J. B. Goodenough, 'Metallic Oxides', Progress in solid state Chemistry, (Ed. H. Reiss), Pergamon, New York, **5**, 145 (1974).

56. B. Reuter and K. Muller, Naturwissenschften, **54**, 164 (1967).

57. G. V. Subba Rao and C. N. R. Rao, Phys. Stat. Sol. (a), **1**, 597 (1970).

58. G. H. Jonker and J. H. Van Santen, Physica., **19**, 120 (1953).

59. E. G. Larson, R. J. Arnott and D. G. Wickham, J. Phys. Chem. Solids, **23**, 1771 (1962).

60. M. Rosenberg, P. Nicolau, R. Manaila and P. Pausescu, J. Phys. Chem. Solids, **24**, 1419 (1963).

61. P. P. Jogalekar and A. P. B. Sinha, Indian J. Pure and Appl. Phys., **5**, 208 (1967).

62. S. T. Kshirsagar and C. D. Sabane, Japan J. Appl. Phys., **10**, 794 (1971).

63. B. A. Mulla and V. S. Darshane, Indian J. Chem. A, **22**, 143 (1983).

64. A. Meenakshisundaram, N. Gunasekaran and V. Srinivasan, Adv. in Catal. Sc. and Technol., Proc. of 7thNational symposium on catalysis, (Baroda, India) Wiley Eastern Ltd., (T. S. R. Prasad Rao, Ed.), 723 (1985).

65. C. Laberty, M. Verelst, P. Lecante, P. Alphonse, A. Mosset and A. Rousset, J. Solid State chem., **129**, 271 (1997).

66. S. Suseela and A. P. B.Sinha, Indian J. Pure and Appl. Phys., **11**, 112 (1973).

67. S. Suseela and A. P. B. Sinha, Indian J. Pure and Appl. Phys., **11**, 116 (1973).

68. G. T. Bhandage and H. V. Keer, J. Phys. C., 7, L 142 (1974).

69. R. J. H. Voorhoeve, Advanced materials in catalysis, Chapter 5, Academic Press (1977).

70. V. I. Savchenko, Russ. Chem. Rev., **55**, 222 (1986).

71. S. Rajadurai and J. J. Carberry, Proc. Faraday Discuss., No.87 (1989).

72. T. Jin, T. Okuhara, G. J. Mains and J. M. White, J. Phys. Chem., **91**, 3310 (1987).

73. K. H. Kim, S. H. Lee, Y. R. Kim and J. S. Choi, J. Catal., **88**, 283 (1984).

74. G. C. Bond, L. R. Molloy and M. J. Fuller, J. Chem. Soc. Chem. Comm., 796 (1975).

75. S. G. Gagarin and M. O. Rozovskii, Kinet. catal., **24**, 1126 (1983).

76. V. Indovina, A. Cimino and F. Pepe, Acta Sim. Ieoram catal., 9th **2**, 846 (1984).

77. M. Kobayashi, T. Kanno and J. Kimura, J. Chem. Soc. Faraday Trasc., **1**, 84, 2099 (1988).

78. J. Laine, Z. Ferrer and M. Labady, Appl. catal., **44**, 11 (1988)

79. S. F. Jen and A. B. Anderson, Surf. Science., **223**, 119 (1989).

80. T. J. Huang and T. C. Yu, Appl. Catal., **71**, 275 (1991).

81. K. I. Choi and M. A. Vannice, J. Catal., **127**, 465 (1991).

82. K. I. Choi and M. A. Vannice, J. Catal., **127**, 489 (1991).

83. K. I. Kapteijn, S. Stegenga, N. J. J. Dekker, J. W. Bijsterbosch and J. A. Moulijn, Catal. Today., **16**, 273 (1993).

84. R. K. Herz, A. Badlani, D. R. Schryer and B. T. Upchurch, J. Catal., **141**, 219 (1993).

85. J. Szanyi and D. W. Goodman, Catal. Lett., **21**, 165 (1993).

86. G. G. Jernigan and G. A. Somorjai, J. Catal., **147**, 567 (1994).

87. F. Boccuzzi, A. Chiorino, S.Tsubota and M. Haruta, Catal. Lett., **29**, 225 (1994).

88. Y. J. Mergler, Proefschrift., **5**, 50 (1995).

89. G. B. Hoflund, Catalysis:Modern Trends, N. M. Gupta and D. K. Chakrabarty (Eds), Narosa Pub. House, New Delhi, India, 429 (1995).

90. G. Parravano, J. Am. Chem. Soc., **75**, 1497 (1953).

91. D. W. Meadowcraft, Nature, **226**, 847 (1970).

92. J. M. D. Tascon, L. G. Tejuca and J. L. G. Fierro, Adv. Catal., **36**, 237 (1989).

93. D. Y. Rao and D. K. Chakrabarty, Indian J. Chem. A, **23**, 375 (1984).

94. B. Vishwanathan and S. Susan George, Indian J. Techn., **22**, 388 (1984).

142

95. P. K. Gallagher, D. W. Johnson and E. M. Vogel, J. Am. Ceram. Soc., **60**, 28 (1977).

96. Om prakash, P. Ganguly, G. Rama Rao, and C. N. R. Rao, Mater. Res. Bull., **9**, 1173 (1974).

97. N. Gunasekaran, A. Meenakshisundaram and V. Srinivasan, Surface Tech., **22**, 89 (1984).

98. S. J. Korf, H. J. A. Koopmans, B. C. Lippens, A. J. Burggraff and P. J. Gellings, J. Chem. Soc. Faraday Trasc. 1, **83**, 1483 (1987).

99. D. K. Chakrabarty and D. Y. Rao, React. Kinet. Catal., 33, 131 (1987).

100. A. V. Salker, D. K. Chakrabarty and H. V. Keer, Indian J. Chem. A, **28**, 458 (1989).

101. K. S. Chan, J. Ma, S. Jaenicke and G. K. Chuah, Appl. Catal. A, **107**, 01 (1994).

102. G. Blyholder, J. Phys. Chem., **68**, 2772 (1964).

103. N. M. Neshev, A. A. Andreev, D. M. Shopov, Dokl. Bulg. Akad. Nauk., **27**, 519 (1974) (in Russian).

104. L. M. Roev, I. G. Voroshilov, Doklady AN Ukr. SSR **9**, 830 (1973) (in Russian).

105. P. Politzer, S. D. Kaster, Surface Sci. **36**, 186 (1973).

106. V. F. Kiselev, O. V. Krylov, Adsorption and Catalysis on transition metals and their oxides (Robert Gomes Ed.) Springer Verlag, Springer series in surface sc. **9**, 230 (1989).

107. L. H. Little, IR Spectra of Adsorbed Species, Academic Press, New York, 47 (1966).

108. J. A. Rabo, C. L. Angeli, P. H. Kasai and V. Shomaker, Disc. Faraday Soc., **41**, 328 (1966).

109. J. W. London and A. T. Bell, J. Catal., **31**, 32 (1973).

110. W. Hertl, J. Catal., **31**, 232 (1973).

111. H. G. Tompkins, R. G. Greenler, Surface Sci., **28**, 194 (1971).

112. D. V. Pozdnjakov, V. N. Filippov, Zh. Fiz. Khim., **46**, 1011, (1971) (in Russian).

113. J. B. Peri, J. Phys. Chem., **78**, 588 (1974).

114. I. G. Voroshilov, L. M. Roev, G. M. Kozub, M. T. Rusov and N. K. Lunev, Kinetica i Kataliz , **16**, 1267 (1975) (in Russian).

115. Ju. A. Lokhov, A. A. Davydov, Kinetica i Kataliz, **21**, 1523 (1980) (in Russian).

116. V. Bheema Raju, D. Y. Rao and D. K. Chakrabarty, Indian J. Chem. A, **21**, 350 (1982).

117. P. J. Moller, S. A. Komolov and E. F. Lazneva, Surface Sci. Lett., L677, 290 (1993).

118. Qingfeng Ge, P. J. Moller, Appl. Surf. Sci., **82/83** , 305 (1994).

119. P. J. Moller, S. A. Komolov and E. F. Lazneva, Appl. Surf. Sci. **82/83** , 569 (1994).

120. S. S. Fu and G. A. Somorjai, Appl. Surf. Sci., **48/49**, 93 (1991).

121. S. Z. Roginskii, Acta. Physico. Chem., USSR, **9**, 475 (1938).

122. W. E. Garner and F. J. Veal, J. Chem. Soc., 1487 (1935).

123. E. D. Pierron, J. A. Rashkin and J. P. Roth, J. Catal., **9**, 38 (1967).

124. E. R. S. Winter, Adv. Catal., **10**, 196 (1958).

125. K. Hirota, Y. Kera and S. Teratum, J. Phys. Chem., **72**, 133 (1968).

126. M. F. Hughes and G. P. Hill, J. Phys. Chem., **59**, 388 (1955).

127. V. I. Marshneva, G. K. Boreskov and V. D. Sokolovskii, Kinet. Katal., **13**,. 1209 (1972).

128. F. S. Stone, Adv. Catal.,'**13**, 1 (1962).

129. W. E. Garner, T. J. Gray and F. S. Stone, Disc. Faraday Soc., **8**, 246 (1950).

130. W. E. Garner, T. J. Gray and F. S. Stone, Proc. Royal Soc.(London), A **211**, 472 (1952).

131. R. M. Dell and F. S. Stone, Trans. Faraday Soc., **50**, 50 (1954).

132. R. Rudham and F. S. Stone, Chemisorption, Proc. Chem. Soc. Symposium, 1956 (W. E. Garner, ed), Academic Press, N. Y., 205 (1957).

133. G. Blyholder, Proc. 3rd Int. Cong. Catal., North Holland Publishing Co. (1964).

134. W. Hertal and R. J. Ferrauto, J. Catal., **29**, 352 (1973).

135. W. J. Morgan and R. J. Ferrauto, J. Catal., **31**, 140 (1973).

136. G. K. Boreskov, V. S. Muzykantov, V. V. Popovskii, G. I. Panov and R. A. Sharbina Kinet. Catal., **13**, 385 (1972).

137. L. Zanderighi, M. P. Faeda and S. Carra, J. Catal., **35**, 427 (1974).

138. K. R. Krishnamurthi, Ph. D. Thesis, I. I. T. Madras (1975).

139. R. Pitchai, Ph. D. Thesis, I. I. T. Madras, (1979).

140. G. K. Boreskov, Y. A. Borisov, N. N. Bulgakov, V. S. Muzykantov, G. I. Panov and P. G. Tsyrul'nikov, Kinetika i Kataliz, **16(5)**,1246 (1975).

141. J. W. Hightower, Chem. Engg. Edn., 148 (1982).

142. J. R. Goldstin and A. C. C. Tseung, J. Catal., **32**, 452 (1974).

143. Yu. V. Tyurkin, E. N. Luzhkova, G. N. Pirogova and L. A. Chesalov, Catal. Today, **33**, 191 (1997).

144. M. Shelef, K. Otto and H. Gandhi, J. Catal., **12**, 361 (1968).

145. Y. F. Yu Yao and J. T. Kummer, J. Catal., **46**, 388 (1977).

146. W. Hertal and P. I. Kingsbury Jr., J. Catal., **32**, 333 (1974).

147. R. Pitchai and V. Srinivasan, Indian J. Chem. A, **16**, 751 (1978).

148. Y. F. Yu Yao, J. Catal., **12**, 361 (1968).

149. F. Severino and J. Laine, Ind. Eng. Chem. Prod. Res. Dev., **22**, 396 (1983).

150. K. R. Krishnamurthy, B. Vishwanathan and M. V. C. Sastri, Ind. J. Chem., **154**, 205 (1977).

151. B. Vishwanathan, K. R. Krishnamurthy and M. V. S. Shastri, J. Res. Inst. Catal., Hokkaido Univ., **27**, 79 (1979).

152. G. M. Schwab, E. Roth, Ch. Grintazes and Marvakis, Structure and properties of solid surfaces' (R. Gomes and C. S. Smith Eds.), The University Of Chicago Press, Chicago (1953).

153. Y. Yoneda, Z. Kato and S. Makishima, Kogyo Kagaku Zasshi., **64**, 975 (1961).

154. N. A. Akhundova and M. S. Belenikii, Nefti Gaz **12** , 73 (1960).

155. H. Paetour and Z. Reikert, Ber. Bunsenges Physik. Chem., **83**, 807 (1979).

156. M. Yu. Sultanov, I. S. Al'tshel and Z. Z. Makhmudova., Azerb Khim. Zn. **2**, 3 (1984)(Russ).

157. D. Perti and R. L. Kabel, AIChE. J., **31**, 1420 (1985).

158. Idem, Ibid., **31**, 1427 (1985).

159. B. Piperov and D. Mekhandzhiev, Izv. Khim., **20**, 500 (1987).

160. B. Piperov, Izv. Khim., **21**, 84 (1988).

161. S. Angelov, E. Zhecheva and G. Tyulier, React. solids, **3**, 57 (1987).

162. S. Angelov, D. Mehandjiev, B. Piperov, V. Zarkov, A. Terelecki-Baricevic, D. Jovanovic and Z. Jovanovic, Appl. Catal.,**16,** 431 (1985).

163. D. Mekhendzhiev, A. Terelecki-Baricevic, B. Dyakova, B. Grbic, I. Dimitrova, E. Zhecheva, Heterog. Catal., 6^{th} pt. **2**, 400 (1987).

164. J. Laine, J. Brito, F. Severino G. Castro, P. Tacconi, S. Yunes and J. Cruz, Catal. Lett., **5**, 45 (1990).

165. K. S. R. C. Murthy and J. Ghose, J. Catal., **147**, 171 (1994).

166. J. Ghose and K. S. R. C. Murthy, J. Catal., **162**, 359 (1996).

167. Li. Ping, Zhou, Jian-Lee and Chen Yu, J. Nat. Gas Chem., **4(3)**, 302 (1995).

168. A. Terelecki-Baricevic, B. Grbic and D. Jovanovic, Appl. Catal., **47**, 145 (1989).

169. V. Zharkov and D. Mehandjiev, Appl. Catal., A, **94**, 161 (1993).

170. F. Pepe and M. Occhiuzzi, J. Chem. Soc. Farad. Trans., **90(6)**, 905 (1994).

171. T. Takada, S. Kasahara, K. Omata and M. Yamada, Nippon Kagaku Kaishi., **9**, 793 (1994).

172. G. N. Pirogova, N. M. Panich, R. I. Korosteleva, and Yu. V. Voronin, Russ. Chem. Bull., **43 (10)**, 1634 (1994).

173. G. N. Pirogova, N. M. Panich, R. I Korosteleva, Yu. V. Voronin and G. E. Kalinina, Izv. Akad. Nauk, Ser. Khim., **(1)**, 49 (Russ.) (1996).

174. K. Omata, T. Takada, S. Kasahara, and M. Yamada, Appl. Catal. A, **146**, 255 (1996).

175. G. M. Schwab and A. Kraut, Z. Anorg. Allg. Chem., **295**, 36 (1958).

176. T. M. Yur'eva, G. K. Boreskov, V. V. Popovskii, V. A. Chirgina and L. S. Egorova, Kinetika i Kataliz, **12(1)**, 140 (1971).

177. N. M. Danilova, Yu. V. Likhachova and P. G. Tsyrulenikov, Kinet. Catal., **16**, 937 (1975).

178. E. A. Hassan, K. M. Abd-El-Salaam and A. A. Said, Bull. Chem. Soc. Jpn., **61**, 1331 (1988).

179. T. Mimani, P. Ravindranathan and K. C. Patil, Proc. Indian Acad. Sci., Chem. Sci., **99**, 209 (1987).

180. P. Lahiri and S. K. Sengupta, Catalysis:Modern Trends, N. M. Gupta and D. K. Chakrabarty (Eds) Narosa Pub. House, New Delhi, India, 301 (1995).

181. T. V. Andrushekevitch, G. K. Boreskov, V. V. Popovskii, V. S. Muzykantov, O. N. Kinkhai and V. A. Sazonov, Kinet. Katal.,**10**, 595 (1968).

182. M. Ya. Kushnerev, V. R. Linde and S. Z. Roginskii, Tverdogo Fiz Teta., **3**, 384 (1971).

183. L. Ya. Margolis, O. V. Krylov and O. V. Isaev, Proc. 5th Int. Cong. of Catal. (J.Hightower, Ed.), North Holland American Elsevier, 103 (1972).

184. G. K. Boreskov, V. V. Popovskii, W. E. Lebedeva, V. A. Sazonov and T. V. Andreshekevitch, Kinet. Katal., **11**, 1253 (1970).

185. Yu. P. Tulenin, Recent advances in catalysis and catalytic reaction engineering (P. Kanta Rao, Ed.) R.R.L. Hyderabad, India, 390 (1986).

186. V. Krishnaswamy and S. Chokkalingam, J. Indian Chem. Soc., **29**, 641 (1982).

187. E. Litchner and G. Szalek, Z. Chem., **8**, 314 (1968).

188. C. S. Narsimhan and C. S. Swamy., Appl. Catal., **2**, 315 (1982).

189. F. E. Massoth and D. A. Scarpiello, J. Catal., **21** 294 (1971).

190. L. Jalowiecki, G. Wrobel, M. Daage and J. P. Bonnelle, J. Catal., **107**, 375 (1987).

191. W. L. Kehl, U. S. Patent, 3, 577, 354 and 3, 595, 810.

192. R. J. Rennard and W. L. Kehl, J. Catal. **21**, 252 (1971).

193. A. Cimino, F. Pepe and M. Schiavello, Proc. 5th int. Cong. of Catal (Palm Beach) Paper No.1 (1972).

194. A. Cimino and A. Schiavello, J. Catal., **20**, 202 (1971).

195. T. A. Egerton and J. C. Vickermann, J. Catal., **33**, 299 (1974).

196. A. Cimino, La. Chemica El Industria, **56**, 27 (1974).

197. Idem, Ibid., **56**, 10 (1978).

198. S. T. Hwang and G. Parravano, J. Electrochem. Soc., **114**, 483 (1987).

199. M. Shelef and K. Otto., J. Catal., **10**, 408 (1968).

200. T. M. Yur'eva, G. K. Boreskov, V. I. Zharkov, L. G. Karakchiev, V. V. Popovskii and V. A. Chigrina, Kinetica i Kataliz, **9**, 1291 (1968).

201. H. Bhattacharya and B. N. Samaddar, J. Am. Ceram. Soc, **61**, 279 (1978).

202. K. C. Patil, C. Nesamani and V. R. Pai-Vernekar, Proc. Acad. Sci. (Chem. Sci) **89**, 87 (1980).

203. D. G. Wickham, Inorg.Synth., **9**, (McGraw Hill, New York), 152 (1957).

204. N. Yamamoto, S. Kawano, N. Achiwa, M. Kiyama and T. Takada, Jap. J. Appl. Phys., **12**, 1830 (1973).

205. G. Rienacker and K. werner, Z. Anorg. Chem. **327**, 275 (1964).

206. P. K. Baltzer and E. Lopatin, Proc. Int. Cong. on Magnetism, Nottingham (London and Bristol Institute of Physics), 564 (1964).

207. I. T. Sheftel and Ya V. Pavlotskii, Sov. Phys.-Solid St. 7, 2781 (1966).

208. V. A. M. Brabers and F. Van Setten, J. Phys. D : Appl. Phys., 16 (1983).

209. N. Yamamoto, S. Kawano and N. Achiwa, Funtai Oyobi Funmatsuyakin, **30(2)**, 48 (1983).

210. N. A. Dhas and K. C. Patil, J. Solid St. Chem., **102**, 440 (1993).

211. J. B. Goodenough and A. L. Loeb, Phys. Rev. **98**, 398 (1955).

212. E. J. W. Verwey, P. B. Braun, E. W. Gorter, F. C. Romeijn, J. H. Van Santen, Z. Phys. Chem., **198**, 6 (1951)

213. J. B. Goodenough, J. Phys. Radium, Paris. **20**, 155 (1959).

214. A. P. B. Sinha and K. P. Sinha, Indian J. Pure Appl.Phys., **1**, 286 (1963).

215. D. B. Ghare, A. P. B. Sinha and A. L. Singh, J. Mat. Sc., **3**, 389 (1968).

216. N. R. Sanjana, Ph. D Thesis, Univ. Poona (1958).

217. C. D. Sabane, Ph. D Thesis, Univ. Poona (1960).

218. S. Asbrinc, A. Was'Kawska, M. Drozd and E. Talik, J. Phys. Chem. Solids, **58**, 785 (1997).

219. B. L. Yang, S. F. Chan, W. S. Chang and Y. Z. Chen, J. Catal., **130**, 52 (1991).

220. J. P. Jacob, A. Matha, J. G. H. Reintjes, J. Drimal, V. Ponec and H. H. Brongersma, J. Catal., **147**, 294 (1994).

221. O. V. Crylov, Kinet. Catal. (Eng. Trasl) **22**, 9 (1981).

222. D. S. McClure, J. Phys. Chem. Solids, **3**, 318 (1957).

223. G. L. Castiglioni, A. Vaccari, G. Fierro, M. Inversi, M. L. Jacono, G. Minelli, I. Pettiti, P. Porta and M. Gazzano, Appl. Catal. A: General **123**, 123 (1995).

224. A. Meenakshisundaram, Ph. D. Thesis IIT Madras (1984).

225. V. A. M. Brabers and F. V. Setten, J. Phys. D: Appl. Phys., **16**, L 169 (1983).

226. G. C. Bond, Heterogeneous Catalysis, Principles and Applications, Academic Press, London and N.Y. 13 (1962).

227. A. Bielanski and J. Haber, 'Oxygen in Catalysis' Marcel Dekker, Inc. N. Y., Basel, Hongkong, (1991).

228. Advances in Catalysis, Vol. **24**, Ed. by D. D. Eley, H. Pines and B. Paul, Academic Press NY, San Francisco, London, Weisz 85 (1975).

229. J. K. Dixon, J. E. Longfield, L. B. Ryland, M. Tamele, J. N. Wilson and M. E. Winfield, Catalysis Vol. VII (Paul H. Emmet, Ed.) Reinhold Pub. Corp. N. Y. 303.

230. Recent advances in catalysis and catalytic research engineering (P. Kanta Rao, Ed.) RRL. Hyderabad, 467 (1986).

231. Congress on catalysis, Ed. by W. M. H. Sachtler, G. C. A. Schuit, P. Zwietering, North-Holland Pub. Co., Amsterdam, Vol. I, 214 (1965).

232. S. J. Thomson and G. Webb, Heterogenous Catalysis, Oliver and Boyd Ltd., Edinburg and London, 74 (1968).

233. F. G. Dwyer, Catalysis Review, **6(2)**, 261 (1972).

APPENDIX - I

Publications

1. Catalytic oxidation of carbon monoxide over $Ni_{1-x}Cu_xMn_2O_4$ system

   S.M.Gurav and A. V. Salker

   National workshop on Catalysis RRL Thiruvananthapuram, 1997 (Accepted)

2. Thermal investigations in the preparations of manganite spinels

   S.M.Gurav and A. V. Salker

   11^{th} National symposium on Thermal Analysis, 1998 (Accepted)

3. Solid state properties and catalytic CO oxidation studies on $Zn_{1-x}Cu_xMn_2O_4$ system

   S.M.Gurav and A. V. Salker

   Indian Journal of chemical technology (communicated).